Hydrogen Storage using Physisorption

Modified Carbon Nanofibers and Related Materials

Waterstofopslag door middel van fysisorptie

Gemodificeerde kooldraden en verwante materialen

(met een samenvatting in het Nederlands)

Proefschrift

ter verkrijging van de graad van doctor aan de Universiteit Utrecht op gezag van de Rector Magnificus, Prof. Dr. W. H. Gispen, ingevolge het besluit van het College voor promoties in het openbaar te verdedigen op dinsdag 23 april 2002 des middags te 12:45 uur

door

Marije Gessien Nijkamp

geboren op 24 december 1973, te Paramaribo, Suriname

Promotor: Prof. dr. ir. K. P. de Jong

Co-promotor: Dr. A. J. van Dillen

Verbonden aan de Sectie Anorganische Chemie en Katalyse, Debye instituut, Faculteit Scheikunde, Universiteit Utrecht

Shell International Oil Products is gratefully acknowledged for financially supporting the research described in this thesis.

This thesis was printed by ponsen & looijen bv, Wageningen

ISBN 90-393-3010-7

Look at these cows and remember that the greatest scientists in the world have never discovered how to make grass into milk.

Michael Pupin

Contents

1

Introduction

1.1 Hydrogen storage

The aim of our research, presented in this thesis, is to contribute to the development and design of a suitable adsorbent for a hydrogen storage system for mobile applications.

Hydrogen storage is a key element in the change-over from the less efficient and polluting internal combustion engine to hydrogen fuel cell driven cars. Hydrogen can be used completely pollution-free and can be produced from renewable energy sources, thus eliminating the net production of greenhouse gases.

Although H_2 might be generated on board on a small scale from e.g. methanol or gasoline, the highest efficiencies will be attained when it is produced off board on a large scale. From the production sites it has to be transported to 'the network' of gas stations where measured amounts, sufficient for a driving range of 400-500 km, will be brought on board of the fuel cell cars. Following the approach of Pettersson *et al*. [1], this means that a fuel cell car needs to store at least 5 kg of hydrogen, while the system allows a peak consumption of 1-3 g/sec to bring about the necessary and desired acceleration. Hydrogen storage systems for mobile applications can be based on either low-cost recyclable fuel containers, or on rechargeable vessels. Rechargeable vessels need to operate more than 1000 deep-discharge cycles, associated with a calendar lifetime in excess of 10 years. The self-discharge time or dormancy should be measured in weeks to a month or more [1]. Additionally, for all options for vehicular H_2 storage, the integrated system should work at temperatures above 20 K and exhibit a high mechanical stability towards intrusions due to collisions. The materials have to be reluctant to ignition when, in spite of all security measures, penetration occurs.

Furthermore, the systems should be low cost in purchase and in maintenance during the life span of the vehicle [2].

In general, hydrogen can be stored pressurized, liquefied, absorbed in metals (as hydrides) and physisorbed on a suitable material. And, although nowadays all of these options are investigated extensively and progress is gained, none of these is fully developed and future applications for a specific utilization are mainly based on extrapolation in which it is assumed that a particular scientific and practical breakthrough is effectuated.

Pressurized H_2 demands the use of a large, heavy tank, which takes up a lot of space in the car and which costs will add significantly to the price of the car [3]. The process of pressurization leads to a low energy efficiency stems from [2,4].

Liquefied hydrogen suffers from an even lower energy efficiency, which is caused by its boiling point of 20 K in combination with unfavorable compression-expansion properties. The tank is bulky and also expensive [3,4] and in spite of its thermal isolation H_2 will evaporate. When driving, this is of course no problem, because meanwhile this H_2 is consumed. However, when the car is not in use, evaporation will continue, and the pressure in the tank will inevitably increase. At the present, the maximum time before H_2 will slowly start to vent off is 3 days.

Metal hydrides also have a low energy efficiency, related to the high temperature needed to release H_2 [4-6]. Due to the limited H_2 absorption in weight, the metal alloy mass needed is significant [3]. Another disadvantage of this storage system is the expansion and contraction of the metal lattice, which occurs when H_2 is taken up respectively released. This expansion/contraction causes stress in the material and the metal disintegrates. Dust, thus formed, may block the tubes leading to the fuel cell. A lot of research is being carried out to solve these problems [5,7-9]. At the moment the TiFe- and MnTi-class of hydrides seems to be the best alternative for use in vehicles, although their weight-based hydrogen capacities are low [1]. Research to enhance the hydrogen capacity is currently focused on hydrides based on magnesium. The latter hydrides exhibit a high capacity even after many cycles, but are no solution to the temperature problem because of their slow kinetics in the lower temperature range. A general problem with these systems is, given the nature of the qualified base metals, passivation by small amounts of water vapor, oxygen and carbon dioxide and poisoning by other impurities in the feed. Furthermore, safety might be a serious problem.

The storage based on physisorption potentially may have a higher energy efficiency [10]. The very low boiling point of H_2 (20 K) makes it necessary to apply temperatures of around 70 K to achieve sufficient amounts of adsorbed H_2. Release of physisorbed hydrogen can be quickly and easily effectuated with relatively small pressure and/or temperature changes. No chemical bonds have to be broken, as is needed for release of H_2 from metal hydrides, which costs a lot of energy. Nevertheless, the tank must be cooled by liquid nitrogen and insulated and therefore will be bulky. The adsorbent material must be mechanically strong, safe and

preferably light and cheap. The United States Department of Energy (DOE) has set the target H_2 storage capacity of such an adsorbent to 6.5 wt%, which equals 720 ml (STP)/g in order to have an acceptable driving range.

Because the interaction forces between hydrogen and adsorbent are physical in character, the interaction is more or less non-specific and the amount of adsorbed hydrogen, at set pressure and temperature, will be mainly related to the specific surface, notably to the pore structure and mean pore diameter, and less to the nature of the adsorbent material. A major advantage of such systems is that adsorbing materials can be chosen that are common in nature, are abundantly available and are safe and not toxic by itself. Furthermore, as table 1.1 shows, the expected efficiency of the adsorption system is the highest. Weighing above arguments we decided to focus our research on the development and design of a suitable adsorbent for hydrogen storage. Considering the know how and expertise of our research group in the field of production and design of (catalyst) support materials including the formation carbon nanofibers, we mainly concentrated on various carbon materials.

Table 1.1 Characteristics of hydrogen storage options [1,2,4,11,12].

Storage method	Temperature (K)	Pressure (bar)	Storage cycle efficiency (%)
pressurized hydrogen	298	200-250	80
liquid hydrogen	20	1-5	60
metal hydrides	293-573	1-60	75
physisorbed hydrogen	77	1-10	90

1.2 Activated carbon materials

Since the 1960's, al kinds of ‘activated’ carbon materials, prepared from mineralogical and organic precursors, have been investigated concerning their suitability to adsorb hydrogen [4,10,12-14]. These materials are typically obtained by thermochemical processing and contain many different types of carbon structures that provide a variety of environments for adsorbing hydrogen [15].

In their recent review on hydrogen storage using carbon adsorbents, Dillon and Heben [15] conclude that, in general, there have been very few reports of an activated carbon type adsorbent, capable of improving the capacity of a high-pressure tank at 300 K. It was generally found that more open, microporous carbon materials adsorbed more hydrogen than denser materials. More specifically, a highly microporous material, which is low in macro and mesoporous volume is needed for high storage capacities. Best results were found by Carpetis and Peschka [10], who measured a storage capacity of 5.2 wt% at 41.5 bar and 65 K for a ‘F12/350’ carbon material.

The most important and severe problem with activated carbons is that they are difficult to produce reproducibly and to end up with a uniform and suitable pore structure. In fact, for future application the reproducible large scale production of the uniform micropore structure is a prerequisite.

1.3 Carbon nanofibers

Carbon nanofibers (CNF) have been studied for more than a century [16]. CNF are formed under certain conditions during conversion of hydrocarbons over e.g. (supported) nickel and iron catalysts. Because of their ability to completely destroy a catalyst and even the reactor, until the 1990's most research was aimed at prevention of their growth. After the discovery in 1991 of single walled carbon nanotubes [17] also their larger 'relatives' have become subject of more interest. Nowadays, their applicability in electronic components [18-20], as a polymer additive [18] and especially as catalyst support material [21-23] is being investigated profoundly.

Carbon nanofibers are largely graphitic materials. They consist of stacks of graphite sheets and have diameters from 10 up to 100 nm and length up to several hundreds of μms. The fibers can be built up from graphite cones, stacked on top of each other (the fishbone type), or from concentric cylinders. Especially the cone shaped fishbone type is interesting in view of our efforts to find a suitable adsorbent for hydrogen. Potentially, with graphitic carbon intrinsically a very high micropore volume could be attained if the space between the cones can be made accessible for hydrogen.

The results obtained with carbon nanofibers and nanotubes as a storage medium for hydrogen aroused many debates in the literature. Gadd *et al*. [24] reported in 1997 that carbon nanotubes, which were hot isostatically pressed with argon at 923 K and 170 bar showed the presence of the argon inside the hollow tubes. This was retained after cooling and depressurizing.

That measurements of H_2 uptake are difficult to perform and require extremely well defined experimental conditions to gain reliable information is demonstrated by Dillon *et al*. [15,25-27], Chen *et al*. [28] and Baker *et al*. [29,30].

Dillon *et al*. [15,25-27] reported that nanotubes, which were sonicated in HNO_3, absorb 10 wt% H_2 at room temperature. The sonication treatment was reported necessary to break and thus open the tubes. Hirsch [31] elegantly showed that this H_2 adsorption capacity of the sonicated tubes resulted from the sonication treatment. This sonication is done in 5 M HNO_3 at 10°C, using a titanium tip. During the high intensity sonication small particles of the tip material are formed and deposited inside or on the walls of the nanotubes. After washing and drying, the titanium shows very good H_2 absorption capacities at room temperature and ambient pressure. Hirsch showed the importance of the sonication treatment on the absorption

capacities of the nanotubes by subjecting diamond powder to this treatment. The characteristics of the absorption were similar to nanotubes. All materials showed hydrogen absorption capacities after this treatment, so the majority of the hydrogen storage of all samples has to be ascribed to the titanium particles.

Chen *et al*. [28] claimed that 'Li and K doped nanotubes' showed 20 or 14 wt% hydrogen adsorption at 200 to 400°C under ambient pressure. The doping of Li and K to the nanofibers was carried out by solid-state reactions between the fibers and Li- and K-carbonates and -nitrates. The stored hydrogen - determined only gravimetrically - could be released at higher temperatures and the sorption-desorption cycle could be repeated with little decrease in sorption capacity. However, Yang *et al*. [32] showed that the supposed hydrogen adsorption capacities can be accounted for by the formation of LiOH and KOH, which results from the presence of traces of H_2O in the feed. When this contaminant was present in the H_2 containing feed, it reacted with the present Li- and K-compounds to form LiOH and KOH. Above authors showed that when water was added to the feed, the adsorption increased, but the shape and reversible behavior remained the same. They also showed that when H_2O was eliminated from the feed the materials could be heated up and cooled down without this reversible 'hydrogen storage' behavior.

Park, Rodriquez and Baker [29] claimed very high H_2 absorption capacities in their fishbone (herringbone) nanofibers at room temperature and high H_2 pressures (110 bar). They claimed storage capacities from 11 to 61 wt%, which is equal to 1.4 to 23 Nl H_2/g_{ads}. In a later report [30] they brought the upper limit down to 42 wt% (9 Nl/g_{ads}). They claimed that the H_2 fitted well between the graphite planes of the fibers. This would mean that H_2 is capable of lifting the planes and subsequently inserting itself in between the planes in a stoichiometry of CH_{18} (61 wt%). Authors claimed that $^2/_3$ of this H_2 was physisorbed and $^1/_3$ was chemisorbed. By lowering the pressure, the physisorbed H_2 could be released from the fibers. So far no one has been able to duplicate their results [33] and it is generally believed that these are incorrect [34].

Several groups performed theoretical calculations on the adsorption of H_2 in carbon nanofibers, nanotubes and several carbon pores in the shape of slits or cylinders. These calculations were performed using Monte Carlo calculations [35,36], Molecular Dynamics (MD) calculations [37] and MD calculations combined with experiments [38]. In this way the feasibility of results as reported by Dillon or Baker were checked. It was concluded that the high hydrogen storage capacity as reported by Baker *et al*. could not be attained with these fibers, because the 'pores' between the graphite planes are too narrow to allow H_2 to enter. It was concluded that maximum H_2 storage would be attained at 77 K using slit- or cylindrically shaped pores with a diameter of 1 nm, at pressures of around 110 bar. The results of the calculations are summarized in table 1.2 below.

Table 1.2 Results of theoretical calculations on the maximum H_2 storage capacity of carbon sorbents at indicated temperatures and 110 bar [38].

Material	T (K)	P (bar)	Pore diameter (nm)	wt% H_2 adsorbed
Baker (claims 68 wt%)	298	110	0.34	0
optimized Baker	298	110	0.7	1
nanotube	300	110	1.0	0.7
slitpore	300	110	1.0	1.2
nanotube	77	110	1.0	6.8
slitpore	77	110	1.0	2.5

Wang and Johnson [37] concluded that the experimental results of Baker were not consistent with any reasonable physisorption model. Their calculations showed that maximum adsorption of 0.46 wt% at room temperature and 100 bar would be reached with 0.9 nm wide slitpores.

1.4 Scope of this thesis

In **chapter 2** we report on the adsorption of hydrogen onto a number of activated carbons and some amorphous as well as some well crystallized microporous oxidic materials in order to reveal the adsorption capacities at 1 bar and 77 K. It will be argued that with the zeolitic materials the chance to find the optimal pore diameter seems realistic, but that their unavoidably low micropore volume limits their scope. With the activated carbons a more optimistic perspective will be offered. Because it was decided to turn to fishbone CNF as the storage medium these fibers had to be produced reproducible and in sufficient amounts. With the at that time available labscale production methods only a few grams per batch could be grown. We therefore designed a fluidized bed reactor which development and use are dealt with in **chapter 3**. In **chapter 4** we report on the micro and macro structure of the thus obtained fibers as well as on our investigation of the influence of heat treatment of the fibers at very high temperatures on their morphology and microstructure. With graphitic carbons intrinsically very high micropore volumes can be calculated. To make this slitshaped porous volume accessible for hydrogen, space between the layers should be enlarged. This enlargement of the d-spacing of graphitic materials can be effectuated by intercalation of another suitable compound like alkali metals and metal halides. In **chapter 5** we turn to the adsorption of hydrogen on potassium intercalated fibers and graphite. In **chapter 6** we describe our efforts to intercalate iron(III)-chloride into the fibers. We also describe the influence of the intercalation on the storage capacity of the fibers. In addition we present our results obtained with iron(III)-chloride intercalated graphite and with the reduced intercalated product. Reduction was performed to enhance the accessible pore volume. Finally, in **chapter 7** we give a summary of the major results of the preceding chapters and give suggestions for further research in this field.

References

1. J. Pettersson and O. Hjortsberg, Hydrogen storage alternatives (KFB-Meddelande, Volvo Teknisk Utveckling AB, 1999).
2. R. Wurster and W. Zittel, Proceedings of the Workshop on Energy technologies to reduce CO_2 emissions in Europe: prospects, competition, synergy (1994).
3. G.D. Berry, A.D. Pasternak, G.D. Rambach, J.R. Smith and R.N. Schock, Energy 21 (1996) 289.
4. J.A. Schwarz, J.S. Noh and R.K. Argawal, United States Patent 4,960,450 (1990).
5. E.L.J. Vercammen, PhD Thesis, Utrecht University (1996).
6. T. Petkov, T.N. Veziroglu and J.W. Sheffield, International Journal of Hydrogen Energy 14 (1989) 449.
7. A. Reiser, B. Bogdanovic and K. Schlichte, International Journal of Hydrogen Energy 25 (2000) 425.
8. J. Huot, G. Liang and R. Schulz, Applied Physics A 72 (2001) 187.
9. A. Zaluska, L. Zaluski and J.A. Stroem-Olsen., Applied Physics A 72 (2001) 157.
10. C. Carpetis and W. Peschka, International Journal of Hydrogen Energy 5 (1980) 539.
11. U. Buenger and W. Zittel, Applied Physics A 72 (2001) 147.
12. K.A.G. Amankwah and J.A. Schwarz, International Journal on Hydrogen Energy 14 (1989) 437.
13. J. Jagiello, T.J. Bandosz, K. Putyera and J.A. Schwarz, Journal of the American Chemical Society, Faraday Transactions 91 (1995) 2929.
14. A.J. Kidnay and M.J. Hiza, Advances in Cryogenic Engineering 12 (1967) 730.
15. A.C. Dillon and M.J. Heben, Applied Physics A 72 (2001) 133.
16. T.V. Hughes and C.R. Chambers, US patent 405,480 (1889).
17. S. Iijima, Nature 354 (1991) 56.
18. H.G. Tennent, US Patent 4,663,230 (1987).
19. C. Niu, E.K. Sichel, R. Hoch, D. Moy and H. Tennent, Applied Physics Letters 70 (1997) 1480.
20. G. Che, B.B. Lashmi, E.R. Fisher and C.R. Martin, Nature 393 (1998) 346.
21. K.P. de Jong and J.W. Geus, Catalysis Reviews- Science and Engineering 42 (2000) 481.
22. M.L. Toebes, J.A. van Dillen and K.P. de Jong, Journal of Molecular Catalysis A: Chemical 173 (2001) 75.
23. D. Moy and R. Hoch, Catalyst supports, supported catalysts methods of making the same and methods of using the same, WO 93/24214 (1993).
24. G.E. Gadd, M. Blackford, S. Moricca, N. Webb, P.J. Evans, A.M. Smith, G. Jacobsen, S. Leung, A. Day and Q. Hua, Science 277 (1997) 933.
25. A.C. Dillon, K.M. Jones, T.A. Bekkedahl, C.H. Kiang, D.S. Bethune and M.J. Heben, Nature 386 (1997) 377.
26. A.C. Dillon, K.M. Jones and M.J. Heben, Proceedings of the US DOE Hydrogen Program Review 1996 Golden Colorado (1996) 747.

27. M.J. Heben, A.C. Dillon, J.L. Alleman, K.M. Jones and P.A. Parilla, Abstracts 2000 MRS Fall Meeting, p. 17.

28. P. Chen, X. Wu, J. Lin and K.L. Tan, Science 285 (1999) 91.

29. A. Chambers, C. Park, R.T.K. Baker and N.M. Rodriquez, The Journal of Physical Chemistry B 102 (1998) 4253.

30. C. Park, P.E. Anderson, A. Chambers, C.D. Tan, Hidalgo and R. Rodriquez, Journal of Physical Chemistry B. 103 (1999) 10572.

31. M. Hirscher, M. Becher, M. Haluska, U. Dettlaff-Weglikowska, A. Quintel, G.S. Duesberg, Y.-M. Choi, P. Downes, M. Hulman, S. Roth, I. Stepanek and P. Bernier, Applied Physics A 72 (2001) 129.

32. R.T. Yang, Carbon, Letters to the Editor 38 (2000) 623.

33. C.C. Ahn, Y. Ye, V. Ratnakumar, C. Witham, R.C.Jr. Bowman and B. Fultz, Proceedings of the Battery Conference on Applications and Advances 14 (1999) 67.

34. C. Zandonella, Nature 410 (2001) 724.

35. F. Darkrim and D. Levesque, Journal of Chemical Physics 109 (1998) 4981.

36. F. Darkrim and D. Levesque, The Journal of Physical Chemistry B 104 (2000) 6773.

37. Q. Wang and J.K. Johnson, The Journal of Physical Chemistry B 103 (1999) 277.

38. M. Rzepka, P. Lamp and M.A. de la Casa-lillo, Journal of Physical Chemistry B 102 (1998) 10894.

2

Hydrogen Storage using Physisorption - Materials Demands

Abstract

A survey is presented of the hydrogen storage capacities of a large number of different adsorbents at 77 K and 1 bar. Results are evaluated to examine the scope of storage based on physisorption of hydrogen on solid adsorbents. It is concluded that microporous adsorbents, e.g. zeolites and activated carbons, display appreciable sorption capacities. Based on their micropore volume (~1 ml/g) carbon-based sorbents display the largest adsorption capacity, viz. 238 ml (STP)/g, at the prevailing conditions. Optimisation of sorbent and adsorption conditions is expected to lead to adsorption of ~560 ml (STP)/g, close to targets set for mobile applications.

2.1 Introduction

In the last two decades there has been an increasing interest in the development of (transportable) reversible systems for hydrogen storage with a high capacity, which is critical to the large-scale application of hydrogen fuel cells in particular for mobile applications [1]. Up to now focus has mostly been on liquid hydrogen, pressurized hydrogen and metal hydrides systems, which all have low energy efficiencies [2]. The energy efficiency of these systems is at most 80%. A higher energy efficiency (90%) is attainable with systems in which hydrogen is concentrated by physical adsorption above 70 K using a suitable adsorbent [3-5]. Such an absorbent should be safe, light and cheap and of course have a high adsorption capacity. In order to obtain a suitable driving range for automotive applications the United States Department of Energy (DOE) target has been set to 6.5 wt% H_2, which equals 720 ml (STP) H_2/g_{ads}. Schwarz and co-workers [6-8] studied the applicability of molecularly engineered activated carbons and came with promising results. Much excitement has arisen from recent reports on the use of carbon nanofibers [9,10] and carbon nanotubes [11,12] but because of further research [13] the exciting results have become questionable. Chapter 1 deals with these reports in more detail.

In this chapter we present a survey of the storage capacity for molecular hydrogen at 77 K and 1 bar of a large number of different types of adsorbents, such as silicas, aluminas, zeolites, graphite, activated carbons and carbon nanofibers. Care has been taken to make sure that these adsorbents include a wide range of specific surface areas and different textures. The carbon nanofibers, aerosil and graphite are materials, which structure only contains large mesopores and macropores. We have studied an all silica material, MCM-41, which completely consists of very regular, 3 nm diameter pores. Some of the activated carbons are mesoporous as well. The zeolites, activated graphite, activated carbon fibers and activated carbon that were studied, are microporous materials. It was made sure that this selection contained materials with small micropores, ~1 nm diameter, as well as materials with larger (super-) micropores, between 1 and 2 nm diameter. The materials were not modified to change their adsorptive properties before their hydrogen adsorption capacity was measured.

2.2 Experimental

A large number of carbonaceous (see table 2.1) and silica-alumina based (see table 2.2) sorbents were characterized using N_2 physisorption at 77 K and up to a pressure of 1 bar. The sorbents were chosen to represent a large variation in surface areas and (micropore) volumes. The materials were used as synthesized, or as obtained commercially, without modification to change their adsorptive properties. Both non-microporous materials, such as aerosil and graphites, and microporous sorbents, such as activated carbons and zeolites, were selected. First we provide a brief description of the samples selected with the sample numbers between brackets. Activated carbons are highly micro- and mesoporous carbon materials. They have been steamed or chemically activated. Steam-activated carbons (7,8,11,12,14-19) have been

prepared from raw materials (e.g. peat, lignite, coal) and carbonized and reacted with steam at 1000°C. In this way part of the carbon atoms are removed by gasification, which yields a very porous structure. Chemically activated carbons (20) are produced by mixing an activation chemical (usually phosphoric acid) with a young carbonaceous material (usually sawdust), and carbonizing the resultant mixture at 500°C. The resulting very porous carbon structure is filled with activation agent, which is removed from carbon by washing [14]. Activated carbon fibers (5,6,12) have been prepared by controlled pyrolysis of various structures, e.g. the synthetic polymer polyacrylonitrile (PAN) or coal-tar pitch [15]. These fibers are subsequently subjected to activation as described for the activated carbons. Activated graphite (3,9) is synthetic graphite which has been activated in the same way as described for the activated carbons. Carbon nanofibers (2,4,10,21) have been catalytically synthesized, as described in chapter 3. These fibers consist of conical (fishbone, 2,4,10) or tubular (parallel, 21) graphite planes [16]. Zeolites are highly crystalline, microporous materials, consisting of silica and alumina. Zeolite L (23) consists of uni-dimensional 12-ring pores, with 0.9 nm diameter. Ferrierite (25) is a two dimensional pore network, consisting of pseudo-spherical cages with 8-ring openings (0.35*0.48 nm) and interconnecting 10-ring pores (0.42*0.55 nm). ZSM-5 (24) consists of tri-dimensional interconnecting 10-ring pores of dimensions 0.51*0.55 nm [17]. The silicas and aluminas (22,26-34,36) are all commercially available inert catalyst supports selected for their lack of microporosity. MCM-41 (35) is an all-silica material, consisting of highly regular, 3 nm diameter channels [18,19].

From the N_2 physisorption data, obtained with a Micromeritics ASAP 2400 apparatus, the BET surface area, total pore volume (PV), micropore volume (MPV) and t-surface (S_t) were derived. All pore volumes are expressed in ml/g, the micropore volume is defined as the pore volume of the pores < 2 nm. The BET surface area (S_{BET}, m^2/g) is the surface area of the sorbent according to the model formulated by Brunauer, Emmet and Teller [13] for planar surfaces. The BET-equation is formulated to assess multilayer adsorption of small inert molecules on substrates. The t-surface area (S_t, m^2/g) is derived from the t-plot and is the mesoporous (> 2 nm) surface area of the sorbent, i.e. the surface area excluding the micropores [20].

The H_2 adsorption measurements were performed volumetrically with a Micromeritics ASAP 2010 at 77 K in the pressure range 0-1 bar. From adsorption-desorption experiments it is evident that reversible physisorption exclusively takes place with all samples.

The micropore analysis was also performed with a Micromeritics ASAP 2010 at 77 K in the pressure range 0-1 bar with nitrogen. The pore diameters, assuming slit-shaped pores, were calculated with the DFTPLUS algorithm provided by Micromeritics.

2.3 Results and discussion

The results of the N_2- and H_2-physisorption measurements are shown in table 2.1 and 2.2 In these tables CNF is used to designate carbon nanofibers, ACF is used for activated carbon fibers and AC for activated carbon. Representative adsorption isotherms are shown for oxides (figure 2.1) and carbon materials (figure 2.2).

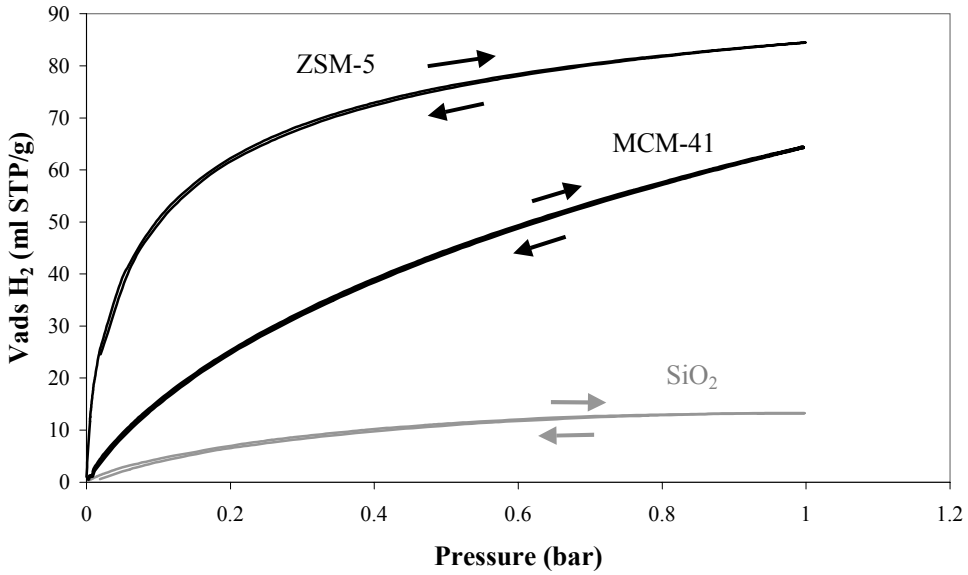

Figure 2.1 Adsorption isotherms for aerosil, MCM-41 and zeolite (ZSM-5).

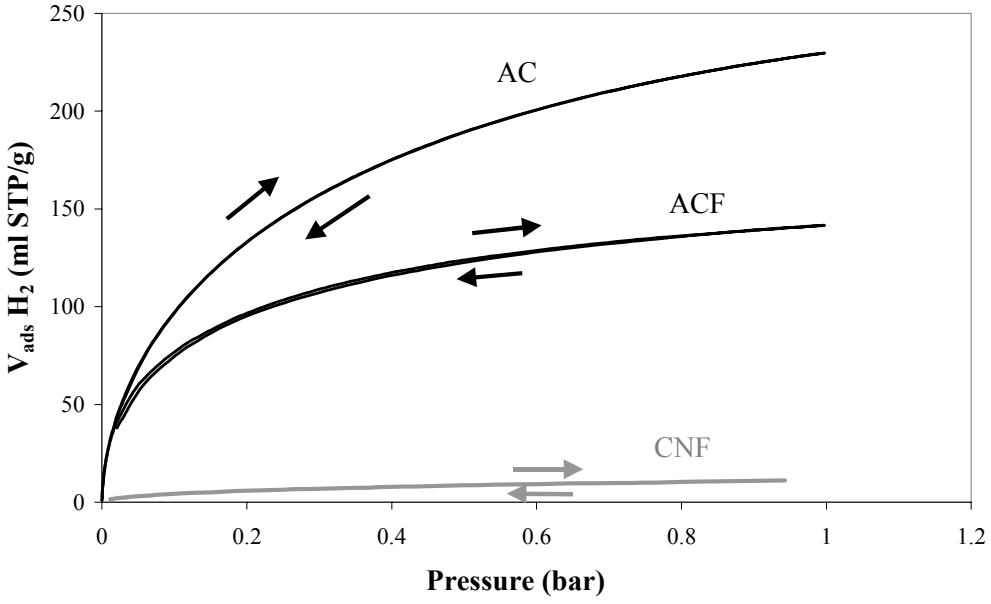

Figure 2.2 Adsorption isotherms for CNF, ACF and AC.

Table 2.1 Texture analysis and hydrogen adsorption capacities at 77 K and 1 bar for carbonaceous materials.

No.	Material	PV (ml/g)	S_{BET} (m^2/g)	S_t (m^2/g)	MPV (ml/g)	H_2 total (ml (STP)/g)	H_2 meso (ml (STP)/g)	H_2 micro (ml (STP)/g)
1	Synth. graphite	0.04	7	7	0.00	0	0	0
2	Large diam. CNF	0.10	49	26	0.01	6	2	4
3	Act. Graphite 100	0.26	119	85	0.02	14	6	8
4	Medium diam. CNF1	0.28	120	120	0.00	12	11	1
5	ACF 400	0.40	883	12	0.34	143	1	142
6	ACF 1200	0.42	899	7	0.37	184	1	183
7	AC Norit 990721	0.43	988	17	0.43	142	2	140
8	AC Norit ROZ 3	0.50	287	84	0.05	36	6	28
9	Act. Graphite 300	0.51	287	183	0.05	36	16	19
10	Medium diam. CNF2	0.55	65	65	0.00	7	7	0
11	AC Norit SX 2	0.60	841	194	0.27	150	17	133
12	ACF 500	0.61	988	173	0.40	142	15	127
13	AC Norit UOK A	0.65	1195	110	0.47	188	10	178
14	AC Norit SX 1	0.67	922	206	0.31	168	18	150
15	AC Norit SX 1G AIR	0.68	1030	180	0.36	171	16	155
16	AC Norit GSX	0.78	933	302	0.26	161	27	134
17	AC Norit SX plus	0.79	1051	238	0.35	165	21	144
18	AC Norit SX 1 G	0.83	1176	229	0.40	187	20	167
19	AC Norit 990293	1.03	2029	78	0.92	238	7	231
20	AC Norit Darco KB	1.39	1462	610	0.42	146	54	92
21	Hyperion CNF	2.75	238	238	0.00	22	22	0

Table 2.2 Texture analysis and hydrogen adsorption capacities at 77 K and 1 bar for oxides.

No.	Material	PV (ml/g)	S_{BET} (m^2/g)	S_t (m^2/g)	MPV (ml/g)	H_2 total (ml (STP)/g)	H_2 meso (ml (STP)/g)	H_2 micro (ml (STP)/g)
22	SiO_2 90	0.23	79	64	0.01	4	4	0
23	Zeolite L	0.25	344	26	0.12	59	1	58
24	Zeolite ZSM5	0.28	431	43	0.16	80	2	78
25	Zeolite ferrierite	0.32	344	41	0.12	65	2	63
26	SiO_2 D051A	0.48	172	172	0.00	9	9	0
27	SiO_2 1614E	0.51	97	97	0.00	9	9	0
28	SiO_2 Caboxil M5	0.59	185	183	0.00	11	11	0
29	S980G	0.60	67	67	0.00	5	5	0
30	SiO_2 Aerosil 200	0.66	167	167	0.00	0	0	0
31	SiO_2 Becker AD 050	0.74	330	330	0.00	18	18	0
32	SiO_2-60-1	0.75	61	52	0.00	3	3	0
33	Al_2O_3 preshaped	0.80	233	233	0.00	7	7	0
34	SiO_2 380	0.87	322	273	0.03	27	15	12
35	MCM-41	1.04	1017	1017	0.00	65	65	0
36	S970SH	1.08	290	268	0.01	28	15	13

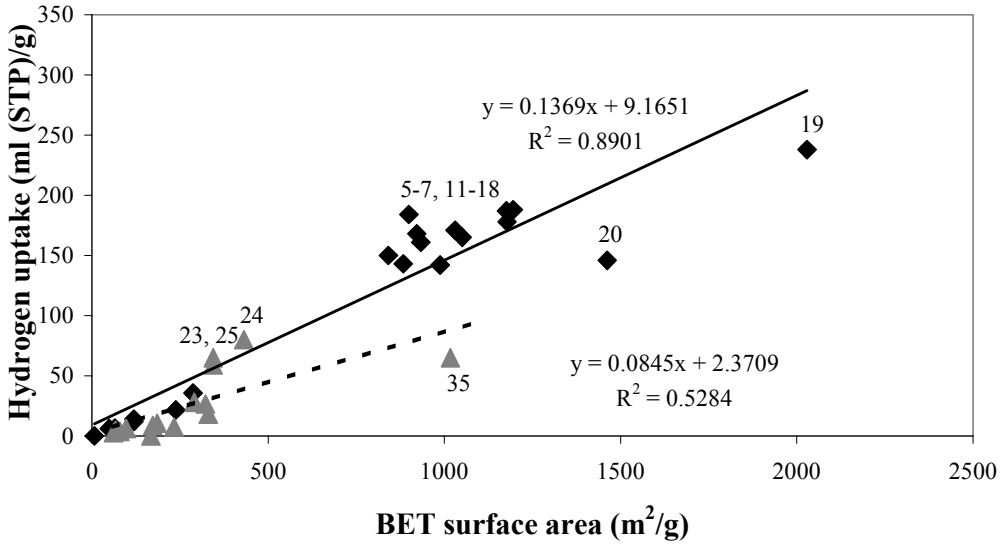

Figure 2.3 Hydrogen adsorption versus at BET surface area 77 K and 1 bar for carbon (◆), silica and alumina (▲).

In a first approach the total amounts of hydrogen taken up per gram of adsorbent at 77 K and 1 bar are correlated with S_{BET}. From figure 2.3 it can be concluded that this correlation exist, but is not very straightforward. It is apparent that with the mesoporous silicas and aluminas a low H_2 capacity is found, even with the MCM-41 sample (35) exhibiting a S_{BET} of 1017 m^2/g. Only with the zeolites (23,24,25), with S_{BET} values of 344, 431 and 344 m^2/g, an enhanced capacity, relative to the linear correlation for oxides, is measured, probably because of their microporous texture. This also holds for the mainly microporous carbon samples (5-7,11-18).

Above results suggest that a better correlation is to be expected between the micropore volumes and the respective adsorption capacities for H_2. However, it is important to realize that hydrogen not exclusively adsorbs in the micropores but also on the surface of the mesopores. Therefore, to find the actual H_2-uptake in the micropores we have corrected the total H_2 uptakes for the amounts adsorbed on the mesopore surface area.

We calculated the contribution by the mesopores using the correlation which exists, as shown in figure 2.4, between the adsorbed volumes and the t-surfaces of the various non-microporous silica (27,31), alumina (29) and carbon samples (4,10,21, all carbon nanofibers). Obviously hydrogen adsorbs more strongly on carbon surfaces: the oxidic surfaces take up 0.06 ml (STP)/m^2 at 1 bar, the carbon surfaces 0.09 ml (STP)/m^2. Using the above correlations and the t-surface areas as derived from the N_2 physisorption measurements the surface coverage of H_2 at 1 bar can be calculated, if the average area, occupied by one H_2 molecule (a_M) is known. Following the approach of Emmet and Brunauer [21], we estimated a_M to be 0.14 nm^2. With this a monolayer capacity for H_2 can be calculated of 7.10^{18} molecules/m^2. Thus, for the oxidic surfaces we arrive, at 77 K, at a coverage of 22% while with the carbon surfaces a coverage of 34% is attained at 1 bar.

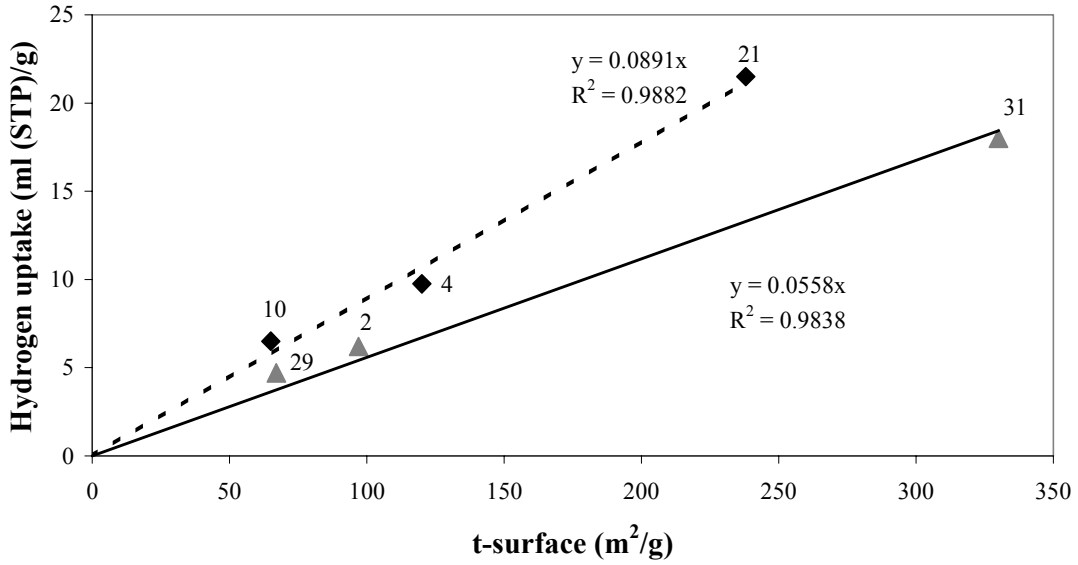

Figure 2.4 Hydrogen adsorption versus t-surface at 77 K and 1 bar for carbon (◆), silica and alumina (▲).

In figure 2.5 the t-surface corrected hydrogen uptakes of various microporous silica (34), alumina (36) and zeolite (23,24,25) samples are plotted against their micropore volumes.

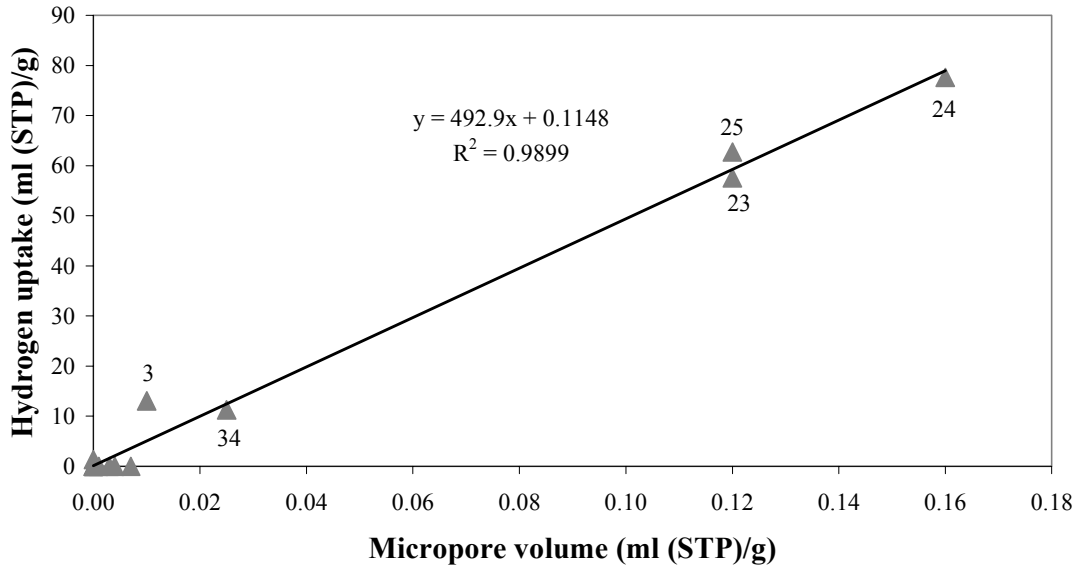

Figure 2.5 t-surface corrected hydrogen adsorption versus micropore volume at 77 K and 1 bar for silica and alumina.

In figure 2.6 this is shown for the microporous carbon samples.

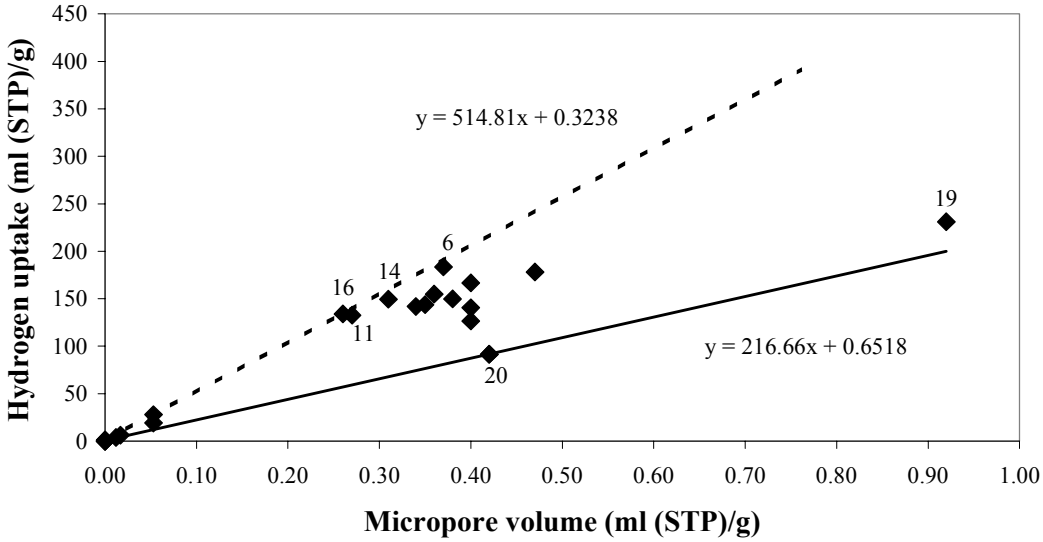

Figure 2.6 t-surface corrected hydrogen adsorption versus micropore volume at 77 K and 1 bar for carbon.

A good correlation is found with the oxidic samples (figure 2.5). The scatter of the data points at low hydrogen uptakes is due to the relatively large error in the calculated micropore volumes. Based on the derived linear correlation the H_2 uptake per ml of micropore volume amounts to 490 ml (STP)/g. The apparent density of H_2 inside the zeolite micropores amounts to 0.044 g/ml, that is 63% of the density of liquid hydrogen (0.07 g/ml). For carbon-based sorbents a large scatter between the data for the H_2 uptake and the micropore volume is observed (figure 2.6). A lower limit for the correlation is given mainly by samples 19 and 20. The lower line shown in figure 2.6 relates to an H_2 uptake of 220 ml (STP)/ml or an H_2 density of 0.020 g/ml (28% of liquid H_2). The upper limit (6,11,14,16) gives 515 ml (STP)/ml or a H_2 density of 0.046 g/ml (66% of liquid H_2). For microporous carbons the details of the pores (size and shape) apparently affect the specific H_2 uptake to a large extent.

A preliminary study to relate the effect of the details of the microporosity to the specific H_2 uptake is reported. Using DFT calculations and assuming slit-shaped pores the pore diameter distributions have been established. The calculated pore sizes range from 0.5 to 2.0 nm (table 2.3, figure 2.7). Realizing that the results have been obtained from N_2 physisorption (N_2 molecule diameter ~0.4 nm), the 'resolution' of the technique is not better than ~0.4 nm. However, the samples 13 and 19 containing super-micropores (1-2 nm) give rise to a lower average H_2 density in the pores than samples 5-12 (0.5-1 nm pores). Tentatively, we conclude that micropores < 1 nm are beneficial to enhance H_2 uptake capacity. At a molecular scale, this implies that graphite structures with 2-3 graphene sheets missing are desirable.

Table 2.3 Pore diameters of several carbon compounds.

No.	Material	Average pore diameter (nm)	H_2 density (g/ml)
5	ACF 400	0.5-0.8	0.038
6	ACF 1200	0.6-0.8	0.046
7	AC Norit 990721	0.8-1.0	0.029
12	ACF 500	0.7-1.0	0.029
13	AC Norit UOK A	0.9-1.5	0.034
19	AC Norit 990293	0.8-2.0	0.023

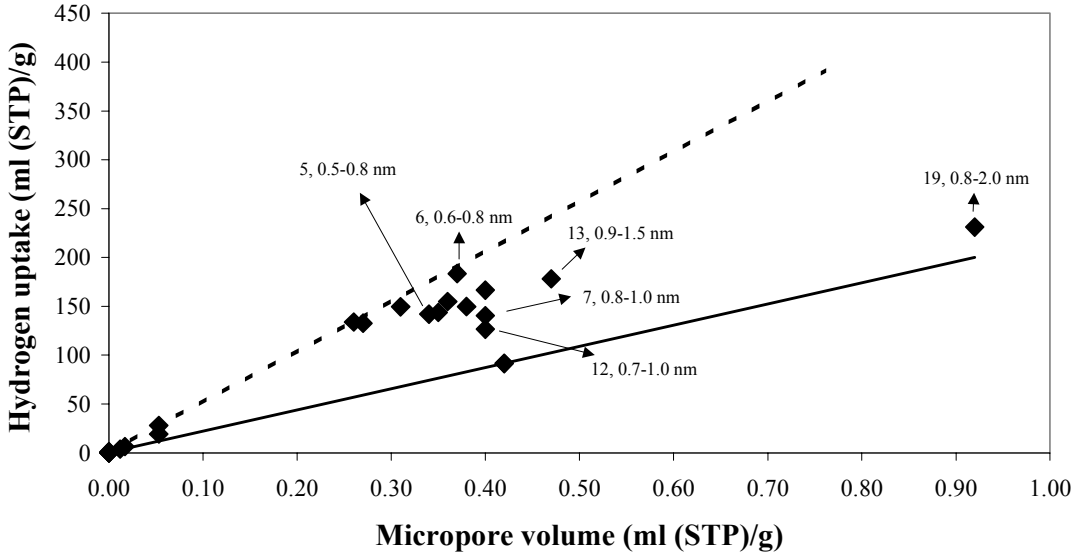

Figure 2.7 Corrected H_2 uptake versus micropore volume of carbon compounds, with diameters of the micropores of several of these carbon compounds reported.

However, the used method for the determination of the pore diameter has limitations and possibly the accuracy of the results could be improved by using another method. Recently a lot of research has been performed on determination of pore sizes with adsorption isotherms, using other computational methods or different adsorption gasses [22-30]. It should be possible to find a more suitable method or adsorption gas to probe the dimensions of these micropores. If so, it would be possible to draw more definitive conclusions on the most suitable pore dimensions for hydrogen storage. Another possibility is that not only the size, but also the specific shape of the pores has a large influence on the adsorption capacity.

In comparing microporous oxides (zeolites) and carbons (activated carbons) it turns out that similar hydrogen densities (0.04-0.05 ml/g) are observed at 77 K and 1 bar. For mesoporous surfaces (figure 2.5) carbon interacts somewhat stronger with H_2 than oxides do. For micropores this difference vanishes, probably due to the different shape of the micropores for activated carbons (slits) and zeolites (cylinders). The main advantage of carbon over oxides resides with the range of micropore volumes that can realistically be achieved. Zeolites with a micropore volume of say 0.5 ml/g or above do not exist, whereas with activated carbon 1 ml/g is common practice. The details of the pore size and shape are very important with the latter, though.

The importance of the size of pores in hydrogen uptake can be illustrated further with the hydrogen adsorption capacity of MCM-41. This oxidic material has very regular, 3 nm diameter pores, which makes it a completely mesoporous material. It adsorbs 65 ml (STP)/g, which is a 12% higher uptake than found with other mesoporous oxides (see table 2.2). This shows that the hydrogen in the mesopores of MCM-41 is slightly more stabilized than by other oxidic mesoporous surfaces. It is however not stabilized as much as H_2 in micropores of zeolites (see figure 2.3).

The density of H_2 in the micropores of carbon at the prevailing conditions (77 K, 1 bar) ranges from 0.02-0.05 g/ml, that is 30-70% of the density of liquid H_2. With the current types of carbon sorbents at the prevailing sorption conditions a maximum uptake of 238 ml (STP)/g has been measured, amply below the DOE target of 720 ml (STP)/g for mobile applications. In case we could realize a micropore volume of 1 ml/g, with a H_2 density of 0.05 g/ml the uptake would rise to 560 ml (STP)/g, much closer to the DOE target. By optimization of both sorbent and sorption conditions (P, T) the H_2 density might approach that of liquid H_2 giving rise to an uptake of 780 ml (STP)/g.

2.4 Conclusions

Our results demonstrate that a large storage capacity for hydrogen by physisorption under the chosen conditions (77 K, 1 bar) is only obtained with adsorbents containing a large volume of micropores with a suitable diameter. Although with zeolite-like materials the chance to find an optimal pore diameter seems realistic, their unavoidably limited micropore volume makes their applicability less likely. With carbonaceous adsorbents (e.g. activated carbons) a more optimistic perspective can be offered. Their intrinsic interaction with hydrogen seems to be slightly stronger than that with oxidic adsorbents, their micropore volume can probably be increased to a value above 1 ml/g, while by increasing the storage pressure or by tuning the pore diameter the storage capacity can be raised up to the targets set for mobile applications. Because of the various sizes and shapes of the micropores in activated carbon it is as yet impossible to comment in details on the optimum pore size and shape. Preliminary results indicate that pores of 0.5-1.0 nm are more beneficial than those of 1.0-2.0 nm. Future research should be focused on a more precise identification of the optimal pore diameter and on the

development of experimental procedures to provide carbon materials with a high volume of these suitable pores.

For our research it is decided that an adsorbent has to be created with a micropore volume as large as possible in order to achieve a high hydrogen storage capacity. We choose a carbon material, because with carbon intrinsically a much higher micropore volume can be attained than with a silica or alumina material. To create micropores the space between subsequent graphene sheets in graphite has to be enlarged. An option to achieve this is via intercalation. A lot of different materials can be intercalated into graphite, for instance alkali metals and metal halides [31,32]. We expect that if we enlarge the d-spacing to 1 nm we may attain enhanced hydrogen storage capacity, based on the results of calculations done by Darkrim *et al*. [33], Rzepka *et al*. [34] and Wang *et al*. [35]. Because we aimed at the development of a material which is suitable as a hydrogen storage device for automotive applications, the material also must be strong. Carbon nanofibers are mechanically strong [16] and may meet the demands for automotive applications. The fibers have the added advantage of short graphite planes, which can diminish diffusion times of the hydrogen into the adsorbent. This will shorten re-fuelling times and problems with hydrogen to fuel cell diffusion inside the car. The results of these intercalation experiments with carbon nanofibers and graphite and the influence on the hydrogen adsorption capacity are described for iron(III)-chloride in chapter 5 and potassium in chapter 6.

Acknowledgements

We wish to acknowledge John Raaymakers for performing the N_2 and H_2 physisorption measurements. We would like to thank Norit for providing the activated carbons. We would like to thank dr. Ben Dekkers for discussions about the BET results.

References

1. G.D. Berry and S.M. Aceves, Energy Fuels 12 (1998) 49.
2. G. Sandrock, Journal of Alloys and Compounds 293-295 (1999) 877.
3. C.C. Ahn, Y. Ye, V. Ratnakumar, C. Witham, R.C. Bowman, Jr. and B. Fultz, Proceedings of the Battery Conference on Applications and Advances 14 (1999) 67.
4. C. Nutzenadel, A. Zuttel, D. Chartouni and L. Schlapbach, Electrochemical and Solid State Letters 2 (1999) 30.
5. F. Darkrim and D. Levesque, The Journal of Physical Chemistry B 104 (2000) 6773.
6. K.A.G. Amankwah and J.A. Schwarz, International Journal on Hydrogen Energy 14 (1989) 437.
7. J. Jagiello, T.J. Bandosz, K. Putyera and J.A. Schwarz, Journal of the American Chemical Society, Raraday Transactions 91 (1995) 2929.
8. J.A. Schwarz, J.S. Noh and R.K. Argawal, United States Patent 4,960,450 (1990).
9. A. Chambers, C. Park, R.T.K. Baker and N.M. Rodriquez, The Journal of Physical Chemistry B 102 (1998) 4253.
10. C. Park, P.E. Anderson, A. Chambers, C.D. Tan, Hidalgo and R. Rodriquez, Journal of Physical Chemistry B. 103 (1999) 10572.
11. A.C. Dillon, K.M. Jones, T.A. Bekkedahl, C.H. Kiang, D.S. Bethune and M.J. Heben, Letters to Nature 386 (1997) 377.
12. M.J. Heben, A.C. Dillon, J.L. Alleman, K.M. Jones and P.A. Parilla, Abstracts 2000 MRS Fall Meeting, p. 17.
13. M. Hirscher, M. Becher, M. Haluska, U. Dettlaff-Weglikowska, A. Quintel, G.S. Duesberg, Y.-M. Choi, P. Downes, M. Hulman, S. Roth, I. Stepanek and P. Bernier, Applied Physics A 72 (2001) 129.
14. Heterogeneous Catalysis for the Synthetic Chemist, R.L. Augustine (Marcel Dekker, Inc., 1996) p. 167.
15. Carbon nanotubes and related structures, P.J.F. Harris (Cambridge University Press, 1999) p. 187.
16. K.P. de Jong and J.W. Geus, Catalysis Reviews- Science and Engineering 42 (2000) 481.
17. Catalysis and Zeolites, J. Weitkamp and L. Puppe (Springer-Verlag Berlin Heidelberg, 1999) p. 288.
18. A.T. Kresge, M.E. Leonowicz, W.J. Roth, J.C. Vartuli and J.S. Beck, Nature 359 (1992) 710.
19. J.S. Beck, J.C. Vartuli, W.J. Roth, M.E. Leonowicz, C.T. Kresge, K.D. Schmitt, C.T.-W. Chu, D.H. Olson, E.W. Sheppard, S.B. McMullen, J.B. Higgins and J.L. Schlenker, Journal of the American Chemical Society 114 (1999) 10834.
20. A.C. Lippens, B.G. Linsen and J.H. De Boer, Journal of Catalysis 3 (1964) 32.
21. P.H. Emmett and S. Brunauer, Journal of the American Chemical Society 59 (1937) 1553.
22. F. Stoeckli, A. Guillot, D. Hugi-Cleary and A.M. Slasli, Carbon 38 (2000) 929.
23. P.I. Ravikovitch, A. Vishnyakov, R. Russo and A.V. Neimark, Langmuir 16 (2000) 2311.
24. T. Ohba, T. Suzuki and K. Kaneko, Carbon 38 (2000) 1879.
25. M. El-Merraoui, M. Aoshima and K. Kaneko, Langmuir 16 (2000) 4300.
26. R.H. Bradley, I. Sutherland and E. Sheng, Journal of Colloid and Interface Science 179 (1996) 561.

27. K. Wang and D.D. Do, Langmuir 13 (1997) 6226.
28. J. Jagiello, T.J. Bandosz and J.A. Schwarz, Langmuir 12 (1996) 2837.
29. M. Jaroniec and J. Choma, Colloids and Surfaces 37 (1989) 183.
30. K. Kaneko, Journal of Membrane Science 96 (1994) 59.
31. H. Selig and L.B. Ebert, Advances in Inorganic Chemistry and Radiochemistry 23 (1980) 281.
32. P.C. Ecklund, NATO ASI Series, Series B 148 (Intercalation Layered Materials) (1986) 309.
33. F. Darkrim and D. Levesque, Journal of Chemical Physics 109 (1998) 4981.
34. M. Rzepka, P. Lamp and M.A. de la Casa-lillo, Journal of Physical Chemistry B 102 (1998) 10894.
35. Q. Wang and J.K. Johnson, The Journal of Physical Chemistry B 103 (1999) 277.

3

Development of a Lab-scale Fluidized Bed Reactor for Carbon Nanofiber Growth

Abstract

Lab scale batches (10-30 grams) of carbon nanofibers can be produced in a fluidized bed carbon nanofiber growth system. Of the tested catalysts the commercially available Engelhard catalyst turns out the most suitable, because it resists the attrition forces in the fluidized bed very well and because its high Ni loading gives high fiber yields. Duration tests with fluidization of the Engelhard catalyst in a N_2 flow proved that it withstands the attrition of the fluidized bed even for a prolonged period of 72 hours without significant desintegration. Carbon fiber granules subjected to the same treatment show attrition and formation of small dust-like fiber granules. Adjusting the gas flow to keep the fluidization profile intact during growth proved unnecessary. We found no indications for structural differences between the fibers grown in the fluidized bed and fibers grown in a fixed bed set-up. The microscopic as well as the macroscopic structure (specific surface area and pore volume) are comparable. The shape of the macroscopic particles resembles the shape of the original catalyst particles.

3.1 Introduction

Carbon nanofibers are a rather new and increasingly important material, which properties, such as high surface area, electrical conductivity and high mechanical strength suggest a wide range of potential uses. They are commercially applied as additive in polymers. The properties of these fibers are much better defined and more reproducible than those of activated carbon and therefore they may replace activated carbon in a number of applications, such as gas adsorbent and catalyst supports [1,2]. Fishbone carbon nanofibers have a BET surface area of 100-200 m^2/g, no micropore volume and an adjustable and large meso- and macropore volume. The absence of micropore volume makes these materials suited as catalyst support for liquid phase reactions.

Carbon nanofibers can be grown by a catalytic process in which a carbon-containing gas is decomposed over a supported metal catalyst. The growth mechanism has been widely studied, especially during the last decade [3-14].

In figure 3.1 the fiber growth mechanism is depicted schematically. During the growth procedure a carbon containing gas, for instance methane, is led through the reactor, where at 550-600°C it partly decomposes to carbon and hydrogen on the surface of the nickel particle (initiation). From literature it is known that carbon either diffuses over the surface of the particle or forms a metal carbide and diffuses through the particle [3-8,10,13,15]. On another surface of the nickel particle, most probably a nickel (111) plane, carbon is precipitated in the form of graphite [9,11,12], segregated from the particle, forming a fiber, while part of the nickel surface remains capable to dissociate CH_4 (propagation). Finally, due to deactivation, the particle stops dissociating methane, the fiber formation stops and the metal particle is encapsulated by carbon (termination). We have determined that the fiber formation period can be maintained up to 16 hours, so the fibers can become very long, up to several hundreds of micrometers. The diameter of the fibers is governed by the diameter of the original nickel particles on the catalyst [15]. From this mechanism it is obvious that the growth catalyst is completely destroyed during growth and the nickel and support material remain in the fiber mass after growth.

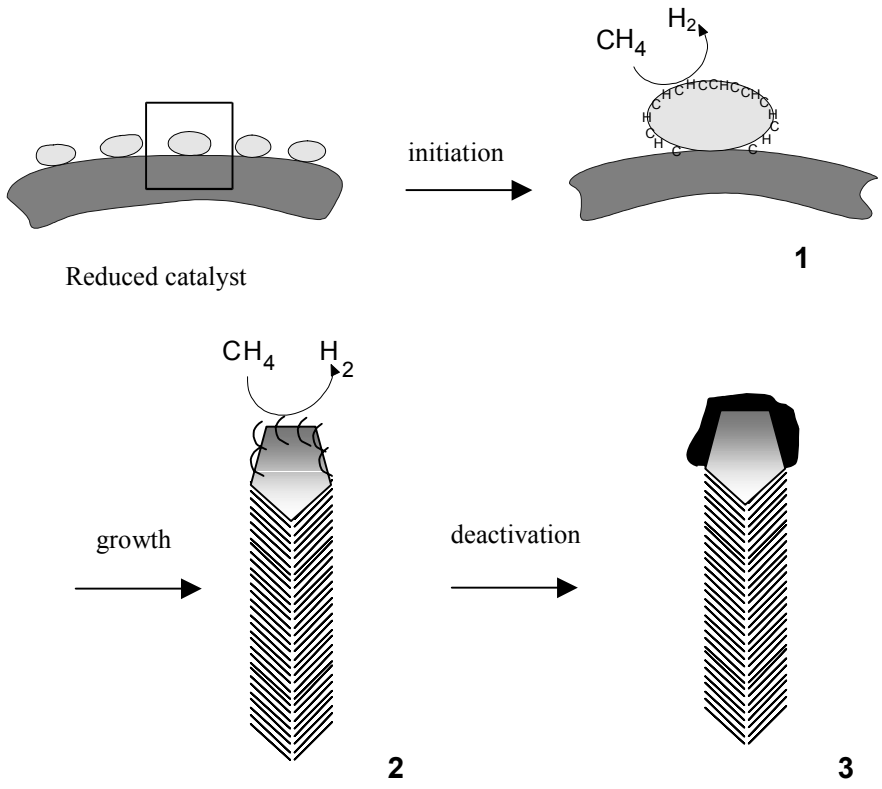

Figure 3.1 Mechanism of carbon nanofiber growth.

We have chosen to use methane as the carbon source, but as carbon containing gas also synthesis gas, a mixture of carbon monoxide and hydrogen, or ethylene can be used for carbon fiber growth. With synthesis gas at 600°C, nickel catalysts will grow parallel carbon nanofibers in stead of fishbone fibers, however we have mostly used methane throughout this work. When we want to use carbon nanofibers for hydrogen physisorption, micropores have to be created (see chapter 2) and fishbone fibers are preferred, because they have potentially accessible micropores between the graphite planes, which is not the case with parallel fibers.

Most of these studies focused on laboratory scale production and applications [2,16,17] and very little is known about mass production of homogeneous batches of fibers. Most of the preparation methods reported are batch-type processes [15,18,19], which are less suitable for scaling up. The reactor is very susceptible to overflowing of the grown fibers into the rest of the set-up or breaking, because of the fiber growth. Also, cleaning of the reactor is quite difficult. The carbon fibers grow in all directions, so they may also grow into the grid. Cleaning of a laboratory reactor is often performed by heating it up in a flame in flowing air to burn off all the carbon, which is not very practical for large scale applications.

Parmon *et al*. from the Boreskov Institute in Russia have published a method to produce hydrogen and filamentous carbon (carbon nanofibers) using a pilot-plant scale (5l) fluidized bed and Ni-based catalysts [20,21]. They use natural gas and produce carbon fibers in the form of granules. To prevent agglomeration of the growing particles they add some inert substrates, such as Al_2O_3, to the fluidized bed.

An attractive feature of fluidized bed reactors is that continuous operation could be within reach. The (semi-)continuous addition of growth catalyst and harvesting of carbon fiber product can be envisaged. For homogeneous fiber growth it is important to diminish temperature variations and gas composition over the growth bed, as these features have a marked influence on the morphology of the fibers. The use of a fluidized bed, with its thorough and constant mixing of catalyst particles and reactants and excellent heat transfer, minimizes these variations.

To make commercial applications viable large scale production at low costs is necessary. The economics of this production on an industrial scale are mainly dictated by the scale of production, the feedstock, the reactor type and type of operation, the yield of carbon nanofibers scaled to the intake of catalytic metal and the growth time and temperature [1]. The results, using a high and low cost scenario, shown in table 3.1 have been reproduced from [1]:

Table 3.1 Results of production-cost estimates for carbon nanofibers.

Case	High-cost	Low-cost
scale of production	low	high
reactor type	fixed-bed	fluidized-bed
type of operation	batch	continuous
yield of fibers (gram C/gram Ni)	50	200
growth time (hour)	2	0.5
cost estimate (US$/kg)	**>50**	**<10**

The high-cost scenario (>50 US$/kg) rules out the use of these materials in large volume applications, such as catalyst support material and gas storage. The low cost case (<10 US$/kg) would mean that such applications are within reach. A fluidized bed reactor is an essential element of such a low-cost production scheme.

In our laboratory, until recently, carbon nanofibers were produced on a 1-2 gram scale in a fixed bed. This scale makes it difficult to perform subsequent experiments or characterisations on samples of the same batch. Therefore, to make a step in the development of a large-scale process, we explored the application of a lab-scale fluidized bed production unit. This also makes it possible to acknowledge possible problems and bottle-necks in the further development of such a system. We have chosen to test two Ni on Al_2O_3 catalysts, because these gave the highest fiber yields in the fixed bed system. It is difficult to remove the Al_2O_3 from the resulting fibers, but this was thought less relevant, because the fibers were to be used for hydrogen storage experiments.

This chapter describes the results of CNF growth in a specially designed batchwise operated fluidized bed reactor from methane as the carbon containing gas and Ni on alumina as the growth catalyst on a yield scale of several tens of grams. Furthermore, the optimization problems and implications for scaling up will be discussed.

3.2 Experimental

3.2.1 Catalysts and reactor

A 20 wt% nickel on alumina catalyst was prepared by deposition-precipitation. The deposition-precipitation procedure was performed at room temperature in a 1.5l double-walled Pyrex vessel equipped with stirrer and baffles to ensure homogeneity of the reaction mixture. As support material, 10 grams of a commercially available γ-Al_2O_3 powder (Alon-C 200 m^2/g, Degussa,) was used. The precipitation was executed by injection of ammonia (0.5 M) into a with HNO_3 acidified suspension (pH=4) of this alumina in an aqueous solution (0.086 M) of nickel nitrate (Acros, 99%) under vigorous stirring. The injection was continued until the pH had reached a level of 8. After filtering, washing and drying in static air at 120°C, the catalyst precursor was calcined at 600°C for two hours in static air.

A commercial 60 wt% nickel on alumina catalyst (extrudates, Engelhard, Ni 3288) was also used without further treatment. The catalyst has a BET surface area of 130 m^2/g. The extrudates are crushed and a sieve fraction of 90-150 μm was used.

To obtain an indication of a suitable growth temperature for the fibers, both catalysts were subjected to a treatment in which 100 mg of catalyst was flowed in a fully automated fixed bed micro-flow system with 20 ml/min of methane and 80 ml/min of Ar while heating up the reactor from 450 to 700°C, with a rate of 10°C/min. The consumption of methane and the production of hydrogen was monitored with a HP5890A gas chromatograph equipped with a 12 ft Porapack Q column.

The fluidized bed reactor (see figure 3.2) consisted of a specially designed cylindrical reactor, with the heating wire applied directly onto the quartz wall of the reactor. The gasses were preheated before entering the reactor as shown in figure 3.2b. With two cylindrical quartz walls the reactor was sufficiently insulated to make temperature control possible. On top of the reactor a cyclone is placed to make sure that no dust, which may result from the attrition in the fluidized bed, ended up in the rest of the set-up.

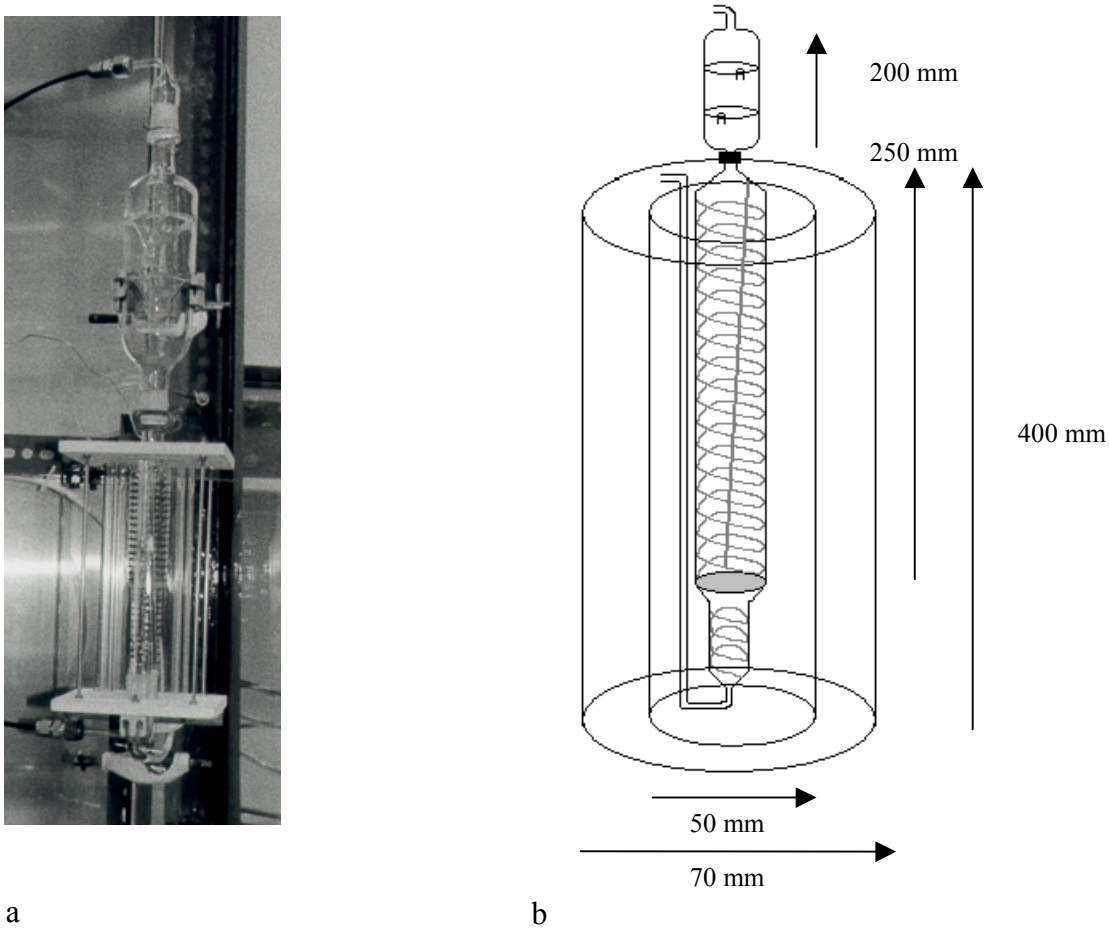

Figure 3.2 Photographic (a) and schematic (b) representation of the fluidized bed reactor and cyclone.

The total length of the reactor was 400 mm, the fluid bed zone was 250 mm. The reactor had a 34 mm external diameter and a 25 mm internal diameter, which shows the thickness of the quartz tube, necessary for placing the heating wire directly on the reactor. The quartz porous grid had been selected using a light microscope to make sure that the holes in the grid were evenly distributed and exhibit approximately the same size over the whole grid. The gas inlet and outlet tubes had an external diameter of 6 mm and a 4 mm internal diameter.

We explored a number of differentially designed reactors:
1. cone shaped
2. cylindrical with two different diameters, bottom small, top wider and
3. cylindrical with constant diameter

Experiments with cone-shaped reactors demonstrated that the fluidization profile in those reactors was not optimal. The 'two diameter cylinder' reactor was designed to suppress fluidization problems caused by the difference in density between catalyst and carbon fibers. The diameter difference did not improve the fluidization performance and the area where the two cylinders are connected does not have much gas flow and turbulence and therefore always shows accumulation of catalyst and fibers. The constant diameter cylindrical reactor turned out to function satisfactory.

After growing a batch of fibers, the reactor walls and the grid were usually covered with small amounts of fibers, which could not be removed manually. The reactor was cleaned by heating it up to 700°C with a gas stream of 20% O_2 in N_2 of 400 ml/min for 30 minutes.

Carbon nanofiber growth experiments were carried out in the fluidized bed reactor. A weighed catalyst sample (usually 0.50-1.00 grams, sieve fraction 90-150 μm) was placed in the fluidized bed and carefully reduced, using the reactor in the fixed bed mode, in a 20 vol% hydrogen in nitrogen flow (total flow 400 ml/min). The sample was heated with 5°C/min up to 650°C and maintained at this temperature for 2 hours. For growth of carbon nanofibers from the nickel catalysts subsequently a stream of methane (minimum 20 vol% and maximum 25 vol%) in nitrogen (total flow between 500 and 1500 ml/min) was passed through the reactor at 570°C, which started the growth of the fibers. The growth process was stopped as soon as the volume of the reactor had been filled completely or when the consumption of methane had stopped.

3.2.2 Characterization

The fibers were examined in a Philips CM-200 FEG electron microscope operated at 200 kV. Samples were prepared by suspending a small amount of CNFs in ethanol under ultrasonic vibration. One drop of the thus prepared suspension was brought onto a holey carbon film on a copper grid and the solvent was evaporated. Scanning Electron Microscopy, performed with a Philips XL30 FEG apparatus, was used to assess the morphology of the samples.

XRD patterns were recorded at room temperature with a Nonius PDS 120 powder diffractometer system equipped with a position-sensitive detector with a 2θ range of 120°. The radiation used was Co $K\alpha_1$ (λ=1.78897 Å). Mean particle diameters were calculated using the Scherrer equation, using the widths of the peak at half height.

Texture analysis was performed with N_2 physisorption at 77 K, up to a pressure of 1 bar. From the N_2 hysisorption data, obtained with a Micromeritics ASAP 2400 apparatus, the BET surface area, total mesopore volume and micropore volume were derived. Prior to the physisorption measurements, the fibers were evacuated in situ at 300°C.

3.3 Results and discussion

3.3.1 Growth conditions and fluidization

To obtain an indication of a suitable growth temperature for the fibers, both catalysts were subjected to a treatment in which 100 mg of catalyst was flowed in a fully automated fixed bed micro-flow system with 100 ml/min of methane while heating up from 450 to 700°C, with a rate of 10°C/min. The consumption of methane and the production of hydrogen was monitored with a gas chromatograph.

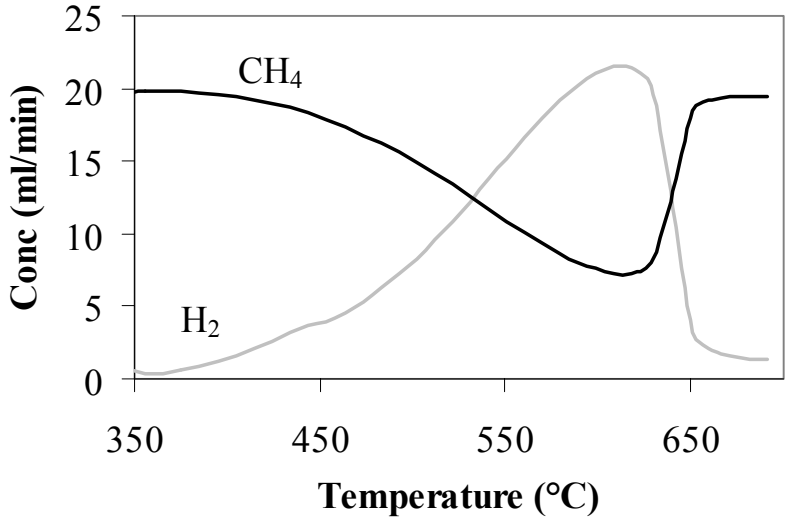

Figure 3.3 Consumption of methane and production of hydrogen versus temperature. Catalyst 60 wt% Ni on Al_2O_3, Engelhard. Gas flow 100 ml/min CH_4.

The peak in the consumption of methane measured with the Engelhard catalyst as well as with the 20 wt% Ni on Al_2O_3 catalyst turned out to occur between 550 and 625°C. Therefore, most growth experiments executed in the fluidized bed were performed in this range, more precisely at 570°C. Yields obtained at 550°C and at 625°C were significantly lower with the same amount of catalyst and maintaining the fluidization profile was more difficult. It was concluded that 570°C is an optimal growth temperature for nickel catalysts in this fluidized bed under the prevailing conditions.

Carbon fibers of the fishbone type were successfully grown in the fluid bed reactor from the Engelhard nickel catalyst with methane at 570°C after the described temperature-programmed reduction in H_2. On average, from 0.5 gram of catalyst after 10 hours of growth 13.5 gram fibers were obtained. The reduction was performed in fixed bed mode of operation, with a total flow of 400 ml/min. Reduction in a fluidized bed mode almost always led to problems with the fluidization profile. Probably, these problems were caused by the presence of reduced nickel at the exterior of the catalyst particles. Reduced nickel sinters very easily and because of the high weight percentage Ni of this catalyst, most of the outside of the catalyst consisted

of Ni, which may stick together when reduced. It is also possible that the water which is formed during reduction may cause the catalyst particles to stick together during the reduction. It proved impossible to restore proper fluidization conditions after the reduction. If the reduction was performed in the fixed bed mode this problem did not arise.

We observed that it was hardly necessary to adjust the gas flow in the reactor during fiber growth to maintain a good fluidization profile. This was unexpected, because it was anticipated that growth of the fibers would cause a weight and density change of these particles, which could necessitate gradual adjustment of the gas flows to keep the fluidization profile intact. Obviously the change of the parameters determining fluidization compensated each other.

The other catalyst, a HDP 20 wt% on Al_2O_3, was also successful in growing fibers, but displayed poor fluidization properties. The growing fiber particles usually caked together within minutes to one hour after starting the growth. Experiments showed that the fluidization profile improved and remained more stable when the reactor was kept in vibration during the growth. In this way it was ensured that the particles kept an even distribution over the bed and no channeling occurred. This procedure worked well enough to make sure that the 20 wt% Ni on Al_2O_3 catalyst remained fluidized during the growth.

It was found that the used, bare alumina support as such was not able to resist the attritive forces of the fluidized bed. The particles break down to dust-like particles much smaller than that of the desired sieve fraction and therefore the fluidization profile becomes erratic and the whole bed cakes together. The 20 wt% Ni on Al_2O_3 catalyst would cake together within 2 hours after starting the growth without vibration of the bed. Therefore, to enable successful use of a fiber growth catalyst in the fluidized bed it is necessary to ensure that the catalyst itself is resistant towards attrition.

3.3.2 Particle size, shape and strength

Because of its superb fluidization properties and high carbon nanofiber yields, all fishbone fibers used in this thesis were grown from the Engelhard catalyst in the fluidized bed. This catalyst grows 13.5 gram of fibers from 0.5 gram of catalyst in 10 hours. This high yield can be explained partially by the high nickel loading, but when the amounts of fibers produced per gram of Ni of both catalysts are compared as shown in figure 3.4, it is obvious that the Engelhard catalyst is a better fiber growth catalyst in the fluidized bed.

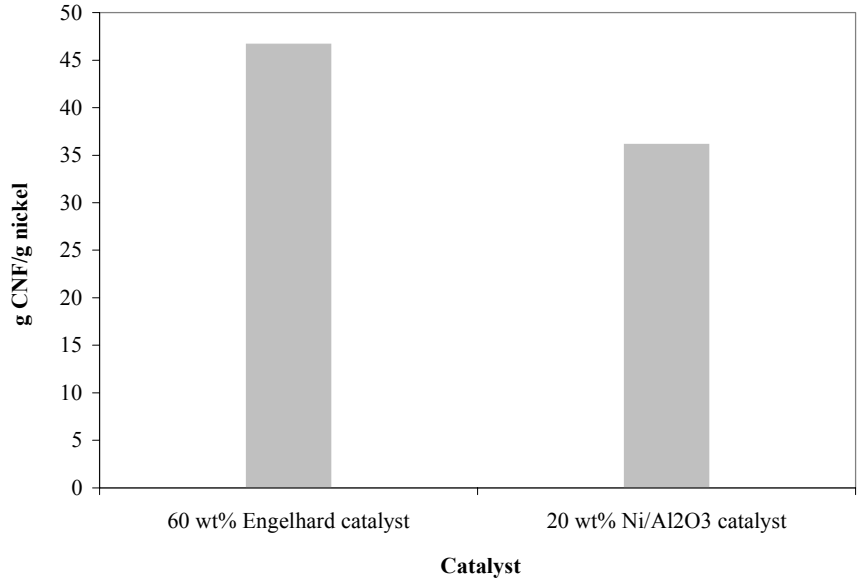

Figure 3.4 Comparison of fiber yields (g CNF/g nickel) from different catalyst in the fluidized bed.

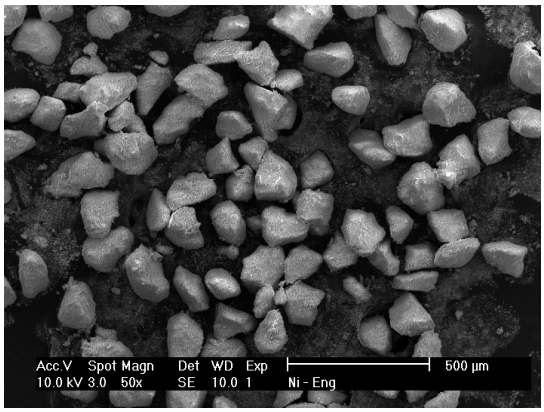

Figure 3.5 SEM image showing the size and shape of the 60 wt% Ni on Al_2O_3 catalyst particles before fluidization.

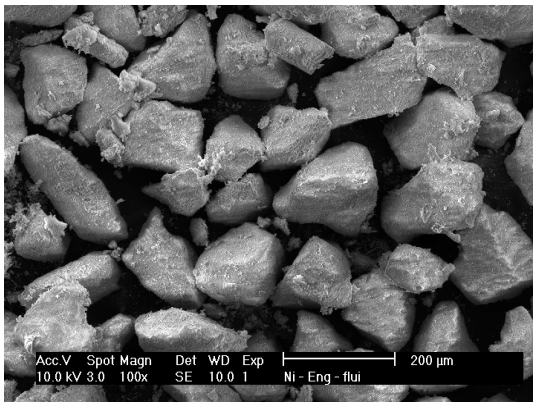

Figure 3.6 Size and shape of the catalyst particles after fluidization at 570°C in nitrogen for 72 hours.

In the SEM image of the original Ni on Al_2O_3 catalyst (figure 3.5) it is clearly visible that the particles were within the range of the sieve fraction, i.e. between 90 and 150 µm. Some particles have sharp edges and corners, while others are more rounded off. If the catalyst was subjected to fluidization in nitrogen for 72 hours at 570°C it is observed (figure 3.6) that the particles were still mainly sized between 90 and 150 µm. There are some smaller particles visible also and the cyclone contained only a small amount of small, irregularly shaped catalyst particles (figure 3.7). Therefore we conclude that the catalyst quite well withstands the attrition forces of the fluidized bed for a prolonged period of time.

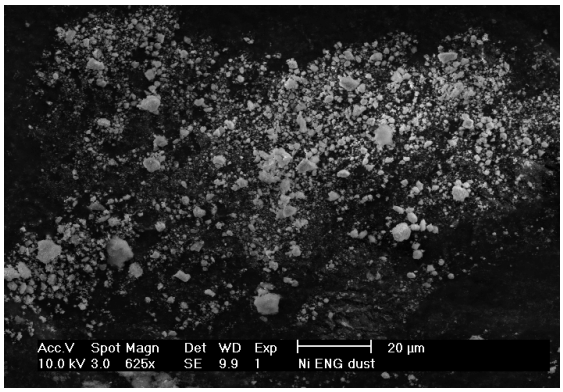

Figure 3.7 Irregularly shaped catalyst bodies, collected from the cyclone after fluidization in nitrogen at 570°C for 72 hours.

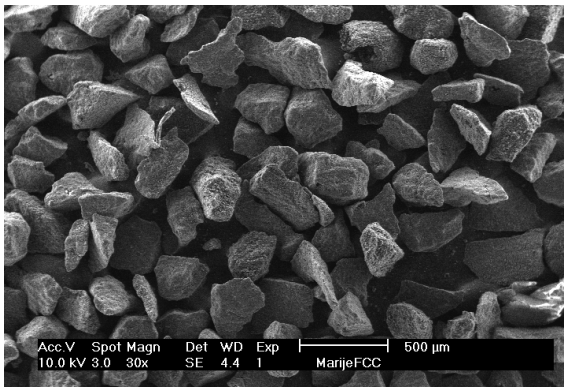

Figure 3.8 SEM image showing the specific rectangular shape of resulting granules of fishbone fibers grown in a fluidized bed from Ni 3288, 60 wt% Ni on Al_2O_3, from CH_4 at 570°C.

SEM analyses showed that the grown fibers form rectangularly shaped granules with sharp corners, like the original catalyst particles (see figure 3.8), with most of the granules sized between 250 and 500 µm. This means a size increase with a factor 3 to 4. This is consistent with results described by Teunissen [22]. She impregnated pre-shaped alumina spheres of a size of 1000 µm with a nickel nitrate solution. After calcination and reduction, methane was passed over during 10 hours at 570°C. Replication of the original catalyst was observed. The original catalyst particles had enlarged 3-4 times, while remaining the same, spherical shape.

When carbon nanofiber granules (see figure 3.8) were subjected to the same treatment (fluidization in N_2 for 72 hours at 570°C) we obtained granules of the same size and shape (see figure 3.9), but there are also smaller particles visible and some of the granules expose a rounded- off form and the surfaces look smoothed. In addition the dust-collector contained a lot of small, irregularly shaped carbon fiber particles (figure 3.10). Above observations demonstrate that the carbon fiber granules can withstand the fluidized bed only for a limited period of time. This may also limit the period of growth to obtain larger, mechanically intact particles.

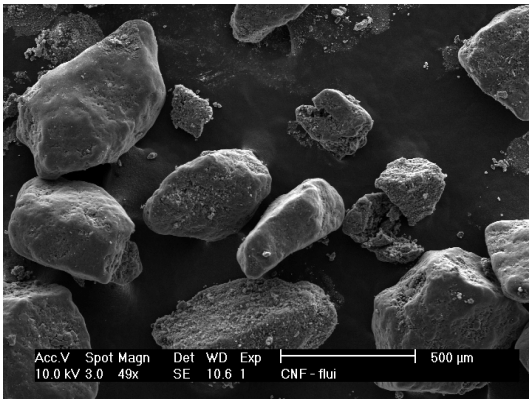

Figure 3.9 Size and shape of the CNF granules after fluidization at 570°C in nitrogen for 72 hours.

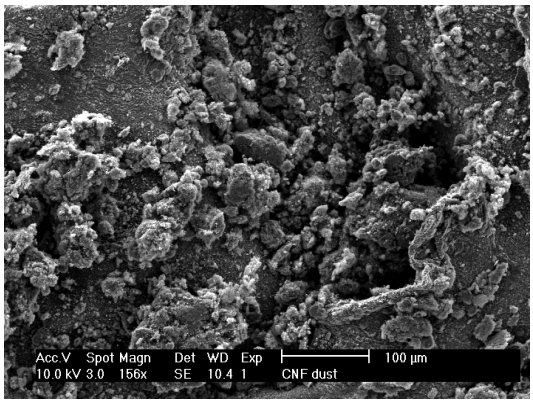

Figure 3.10 Irregularly shaped fiber granules, collected from the dust collector after fluidization in nitrogen at 570°C for 72 hours.

3.3.3 Structure of the fibers

From SEM and TEM results, as shown in figures 3.11 and 13.2, it is also obvious that the diameters of the fibers grown from the Engelhard catalyst vary between 20 and 90 nm, with most of the fibers having diameters between 40 and 70 nm.

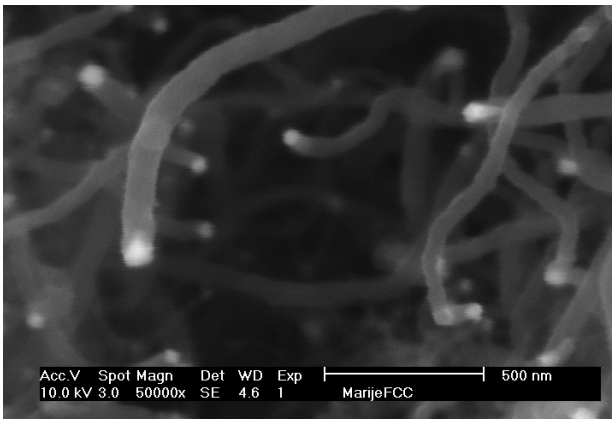

Figure 3.11 SEM picture of carbon nanofibers grown from Engelhard Ni catalyst.

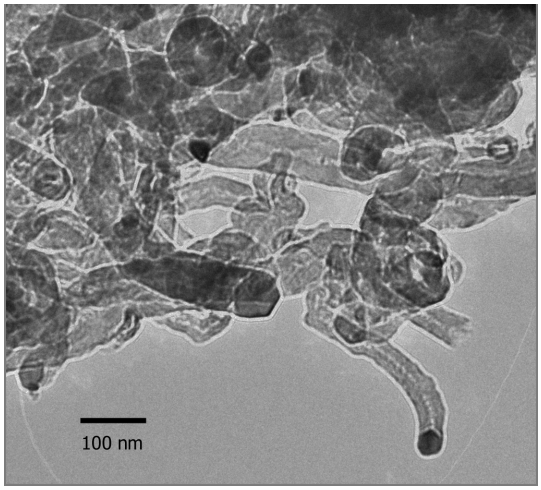

Figure 3.12 TEM picture of carbon nanofibers grown from Engelhard Ni catalyst.

In figure 3.13 an X-ray diffractogram of the Engelhard catalyst is shown. The diameters (in nm) of the particles, as determined from the half height of the respective peaks, are shown.

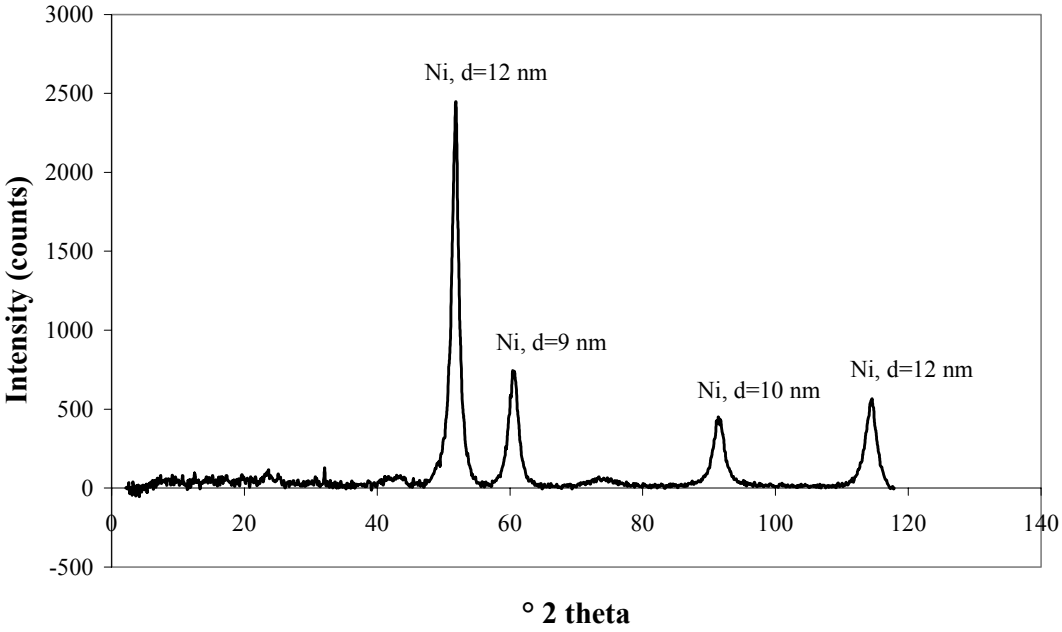

Figure 3.13 X-Ray diffractogram of the 60 wt% Ni on Al_2O_3 catalyst after reduction at 700°C for 2 hours with the diameters of the Ni particles as determined by the Scherrer equation.

When the reduced catalyst is studied with XRD only Ni-peaks are present. The mean diameter of the Ni particles after reduction lies between 9 and 12 nm. This is much smaller than the diameter of the Ni particles on the tips of the fibers as determined by TEM analysis at high resolution, which showed fiber and Ni particle diameters mainly between 20 and 90 nm, with most fibers and Ni particles between 40 and 70 nm. It is therefore postulated that prior to growth of the fibers, the Ni particles coalesce and form bigger particles.

When the reduced Engelhard catalyst is exposed to a flow of 25% CH_4 in N_2 at 570°C for 30 minutes, only some fibers have been grown. In figure 3.14 an XRD pattern of a sample of this catalyst is shown. Because only a limited amount of fiber is present, some of the Ni peaks are not overruled by the graphite peaks. From these peaks the mean Ni particle diameter was calculated to be 15-16 nm, which is significantly larger than that of the original particles. Probably, during the first stages of the fiber growth under influence of the methane dissociation and/or Ni carbide formation smaller particles combine together before fiber growth. The fact that the Ni particles after initial growth are still considerably smaller than the mean diameter of the fibers after prolonged growth cannot be explained as yet. From the SEM and TEM images (see figures 3.11 and 3.12) it appears, however, that many Ni crystallites of 20-90 nm diameter are present in the final carbon fibers.

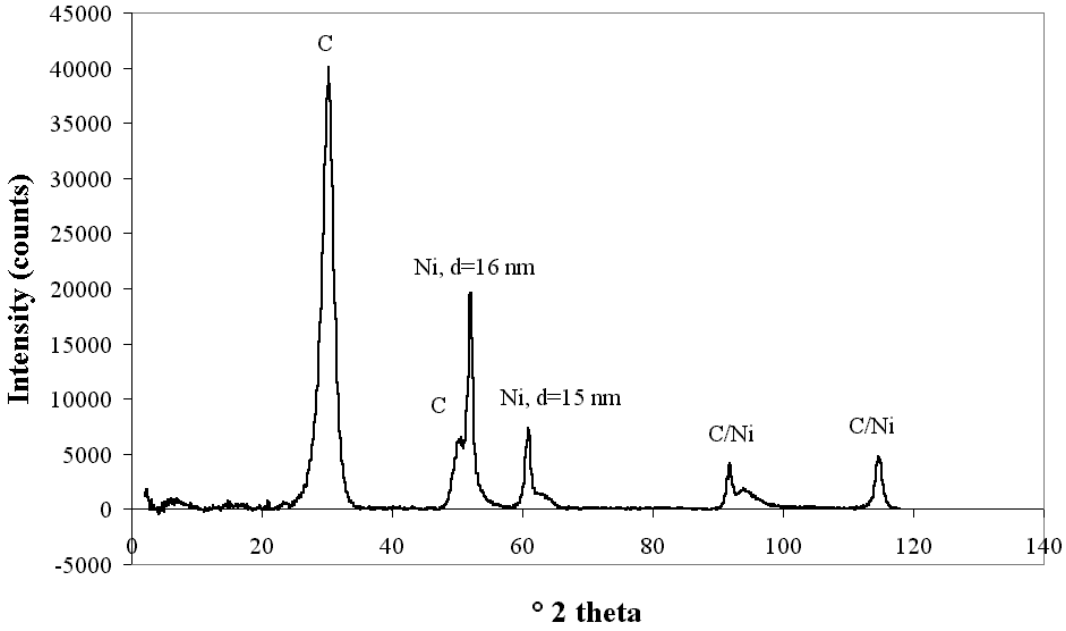

Figure 3.14 X-Ray diffractogram of the reduced 60 wt% Ni on Al_2O_3 catalyst, after 30 minutes CH_4 at 570°C with the diameters from the Ni particles as determined from the Sherrer equation.

TEM analysis at very large magnifications showed that the resulting fibers are indeed of the fishbone type. This is clearly visible in figure 3.15.

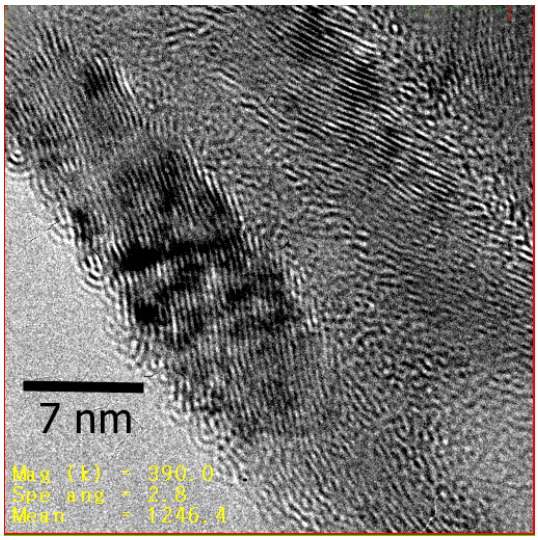

Figure 3.15 TEM image of a fishbone CNF, grown in the fluidized bed from the Ni Engelhard catalyst with CH_4 at 570°C.

The fishbone fibers as grown have a specific surface area of 100 m^2/g. XRD analysis of these materials as shown in figure 3.16 shows a large graphite peak at the d=0.340 nm 2θ=30°, which is slightly larger than that of pure graphite, where d=0.335 nm. Other peaks that are present can be attributed to graphite, nickel and alumina. The slightly enlarged d-spacing can be explained by the turbostratic nature of this material. The graphite planes of the fibers are not completely straight. This subject is dealt with in more detail in chapter 4.

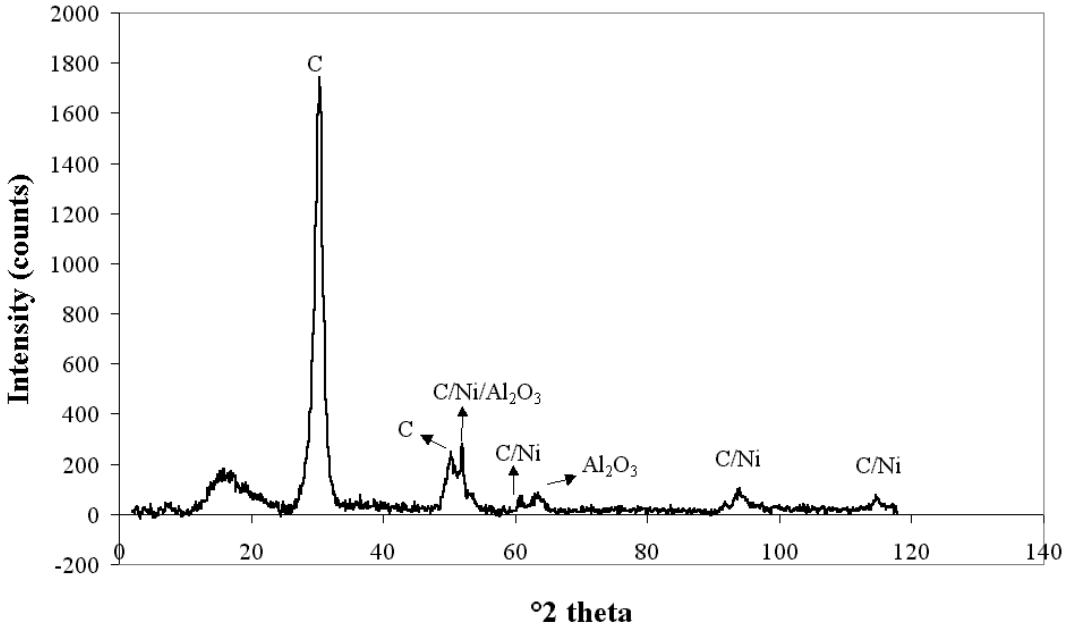

Figure 3.16 X-ray diffractogram of fishbone nanofibers grown in the fluidized bed from methane at 570°C.

In view of an interest in low production costs a few observations are discussed below. Because it is impossible to achieve a high conversion per pass of methane into carbon nanofibers, a once-through set-up is impractical and uneconomical. Therefore, a pilot-plant should be designed with the possibility to recycle the methane feed, following separation of hydrogen produced. It is possible to separate hydrogen and methane at elevated temperatures using metallic, for instance palladium membranes and to re-introduce the methane into the reactor. The fluidized bed for carbon fiber growth proposed by Parmon *et al*. is based on this principle [23-25].

The growth time is determined by the time the catalyst is actively dissociating methane and precipitating graphite in the form of fibers. For optimal growth rate the fibers should be removed from the fluidized bed when the metal particles at the tips start losing their highest activity. We observed that the Engelhard catalyst shows the highest activity during the first 4 hours after starting the growth. The length of this activity period differs per type of catalyst, type and concentration of the feed and depends on the temperature. In our laboratory we prepared several catalysts which show methane dissociating activity for at least 15 hours. It is also imaginable that catalysts can be used with a lower lifetime but with a higher activity.

With such catalysts, a shorter cycle time of fiber harvesting and adding new catalyst and higher yields should be possible. The rate determining step in the growth process is the diffusion of carbon through the nickel particle. The diffusion rate should therefore be enlarged. This might be done by alloying nickel with other metals. This has already been done to influence the morphology and the amounts of fibers grown [10,23,26-37]. With such a catalyst residence time can be limited to avoid attrition.

Currently 50 g CNF can be grown per gram Ni, using the Engelhard catalyst. However, Parmon *et al*. [21] have reported a value of 200 g CNF/g Ni, so it should be possible to further increase the amount of fibers grown per g of catalyst, e.g. by developing a catalyst with an even higher nickel loading. Of course the catalyst must be capable to withstand the attrition forces of the fluidized bed. This might be possible with the high-percentage Ni/Al_2O_3 catalysts, reported by Avdeeva *et al*. [23-25,38].

At this stage the process with respect to the catalyst is batch-wise. We have not explored the possibility of continuous operation. Very important is our observation that during the lab-scale fluid bed process the growth experiments have not shown the need for drastic adjusting of the gas flows to keep the fluidization profile intact. This means that apparently no difference in density or fluidization behavior of the particles develops high enough to separate the active and the deactivated particles.

3.4 Conclusions

The fluidized bed carbon nanofiber growth system is very suitable to produce lab scale batches (10-30 grams) of carbon nanofibers. Our experiments demonstrate that the commercially available Engelhard catalyst, when compared to a HDP 20 wt% Ni on Al_2O_3 catalyst, is the most suitable catalyst for use in a fluidized bed. This is because this catalyst resists the attrition forces in the fluidized bed very well and because the high Ni loading of the catalyst gives high fiber yields. A disadvantage of this catalyst is the wide distribution range of the fiber diameters, i.e. between 20 and 90 nm, with most fibers between 40 and 70 nm. This is probably caused by the Ni particle size distribution. Therefore, if a very narrow diameter distribution of the fibers is desired, this catalyst is less suitable.

From XRD experiments we found that after reduction for 2 hours at 700°C Ni particles are present with a mean diameter between 9 and 12 nm. After 30 minutes of fiber growth, the mean diameter had enlarged to 15-16 nm for the Ni particles. This shows that during the first stage of the growth the Ni particles enlarge under influence of the growth process, e.g. carbide formation and/or methane dissocation. Nevertheless, the mean diameter of the observed Ni particles remains significantly smaller than the average fiber diameter (between 20 and 90 nm) and with this that of the Ni particles present in the fibers, implying that further Ni sintering occurs prior to growth.

The best results we obtained, when the catalyst is reduced in the fixed bed mode before fiber growth in the fluidized bed. If the reduction is performed in the fluidized bed, the catalyst particles cake together, possibly due to sticking behavior of the reduced nickel at the particles surfaces or under influence of water resulting from the reduction process. Adjusting the gas flow to keep the fluidization profile intact during growth proved unnecessary. Tests with fluidization of the Engelhard catalyst for 72 hours in N_2 proved that it withstands the attrition of the fluidized bed for a prolonged period of time without significant desintegration. Carbon fiber granules subjected to the same treatment show attrition and small dust-like fiber granules.

We have found no indications for structural differences between the fibers grown in the fluidized bed and fibers grown in our fixed bed set-up. The microscopic structure as well as the macroscopic structure (specific surface area and pore volume) are comparable. The shape of the macroscopic particles resembles the shape of the original catalyst particles.

To bring down the production costs of carbon nanofibers to 10 US$/kg or less a number of important improvements have to be achieved with respect to the presented lab-scale set-up. In the first place a process should be developed that comprises recycling of the methane. It should also be pursued to develop a catalyst with a very high activity for fiber growth, which would make a short cycle time of adding new catalyst and harvesting grown fibers in a continuous process possible. Also the amount of fibers grown per gram Ni should be enhanced. Considerable engineering challenges remain to develop a full-scale commercial process for the catalytic growth of carbon nanofibers.

Acknowledgements

The development of the fluidized bed reactor for carbon nanofiber growth was executed by Micha Müller within the framework of his graduate research project. We wish to acknowledge John Raaymakers for performing the N_2 physisorption measurements. We thank Marjan Versluijs for performing the SEM measurements.

References

1. K.P. de Jong and J.W. Geus, Catalysis Reviews- Science and Engineering 42 (2000) 481.
2. N.M. Rodriquez, Journal of Materials Research 8 (1993) 3233.
3. R.T.K. Baker and P.S. Harris, Chemistry and Physics of Carbon 14 (1978) 83.
4. J.L. Figueirido, C.A. Bernardo, R.T.K. Baker and K.J. Huttinger, Carbon fibers, filaments and composites, Vol. 177 (Kluwer, Academic Publishers, Netherlands, 1990).
5. R.T.K. Baker, M.A. Barber, P.S. Harris, F.S. Feates and R.J. Waite, Journal of Catalysis 26 (1972) 51.
6. R.T.K. Baker and R.J. Waite, Journal of Catalysis 37 (1975) 101.
7. A. Oberlin and M. Endo, Journal of Catalysis 32 (1976) 335.
8. J. Rostrup-Nielsen and D.L. Trimm, Journal of Catalysis 48 (1977) 155.
9. M. Audier, A. Oberlin and M. Coulon, Journal of Crystal Growth 55 (1981) 549.
10. E. Boellaard, P.K. de Bokx, A.J.H.M. Kock and J.W. Geus, Journal of Catalysis 96 (1985) 481.
11. I. Alstrup, Journal of Catalysis 109 (1988) 52.
12. R.T. Yang and J.P. Chen, Journal of Catalysis 115 (1989) 52.
13. J.W. Snoeck, G.F. Froment and M. Fowlest, Journal of Catalysis 169 (1997) 240.
14. H.P. Boehm, Carbon 11 (1973) 583.
15. M.S. Hoogenraad, Ph.D. Thesis, Utrecht University (1995).
16. W.T. Owens, N.M. Rodriquez and R.T.K. Baker, The Journal of Physical Chemistry 96 (1992) 5049.
17. M. Terrones, N. Grobert, J. Olivares, J.P. Zhang, H. Terrones, K. Kordatos, W.K. Hsu, J.P. Hare, P.D. Townsend, K. Prassides, A.K. Cheetham, H.W. Kroto and R.M. Walton, Letters to Nature 388 (1997) 52.
18. M. Endo, R. Saito, M.S. Dresselhaus and G. Dresselhaus, Carbon nanotubes: preparation and properties, (CRC Press, Boca Raton, 1997) p. 96.
19. C. Menini, C. Park, R. Brydson and M.A. Keane, The Journal of Physical Chemistry B 104 (2000) 4281.
20. G.G. Kuvshinov, Yu.I. Mogilnykh, D.G. Kuvshinov, S.G. Zavarukhin and V.N. Parmon, Hydrogen energy progress XI/Eleventh world hydrogen energy conference, Vol. 1 (Stuttgart, 1996) 655.
21. V.N. Parmon, G.G. Kuvshinov and V.A. Sobyanin, Hydrogen energy progress XI/Eleventh world hydrogen energy conference Vol. 3, (Stuttgart, 1996) 2439.
22. W. Teunissen, Ph.D. Thesis, Utrecht University (2000).
23. O.V. Goncharova, L.B. Avdeeva, V.B. Fenelonov, L.M. Plyasova, V.V. Malakhov, G.S. Litvak and A.A. Vlasov, Kinetics and Catalysis 36 (1995) 268.
24. Sh.K. Shaikhutdinov, L.B. Avdeeva and V.I. Zaikoskii, Applied Catalysis A: General 148 (1996) 123.
25. S.K. Shaikhutdinov, L.B. Avdeeva, O.V. Goncharova, D.I. Kochubey, B.N. Novgorodov and L.M. Plyasova, Applied Catalysis A: General 126 (1995) 125.
26. S. Motojima, S. Hasegawa, S. Kagiya, M. Momiyama, M. Kawaguchi and H. Iwanaga, Applied Physics Letters 62 (1993) 2322.
27. P.C.M. van Stiphout, D.E. Stobbe, F.Th. Scheur and J.W. Geus, Applied Catalysis 40 (1988) 219.
28. M.T. Tavares, C.A. Bernardo, I. Alstrup and J.R. Rostrup-Nielsn, Journal of Catalysis 100 (1986) 545.

29. Y. Nishiyama and Y. Tamai, Journal of Catalysis 45 (1976) 1.
30. C.A. Bernardo, I. Alstrup and J.R. Rostrup-Nielsen, Journal of Catalysis 96 (1985) 517.
31. P.K. de Bokx, A.J.H.M. Kock, E. Boellaard, W. Klop and J.W. Geus, Journal of Catalysis 96 (1985) 454.
32. A. Chambers and R.T.K. Baker, Journal of Physical Chemistry B 101 (1997) 1621.
33. M.S. Kim, N.M. Rodriquez and R.T.K. Baker, Journal of Catalysis 143 (1993) 449.
34. N. Krishnankutty, C. Park, N.M. Rodriquez and R.T.K. Baker, Catalysis Today 37 (1997) 295.
35. W.T. Owens, N.M. Rodriquez and R.T.K. Baker, Catalysis Today 21 (1994) 3.
36. C. Park, N.M. Rodriquez and R.T.K. Baker, Journal of Catalysis 169 (1997) 212.
37. N.M. Rodriquez, M.S. Kim and R.T.K. Baker, Journal of Catalysis 144 (1993) 93.
38. L.B. Avdeeva, O.V. Goncharova, D.I. Kochubey, V.I. Zaikoskii, L.M. Plyasova, B.N. Novgorodov and Sh.K. Shaikhutdinov, Applied Catalysis A: General 141 (1996) 117.

4

A Detailed Structural Study of the Effects of High-Temperature Treatment of Carbon Nanofibers

Abstract

Carbon nanofibers, both fishbone and parallel where subjected to heat treatment at 1600°C (fishbone) and 2000°C (fishbone and parallel). The fibers were studied with N_2 physisorption, XRD, TGA, IR and HR-TEM. Attention was paid to the occurrence of defects inside and at the surface of the fibers. In all types of fibers the graphite planes were shown to be bending and possess defects, both before and after heat treatment. The heat treatments had effect on the aromatic character of the fibers. With IR it is shown that non-aromatic groups disappear from the surface and with TGA the onset of oxidation is shown to shift to higher temperatures. Most importantly, according to HR-TEM the extent of graphitization at the surface of the fibers increases upon heat treatment. Single graphite planes protruding from the fiber surface are observed. In line with this observation the reactivity of the carbon nanofibers with respect to oxidation decreases significantly after heat treatment. The bulk of the fibers does not seem to be affected much, though.

4.1 Introduction

Carbon nanofibers have been studied for more than a century. For most of this time they have been considered a nuisance, because of their ability to completely destroy a catalyst, both on microscopic and a macroscopic scale and to attack and rupture reactor walls [1]. Most of the research in the first years was therefore aimed at prevention of nanofiber growth and there have been excellent results in this area.

Since two decades these fibers are also studied for use as additives in polymers and also as catalyst support material [2-4]. Since Gadd *et al* [5] reported in 1997 that it is possible to trap argon in carbon nanotubes by hot isostatically pressing for 48 hours at 650°C under an argon pressure of 170 MPa much interest has arisen in these materials as possible hydrogen storage materials. Baker and Rodriquez [6,7] claimed very high adsorption capacities of fishbone (herringbone) nanofibers at 298 K and 120 MPa hydrogen. So far no one has been able to reproduce these results [8]. Dillon claims to adsorb up to 7 wt% of hydrogen in very pure single walled carbon nanotubes at room temperatures and ambient pressure (300 torr). Because of further research these results are debatable [8-11].

It is noteworthy that in most of these reports there are TEM pictures of the carbon nanofibers, mostly as proof of their specific structure. But there are no known detailed studies of these materials and especially not of their structural defects and deformities. Mostly these materials are presented as graphite-like materials, but a closer study of the TEM pictures reveals that there are in fact significant differences compared to graphite. Most obvious is the striking amount of defects, dents and kinks in the graphite layers of these materials. The high amount of defects can cause problems and differences in behavior of these materials compared to graphite. Therefore, we have also studied a method to graphitise these materials using heat treatment at 2000°C. It has been reported that vapor-grown carbon nanofibers can be intercalated with metal chlorides after being heat treated for 30 minutes at 3000°C [12]. Chieu *et al*. [13] studied carbon nanofibers with Raman spectroscopy after heat treatments ranging from 1200°C to 3000°C. From this work they concluded that up to 2000°C the fibers graphitised in plane, but not 3-dimensional. Heat treatment at 3000°C for 30 minutes rearranged the fibers such that there structure was very similar to crystallic graphite. Bougrine *et al*. [14] studied single walled carbon nanotubes heat treated for 30 minutes between 1400°C and 2400°C with TEM and Krypton adsorption. Treatment up to 1600°C resulted in the removal of impurities, namely metal particles from the synthesis, which melt at that temperature. Thermal treatment at 2000°C and 2400°C produced changes in the nanotube morphology. The single walled nanotubes changed into multi walled nanotubes, consisting of 2 to 20 graphite layers. At 2000°C they also observed the amorphous carbon, present in the sample before high temperature treatment, becoming ordered, with an interlayer distance of 0.34 nm, as determined by electron diffraction.

To see if high temperatures bring about changes of the graphitic nature of the fibers, they are treated at 1600°C and 2000°C. Subsequently they are studied with SEM, TEM, TGA, XRD, IR and nitrogen physisorption. Here we report the results of these studies on the structure, morphology, d-spacing and defects of these interesting materials.

4.2 Experimental

Fishbone carbon nanofibers (CNF-Eng) were produced in the fluidized bed (see chapter 3) at 570°C using catalytic decomposition of methane on the 60 wt% commercial catalyst from Engelhard (Ni 3288). To remove Ni (2.3 wt% after growth) and Al_2O_3 (1.5 wt% after growth), 10 grams as synthesized fibers were refluxed for 2 hours in 100 ml concentrated HNO_3 to remove both Al_2O_3 and exposed Ni particles. Subsequently the fibers were washed with water and dried for 16 hours at 120°C.

This pre-treatment leads to oxidation of the surface of the fibers, creating for instance carboxyl and carbonyl groups [15]. To prevent interference of these oxygen-containing groups on the chemistry at high temperatures they were largely removed by heating the samples at 800°C for 4 hours in a nitrogen flow.

Parallel fibers (CNF-Hyp) were obtained from Hyperion. These are commercially available parallel carbon nanofibers which are grown from Fe. They were not subjected to any treatments to remove impurities (probably Fe and Al_2O_3).

Carbon nanofibers of the parallel type were produced by catalytic decomposition of syngas, a mixture of CO and H_2, on Ni/Al_2O_3 catalysts. The Ni on Al_2O_3 catalyst with 20 wt% Ni metal loading was synthesized by the deposition-precipitation technique. Alumina (Alon-C, Degussa) was suspended in an acidified (pH=3) aqueous solution (0.086 M) of nickel nitrate (Across, 99%). Diluted ammonia (0.5 M) was added in two hours at room temperature under vigorous stirring until the pH had reached a value of 8.5. After overnight stirring, the suspension was filtered, washed, and dried at 120°C. Finally, the catalyst was calcined at 600°C in stagnant air for three hours. Parallel carbon nanofibers were synthesized in small quantities in a fully automated micro-flow system. For the growth of parallel carbon nanofibers, 100 mg of the 20 wt% Ni/Al_2O_3 catalyst was reduced at 700°C in 20% H_2/Ar (flow rate 100 ml/min) in a micro-flow reactor for two hours. After reduction, the temperature was decreased to 600°C and synthesis gas (20% CO and 7% H_2 in Ar, flow rate 100 ml/min) was passed through the reactor during 10 hours. After reaction, about 0.5 g of parallel fibers were collected [15].

The fibers were heat treated at 1600 and 2000°C. All the samples were kept at the desired temperature for 30 minutes in an Ar atmosphere. The samples were brought into the oven in a tungsten cup, which had been pre-treated at 2000°C to remove possible volatile impurities. The sample was heated up by moving it slowly into the hot zone by means of a tungsten

cable. It remained in the hot zone for 30 minutes and was cooled down by slowly moving it out of the oven. During the whole procedure the sample was exposed to an argon flow. During the transportation into and out of the oven of the more fluffy parallel fibers, CNF-Hyp and CNF-Par, the flow was decreased, because otherwise fibers were blown out of the cup.

Transmission electron microscopy was performed using a Philips CM30UT electron microscope with a field emission gun as the source of electrons operated at 300 kV. Samples were mounted on a carbon polymer supported on a copper grid (Quantifoil®) by placing a few droplets of as suspension of ground sample in n-hexane on the grid, followed by drying at ambient conditions. Samples were also examined in a Philips CM-200 FEG electron microscope operated at 200 kV. With the latter microscope samples were prepared by suspending the solid in ethanol under ultrasonic vibration. One drop of the thus prepared suspension was brought onto a holey carbon film on a copper grid. Scanning Electron Microscopy was performed with a Philips XL30 FEG apparatus.

XRD patterns were recorded at room temperature with a Nonius PDS 120 powder diffractometer system equipped with a position-sensitive detector with a 2θ range of 120°. The radiation used was Co $K\alpha_1$ (λ=1.78897 Å).

From the N_2 physisorption data, obtained with a Micromeritics ASAP 2400 apparatus at 77 K, the BET surface area, total pore volume and micropore volume were derived. Prior to the physisorption measurements, the fibers were evacuated at 300°C.

TGA analyses were carried out on a Netzsch STA-429 thermobalance. The gasses evolved during analysis were monitored by a Fisons Thermolab quadropole mass spectrometer, using a capillary situated directly above the sample cup. Samples of 20-100 mg were heated in 60 ml/min Ar at a rate of 300°C/h to 850°C. For oxidation experiments samples of 20-100 mg were heated in a 20% O_2 in Ar stream, with a total flow of 60 ml/min.

Transmission infrared spectra were recorded with a Perkin Elmer 2000 spectrometer equipped with an air dryer for removal of water vapor and carbon dioxide. One hundred scans were co-added at a resolution of 8 cm^{-1} and a boxcar apodisation. Samples were prepared by thoroughly mixing a small amount of ground nanofibers with pre-dried KBr. Tablets were pressed at 8 tons in vacuum for two minutes. The concentrations of the nanofibers ranged from 0.1 to 1‰ (m/m). All transmission spectra were baseline corrected.

4.3 Results and discussion

4.3.1 XRD results

XRD results (see table 4.1) show that heat treatment has no significant effect on the width at half height of the (d_{002}) graphite peak at d=0.340 nm. This is not surprising, because it was expected that heat treatment up to 2000°C would only influence the in-plane organization of the graphite planes. It is noted that the (d_{002}) reflection results from the subsequent graphite planes or graphene sheets.

Table 4.1 Peak width at half height of d-spacing between graphite planes (d_{002}) before and after heat treatment of fishbone and parallel carbon nanofibers.

Sample	Peak width (°2θ)	L_c (nm)
CNF-Eng	1.27	10.8
CNF-Eng-1600	1.47	9.2
CNF-Eng-2000	1.22	11.3
CNF-Hyp	3.31	3.8
CNF-Hyp-2000	3.28	3.8
CNF-Par	2.33	5.5
CNF-Par-2000	1.97	6.6

Using the Scherrer equation the graphite domain size along the C-axis of graphite, L_c has been calculated (table 4.1). Although heat treatment has no significant effects, the differences of L_c for different fibers is noteworthy. The parallel fibers display smaller values for L_c, in particlar the Hyperion fiber, than the fishbone-type fibers (CNF-Eng). The absolute value of L_c for the Hyperion fibers fits with the values obtained from TEM (see section 4.3.2).

Other graphite peaks which are present in the diffractogram are all either mixed with signals from the Ni particles or mixed with Al_2O_3 signals. From these results it appears that the removal of nickel and alumina using nitric acid reflux has not been very effective. What can be observed in the diffractogram of the heat treated fishbone fibers is that the intensities of the Ni and Al_2O_3 peaks diminish considerably with higher treatment temperatures. This can be explained by considering the melting and boiling points of these materials, which are listed in table 4.2 [16].

Table 4.2 Melting and boiling points of Ni, Al_2O_3, α-Al_2O_3 and Fe.

Material	Melting point (°C)	Boiling point (°C)
Ni	1453	2732
Al_2O_3	2045	2980
α-Al_2O_3	2015	2980
Fe	1535	2750

At 1600°C and above the Ni will have melted, but not evaporated. The Al_2O_3 will probably have melted at least partly at 2000°C. Possibly phase separation between carbon fibers on the one hand, and nickel and alumina, on the other, had occurred. It is suggested that Ni/Al may have reacted with tungsten and more or less pure carbon fibers remain for further analysis. The conclusions, however, are in contrast to results obtained with other samples (figures 4.4 and 4.5). In these two cases the peaks of metal and support are more pronounced after heat treatment.

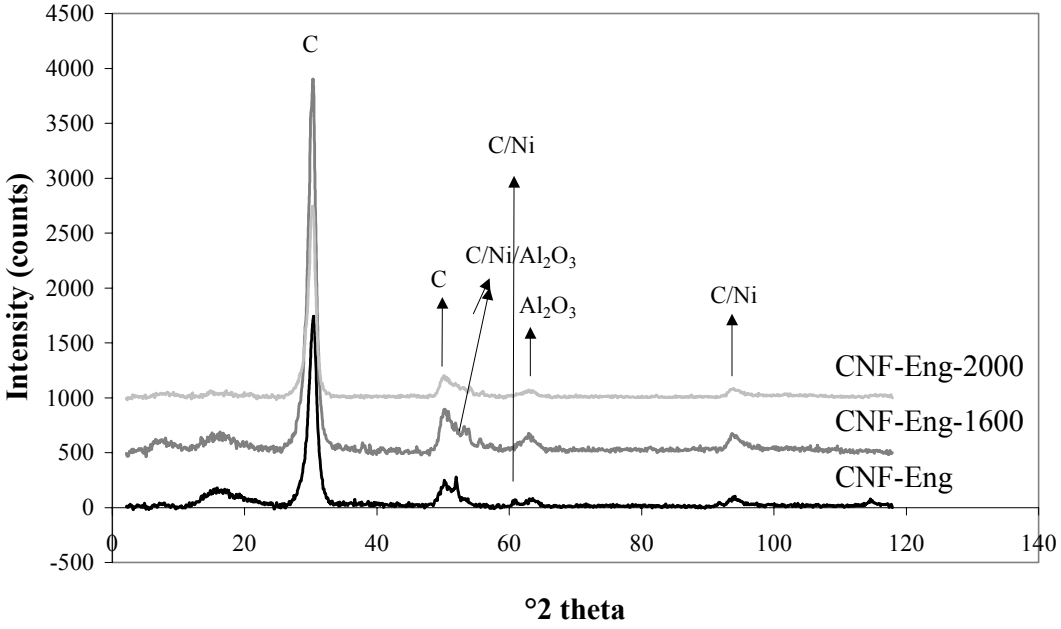

Figure 4.1 X-ray diffractogram of CNF-Eng, CNF-Eng-1600 and CNF-Eng-2000.

Back-scatter SEM images of untreated fibers show the exposed Ni particles at the tips of the fibers. After heat treatment the number of small Ni particles that is visible in the SEM images has diminished considerably. From a large amount of very small particles at the tips of the fibers, the Ni has changed into bigger lumps which have sintered together inside the bird's nests of the fibers. This is clearly visible in the SEM images shown in figures 4.2 and 4.3. Since the total amount of Ni present in these fibers is only 1.5 wt% before acid treatment, and these fibers have had an acid treatment, which removes a large amount of Ni, it is not surprising that these Ni particles are not detected with XRD. The amount of Ni and Al_2O_3 that is still present is below the detection limit of the XRD.

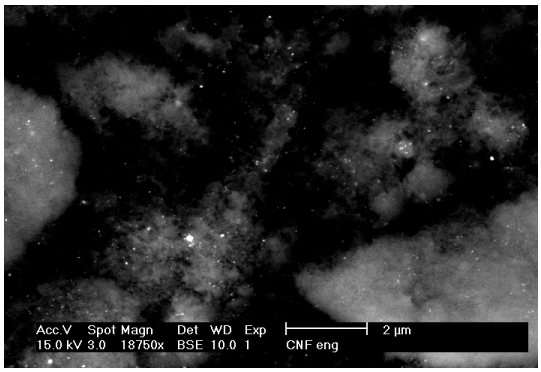

Figure 4.2 Back-scatter image from CNF-Eng.

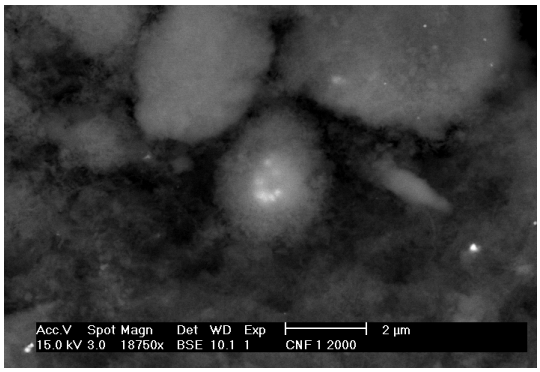

Figure 4.3 Back-scatter image from CNF-Eng-2000.

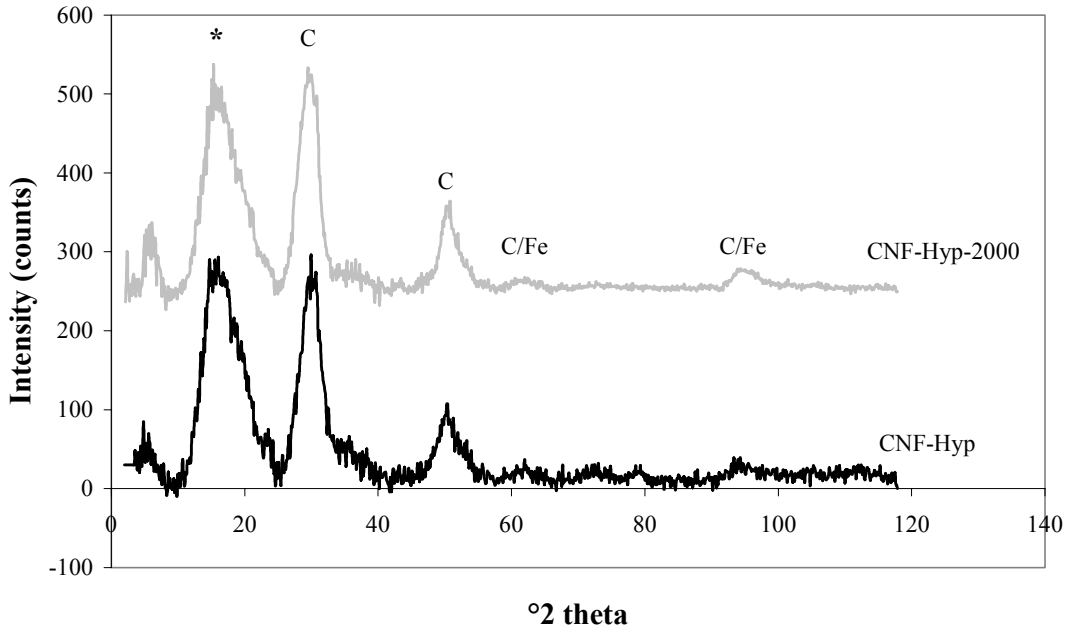

Figure 4.4 X-ray diffractogram of the CNF-Hyp and CNF-Hyp-2000.

The most obvious changes in the X-ray diffractograms can be seen at low °2θ values. A broad peak is visible at 18°2θ (d=0.57 nm). It is much stronger in the Hyperion and parallel fibers than in the fishbone fibers. This peak cannot be accounted for with graphite, Ni or Al_2O_3. We postulate that this peak is the result of the presence of amorphous carbon, which is possibly present in between graphite planes (see section 4.3.2). The amorphous carbon is further confirmed when we study the XRD patterns of two activated carbons obtained from Norit. These carbons also show broad peaks around 18°2θ (see figure 4.6)

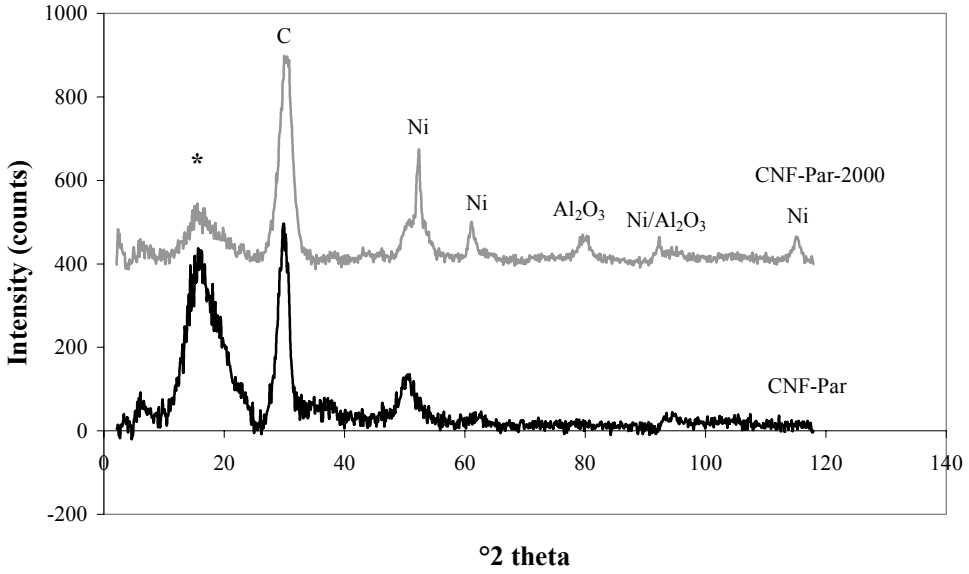

Figure 4.5 X-ray diffractogram of the CNF-Par and CNF-Par-2000.

In fishbone fibers a very small amount of the fibers actually has a parallel character (see also 4.3.2, TEM results), which explains the low intensity of the 18°2θ peak. During the heat treatment of the CNF-Par (figure 4.5) the amorphous carbon probably reacts with traces of air or it is rearranged to a more organized form of carbon. The latter results would be the same as those reported by Bougrine [14]. This would explain why the peak intensity has diminished considerably after the heat treatment. In the Hyperion fibers the peak has a high intensity relative to the (d_{002}) peak, which hardly diminishes after heat treatment. The apparent stability of the amorphous carbon with the Hyperion fibers cannot be explained as yet.

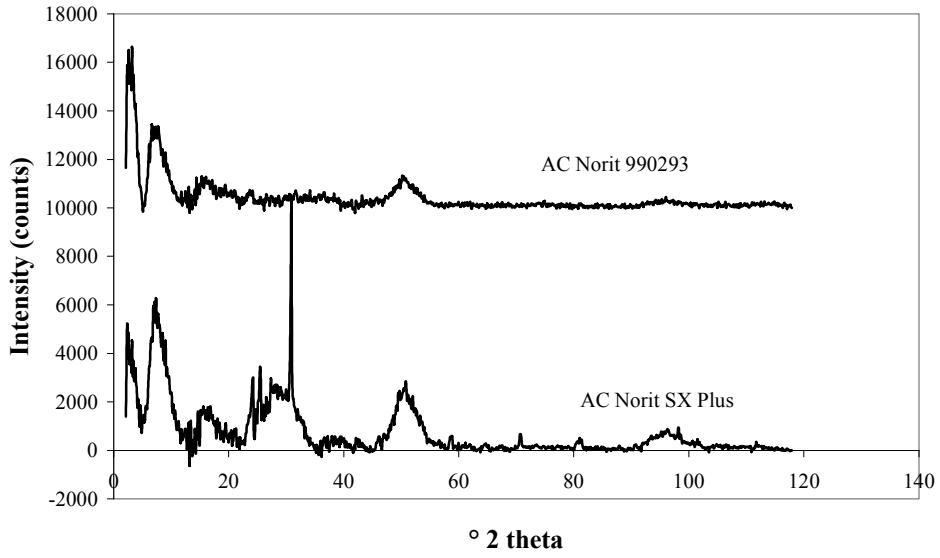

Figure 4.6 XRD patterns of two activated carbons, which show broad peaks around 18°2θ.

4.3.2 TEM results

TEM images taken from the fishbone fibers at high magnifications show that a significant part of the fibers displays graphite planes more or less parallel to the fiber axis (see figures 4.8 and 4.9). Because we have not studied a very large amount of TEM images we are not able to put down a percentage. Furthermore, when the fibers are studied in detail, a large number of defects is found. Often two graphite planes merge into one, the planes are not straight, they bend and are irregular. Also it is apparent that some ends of the planes run parallel to the fiber surface.

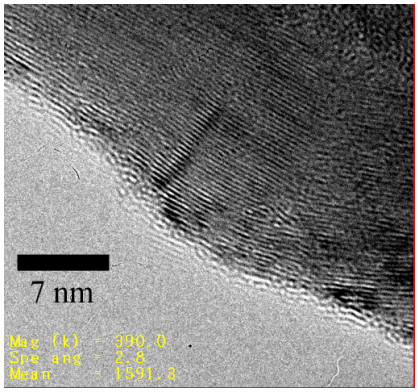

Figure 4.7 HR-TEM image of CNF-Eng.

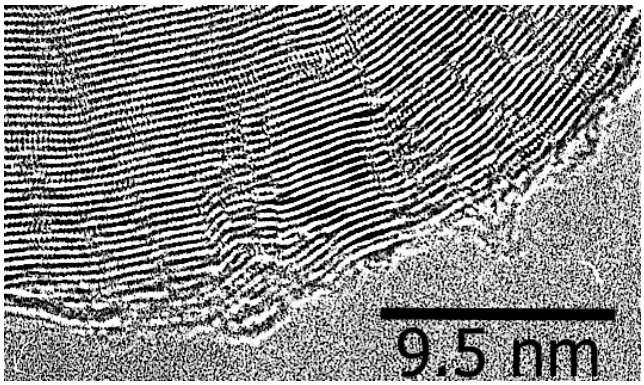

Figure 4.8 HR-TEM image of CNF-Eng with defects in the graphite planes.

In figure 4.7 the graphite planes are quite straight. A defect (2 planes becoming 1) can be seen in the lower right-hand side of the picture (near the edge of the fiber). Also a very large defect can be observed, where the fiber bends. Over the whole diameter of the fiber the graphite planes are disconnected.

In figure 4.8 the fiber shown has a more or less parallel appearance with the graphite planes parallel to the fiber axis, as opposed to the fishbone fibers, where the planes are at an angle with the axis. Large amounts of defects can be observed in the form of graphite planes coming together or splitting up. Also the graphite planes are disconnected in a lot of places.

At some positions in figure 4.8 the graphite planes bend to run in parallel at distances of ~0.6 nm with some carbon visible between the graphite planes. The local expansion of graphite due to 'intercalated carbon' might be a working hypothesis to explain the 18°2θ reflection in XRD (see figures 4.1, 4.4 and 4.5).

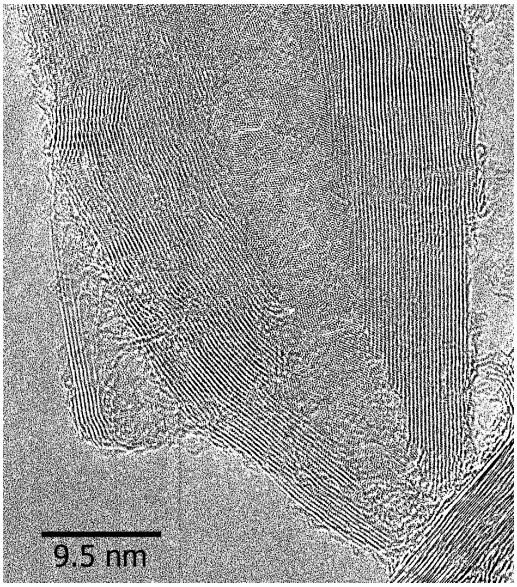

Figure 4.9 HR-TEM image of CNF-Eng with the planes at an angle to the fiber axis.

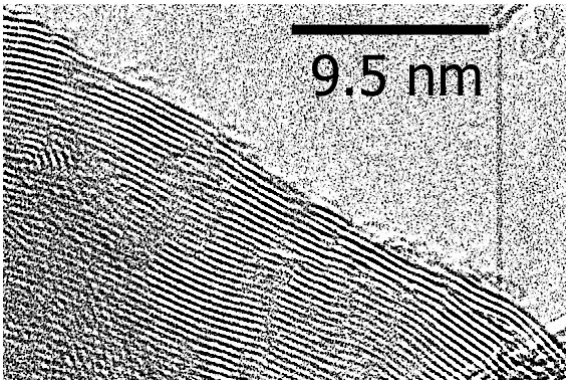

Figure 4.10 HR-TEM image of plane ends on the surface of a fishbone fiber.

In figure 4.9 a part of a fiber can be observed which does have the graphite planes at an angle towards the fiber axis. Some defects can be observed, but in general the graphite planes are straight and largely defect-free.

In figure 4.10 the slabs of planes protruding from the surface of the fiber can be observed very well.

When the fishbone fibers are heat treated for 30 minutes at 2000°C some differences are observed. The amount and nature of the defects and the bending and curving of the graphite planes are not affected. The slabs at the surface of the fibers are affected however. The slabs straighten and protrude from the fiber as opposed to run parallel to the fiber surface (figures 4.11 and 4.12). This effect can already be observed for some slabs after treatment at 1600°C (see figure 4.11) and can be observed very well after heat treatment at 2000°C (figure 4.12).

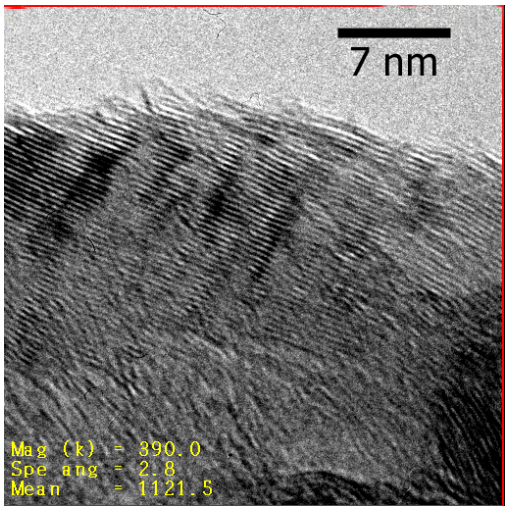

Figure 4.11 HR-TEM image of the slabs protruding from the surface of CNF-Eng-1600.

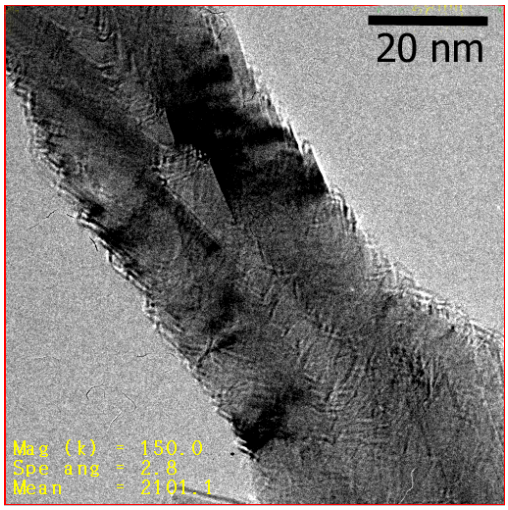

Figure 4.12 TEM image of the slabs protruding from the surface of CNF-Eng-2000.

Also the Hyperion fibers have been studied with HR-TEM. As can be observed in figure 4.13 Hyperion fibers have large diameter channels and thin walls, which often only consist of 4 or 5 graphite planes (figures 4.14, 4.15 and 4.16). The outer diameter distribution of these fibers has been determined from TEM analysis as 9 to 18 nm.

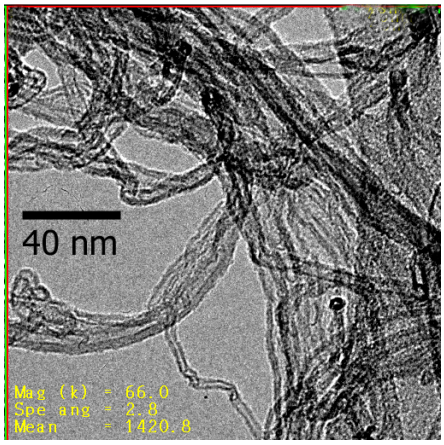

Figure 4.13 Hyperion fibers before heat treatment, as synthesized, CNF-Hyp.

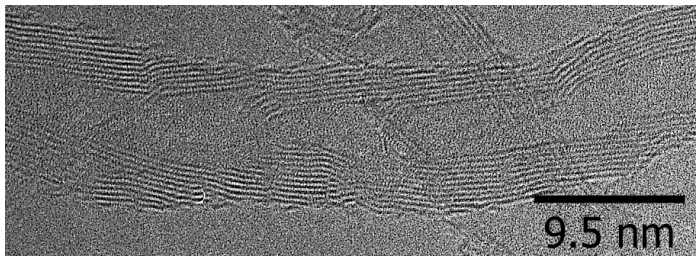

Figure 4.14 HR-TEM of a Hyperion parallel fiber, with a bit of fishbone nature.

As is clearly visible in figure 4.14, in this fiber the planes are not aligned parallel to the fiber axis, but they are under an angle. A lot of plane endings can be observed at the surface of the fiber and inside the channel of the fiber there are also disconnections at regular intervals.

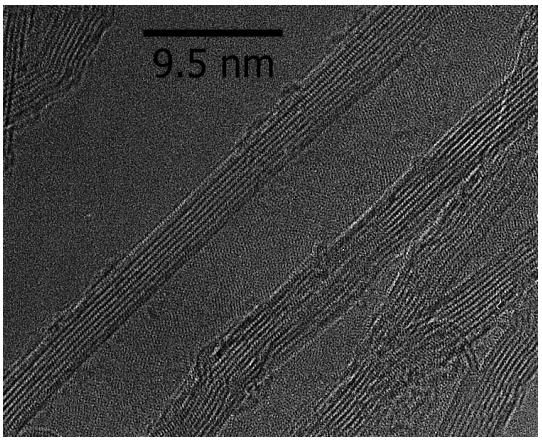

Figure 4.15 HR-TEM image of a very straight and regular Hyperion fiber.

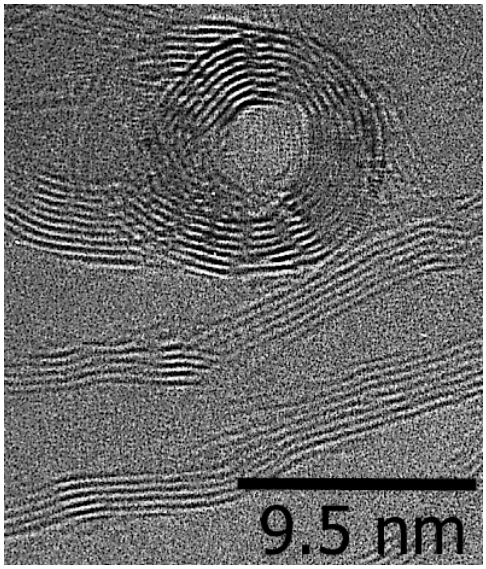

Figure 4.16 HR-TEM image of the top of a Hyperion fiber and plane ends in the inside of the channel.

The fiber in the centre of figure 4.15 has long, straight graphitic domains.

Figure 4.16 displays some bending in the fiber in the lower left hand corner and also an end of a fiber. In the latter the tubular structure of the fiber can be observed very well.

After heat treatment at 2000°C the Hyperion fibers were again studied with HR-TEM. The fibers still contained a large amount of defects and bends in the graphite planes. The planes were not observed to have straightened out under influence of the heat treatment. With TEM no differences could be observed.

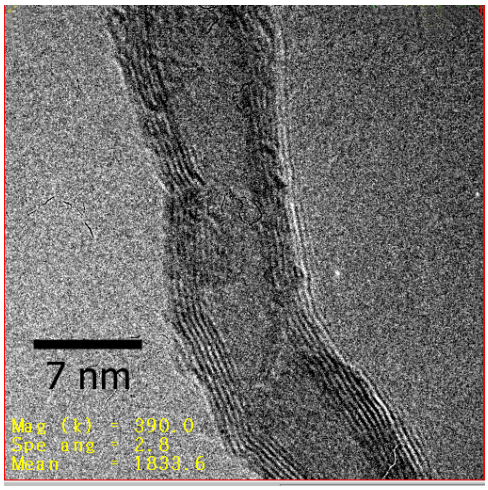

Figure 4.17 HR-TEM image of CNF-Hyp-2000.

The parallel fibers grown from Ni with syngas, CNF-Par, were also studied with HR-TEM. These fibers have a larger diameter than the Hyperion fibers. The walls of these tubes are formed by more graphite planes, usually up to 20. Also it is clearly visible that not all the fibers have a completely parallel structure. Figure 4.17 shows part of a fiber with some fishbone character, with the graphite planes at an angle with the fiber axis.

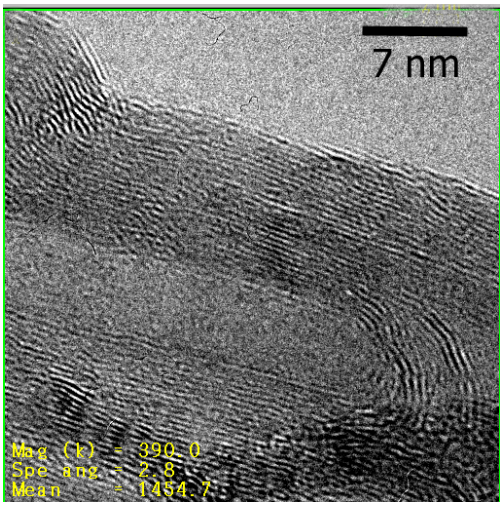

Figure 4.18 HR-TEM image of CNF-Par.

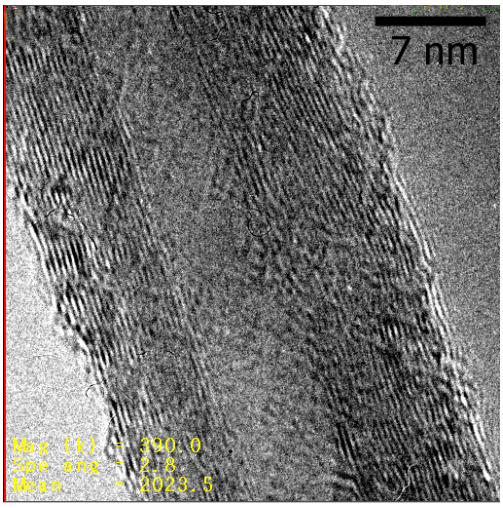

Figure 4.19 HR-TEM image of CNF-Par-2000.

Figure 4.18 shows part of a fiber with a large domain with long, defect-free and straight graphite planes. In the inner tube of the fiber, several curved graphite planes are visible, which bridge the channel of the fiber. On the surface of the fiber the ending of some graphite planes is clearly visible. So the surface of these as synthesized carbon fibers is not free of graphite plane endings and defects.

After heat treatment for 30 minutes at 2000°C the amount of defects in the fiber could not be observed to have diminished. The surface of the fiber shows plane ends and defects are also still present throughout the fiber. The surface might even be considered a bit more rugged and uneven than prior to heat treatment. This breaking up may be the result of the presence of oxygen containing groups on the surface, which are removed as CO or CO_2 during the heat treatment.

In all the fibers the d-spacings have been measured. This has been done by measuring the distance over at least 5 graphite planes and averaging this out. For all the fibers measured the d-spacing between the graphite planes varies between 0.29 and 0.38 nm. This averages out at 0.34 nm, which is consistent with the d-spacing determined by XRD. It was observed that the spacing tends to be larger at parts of the fiber where there are a lot of defects, or where the fiber is bending. It is somewhat smaller in very straight regions. The broadening of the graphite (d_{002}) peak in the XRD image of carbon nanofibers can be explained in part by this phenomenon.

4.3.3 Texture and TGA results

All the fibers were analysed with N_2 physisorption. In table 4.3 the BET surface area and the total porevolume (PV) are shown. From t-plot analysis it appeared that no micropores (diameter < 2 nm) are present in all samples studied.

Table 4.3 Nitrogen physisorption results from untreated and heat treated fishbone and parallel carbon nanofibers.

Sample	BET SA (m^2/g)	PV (ml/g)
CNF-Eng	113	0.40
CNF-Eng-1600	84	0.36
CNF-Eng-2000	71	0.33
CNF-Hyp	238	2.75
CNF-Hyp-2000	265	2.17
CNF-Par	157	1.03
CNF-Par-2000	172	0.99

When studying these nitrogen physisorption results, one has to keep in mind that the meso- and macropore volume of carbon nanofibers are formed by the space between the fibers. Where the fibers are close enough together, a space is formed, that is detected with nitrogen physisorption. Changes in pore volume of these materials can therefore also be the result of slight compression or decompression of the material. When the fibers have undergone a treatment, the orientations of the fibers can change, which will result in a slightly different pore volume. Therefore the difference in the pore volumes of the heat treated and untreated fibers is thought to be insignificant.

The Hyperion and parallel carbon fibers have a slightly enlarged BET surface area, which is considered within the measurement error (5%), so this textural change is also insignificant. The fishbone fibers however have a clearly diminished BET surface area. From the difference we observe in the surface structure of the fishbone fibers we would rather expect an enlarged BET surface area, because the slabs start protruding from the surface, which may create a larger surface. This result may be explained by a difference in surface roughness on atomic scale of the fibers before and after heat treatment. More research is needed to explain these apparently contradictive results.

TGA results are presented in figure 4.20. Untreated as well as heat treated fibers were subjected to a 20% O_2 in Ar stream, while heating up to 1000°C. The monitored weight loss versus temperature is presented in figure 4.20.

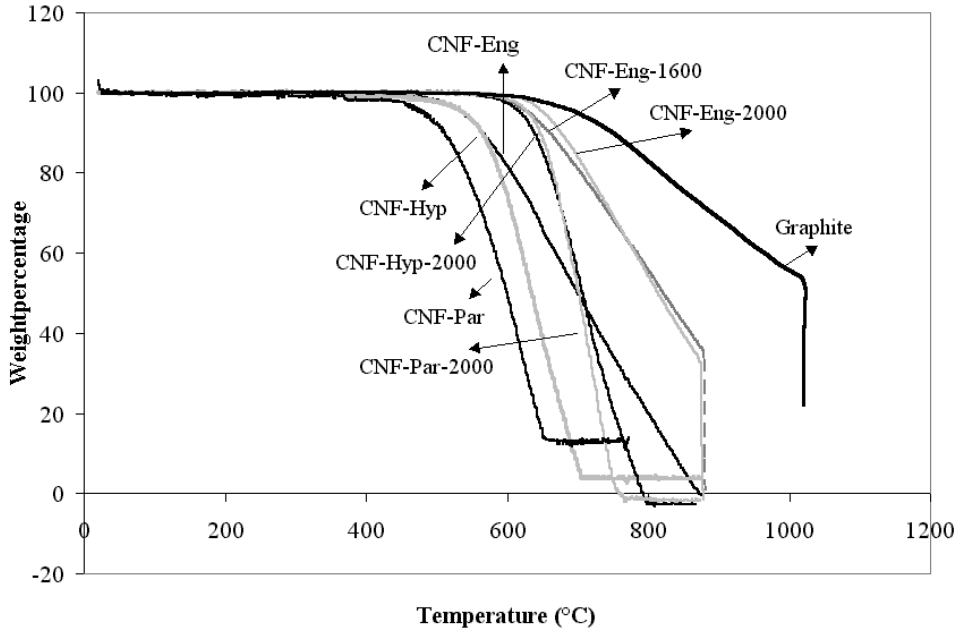

Figure 4.20 Weight loss versus temperature for heat treated and untreated carbon nanofibers.

From this figure it is obvious that the heat treatment has a distinct effect on the onset of the oxidation reaction. The onsets of the oxidation of the untreated fibers (CNF-Eng, CNF-Hyp and CNF-Par) are all at least 75°C below the onset of the oxidation of the heat treated fibers. For comparison also results for the oxidation of synthetic graphite (Fluka Chemika, 99%, BET surface area 6 m^2/g) are plotted. The onset of this oxidation is slightly above that of fishbone fibers heat treated at 2000°C, which is as expected, because the fibers are still not as organized, inert and defect-free as graphite. The faster oxidation of the parallel fibers, both the Hyperion as the parallel CO/H_2 produced fibers may be caused by the shape of the fibers. When the oxidation of a graphite plane of a parallel fiber starts, a larger part of the graphite can be converted to CO_2 than with the fishbone fibers. The fishbone fibers, which consist of many small planes oxidize slower in air, because when a plane is completely oxidized a much smaller part of the fiber is oxidized and to continue a new oxidation-nucleation has to take place. There is only a slight difference observed between the fishbone fibers which are heat treated at 1600 and those treated at 2000°C. The onset of the oxidation of the graphite is at about the same temperature, but the reaction proceeds slower. Higher onset of the oxidation of the heat treated fibers suggests that the heat treatment of the fibers does influence the graphitic nature of the fiber surface. Oxidation probably starts at defect-sites at the surface of the graphite, so a higher onset of oxidation suggests that indeed less defects are present at the surface after heat treatment.

4.3.4 IR results

The fibers were studied with transmission IR to study the nature and amount of the defects of the fibers with a bulk technique to compare the results with those of TEM where a very small part of the material is studied. Ros *et al*. showed that IR is a very promising technique to study the structure of parallel and fishbone carbon nanofibers [17]. The strong absorbance coefficient of the fibers necessitated a very low sample concentration. To allow comparison, transmission levels of all spectra were kept approximately the same. It was established that, within the transmission window used, the intensity of the bands did not depend upon the transmission level of the spectra. In table 4.4 all infrared band assignments are summarised [17].

Table 4.4 Assignments of infrared absorptions found for carbon nanofibers and graphite [17].

Wavenumber (cm^{-1})	Assignment
3012	aromatic C-H stretching
2974	CH_2/CH_3 stretching
2917	CH_2/CH_3 stretching
2846	CH_2/CH_3 stretching
1717-1712	C=O stretching
1633	adsorbed water
1580-1570	aromatic ring stretching
1454	CH_2/CH_3 bending
1384	nitrate
1217-1188	C-C stretching
880-870	isolated aromatic C-H out-of-plane bending

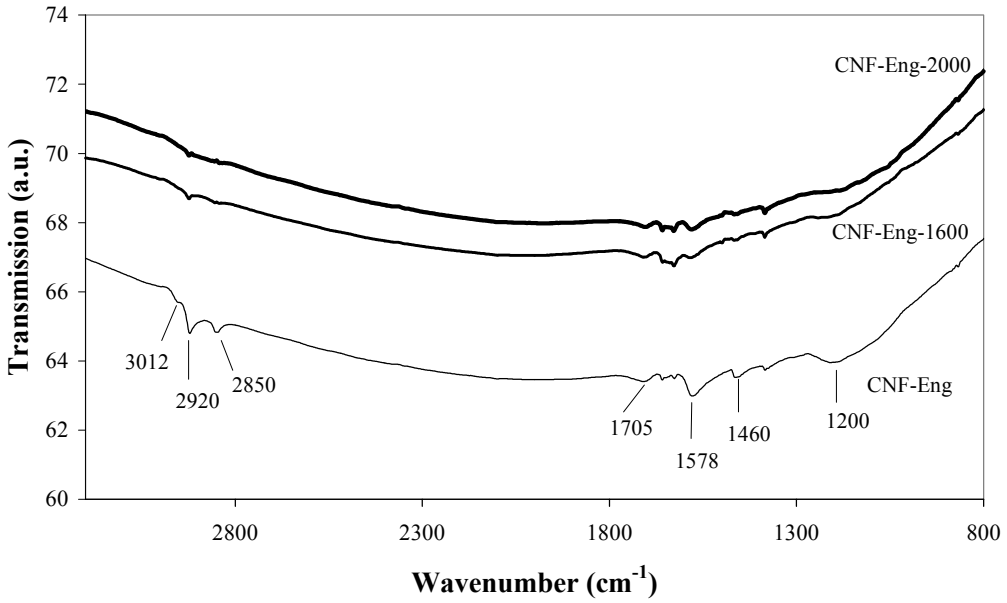

Figure 4.21 IR spectra of CNF-Eng, CNF-Eng 1600 and CNF-Eng-2000.

In figure 4.21 the IR spectra of untreated and heat treated fishbone fibers are shown. It is obvious from this figure that all the bands that can be assigned to non-aromatic vibrations, such as 2920 and 2850 (CH_2/CH_3 stretching), 1460 (CH_2/CH_3 bending) and 1200 (C-C stretching) diminish considerably or even disappear completely after heat treatment. The treatment has probably influenced the surface of the fibers in such a way that a lot of non-aromatic endings have either reacted away or have become more aromatic in nature. The absorption at 1578 can be assigned to aromatic ring stretching. This absorption decreases, which shows that the graphitic regions have enlarged and have become more symmetric, which decreases the absorption coefficient.

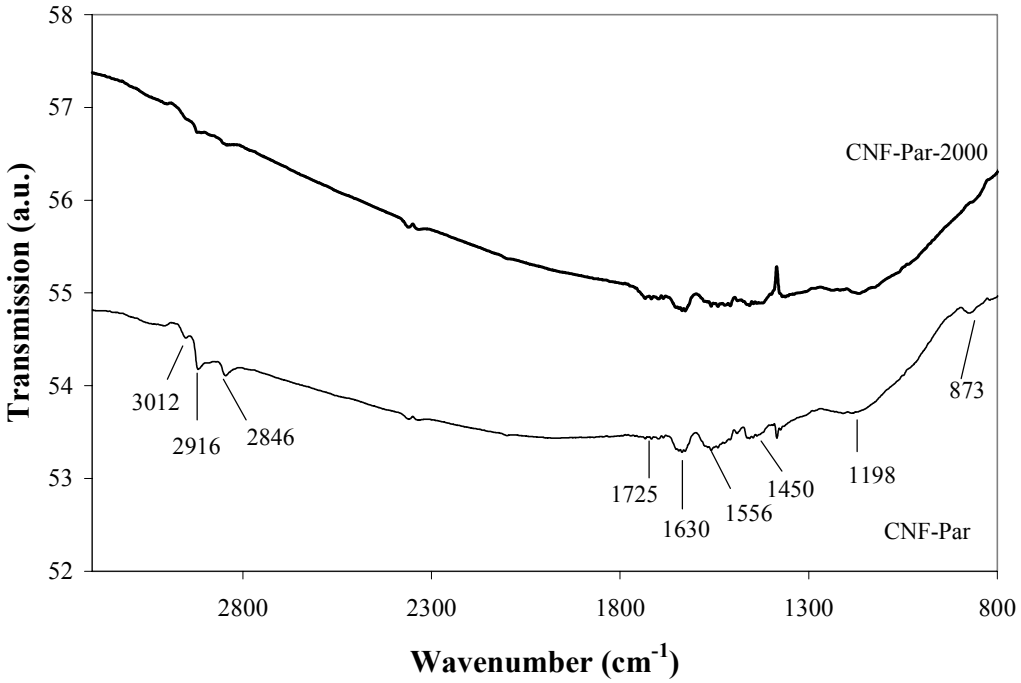

Figure 4.22 IR spectra of CNF-Par and CNF-Par-2000.

The C=O absorption intensity is high and is found at 1705 cm^{-1}, which is consistent with carbonyl groups. The high intensity is consistent with the severe oxidation treatment which was performed on these fibers (two hours refluxing with nitric acid) and the carbonyl groups are found because the fibers were heat treated at 800°C only with nitrogen after the oxidation. This treatment removes the carboxyl groups from the surface, but the carbonyl groups remain [15]. It is striking that this absorption is still present after the heat treatments at 1600°C and 2000°C, which must have removed these oxygen-containing groups from the surface. After the treatment the fibers were, cooled down, mostly under argon, but the last part in air. Probably the oxygen was removed during the treatment, but the oxygen-terminating defect sites remained. These sites were then reoxidized during the cooling down. Not much difference can be observed in the spectra of CNF-Eng-1600 and CNF-Eng-2000. It can be concluded that most of the changes have already taken place at 1600°C.

In figure 4.22 it is obvious that also for the parallel fibers, the non-aromatic CH_2 and CH_3 vibrations diminish or disappear after the heat treatment, for instance at 2916, 2846, 1450 and 1198 cm^{-1}. The absorption at 873 cm^{-1} also disappears almost completely. This absorption is assigned to an isolated aromatic C-H out of plane bending. This implies that the treatment increased the aromatic character of these fibers.

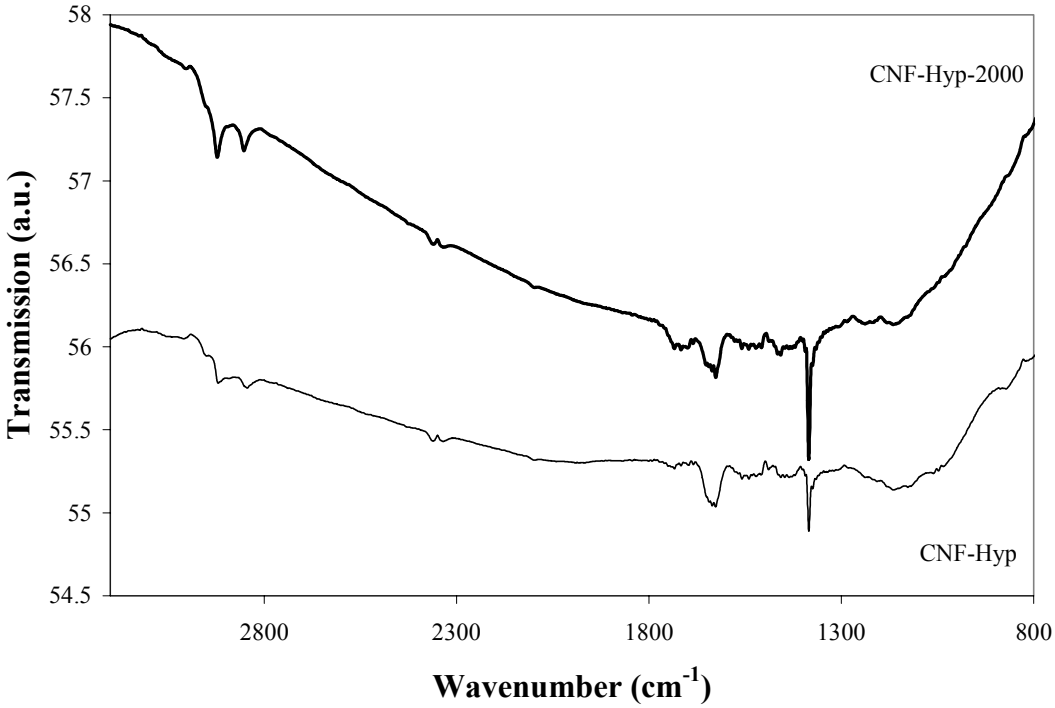

Figure 4.23 IR spectra of CNF-Hyp and CNF-Hyp-2000.

The Hyperion fibers were also studied with IR. Unfortunately the intensities of these measurements are too inconsistent to compare these quantitatively. Qualitatively, see figure 4.23, it can be concluded that there are no peaks which appear or disappear completely, so the Hyperion fibers do not show a large change upon the heat treatment.

4.4 Conclusions

The fishbone nanofibers are shown from TEM analysis to display a significant amount of defects, such as two planes coinciding to one, bending planes, planes more or less parallel to the fiber axis and plane ends parallel to the fiber surface. After heat treatment at 1600°C and 2000°C the fibers showed a similar number of defects. The plane terminates no longer parallel to the surface of the fiber, but protrudes from the surface, as if they had straightened out. The BET surface area of these materials has diminished, however. This may be caused by a lower surface roughness. To gain more insight into this phenomenon, more research is needed. Additionally Ni and Al_2O_3, which are still present in the sample have diminished from the X-ray diffractogram. With SEM it can be seen very clearly that the Ni has melted from the tips of the fibers and has recrystallised inside the mesopores in the bird's nests of the fiber structure. There is very little Ni and Al_2O_3 left in the samples, because they were pre-treated with acid prior to the heat treatment.

In the Hyperion and parallel fibers Fe or Ni and Al_2O_3 have also melted and recrystallised in the pores between the fibers. These materials are still visible in the XRD pattern after heat treatment as sharpened peaks. This is not surprising because these materials were not pre-treated with acid and therefore much larger amounts of Fe or Ni and Al_2O_3 are still present. The parallel and Hyperion carbon fibers contain the same amount and types of defects and also have connecting graphite planes inside the channels. TEM analysis does not show a diminished amount of defects after heat treatment and the BET surface area of these materials does not change.

Thermo Gravimetric Analysis shows that oxidation of heat-treated fibers starts at higher temperature than that of untreated fibers, closer to the onset temperature of graphite oxidation. Because defects at the surface of the fiber are the most logical candidates for the start of the oxidation, the heat treatment must have diminished the amount of these surface defect sites. These results suggest that all the fibers have increased their surface aromaticity.

IR results are consistent with TEM and TGA results. The surfaces of the fishbone and parallel fibers have become much more aromatic. For the fishbone fibers this can also be seen clearly from protruding graphite planes. For the parallel fibers this is not very clear from TEM results, but TGA and IR show a decrease of aliphatic carbon. The results for Hyperion fibers are less consistent. From IR and TEM results the material does not seem to be affected much, but TGA shows an increase in oxidation temperature.

It can be concluded that although the surfaces of the fibers are affected by heat treatment at 2000°C for 30 minutes, the bulk of the fibers is not. To obtain a large influence on the defects inside the fibers higher temperatures and longer treatment times are needed.

Acknowledgements

We wish to thank dr. Roland Vogels of Philips Lighting Components, Eindhoven for providing the heat treatment facilities. We wish to acknowledge dr. Patricia J. Kooyman of the National Center for High Resolution Electron Microscopy, Delft University of Technology, Delft for performing the electron microscopy investigations. We thank prof. dr. ir. J.W. Geus for also performing electron microscopy investigations. We also thank A. Broersma for performing the TGA measurements. We gratefully thank dr. Tijmen G. Ros for performing the IR data and subsequent discussions.

References

1. J.R. Rostrup-Nielsen, Journal of Catalysis 85 (1984) 31.
2. M.S. Hoogenraad, Ph.D. Thesis, Utrecht University (1995).
3. K.P. de Jong and J.W. Geus, Catalysis Reviews- Science and Engineering 42 (2000) 481.
4. D. Moy and R. Hoch, Catalyst supports, supported catalysts methods of making the same and methods of using the same, US Patent WO 93/24214 (1993).
5. G.E. Gadd, M. Blackford, S. Moricca, N. Webb, P.J. Evans, A.M. Smith, G. Jacobsen, S. Leung, A. Day and Q. Hua, Science 277 (1997) 933.
6. A. Chambers, C. Park, R.T.K. Baker and N.M. Rodriquez, The Journal of Physical Chemistry B 102 (1998) 4253.
7. C. Park, P.E. Anderson, A. Chambers, C.D. Tan, Hidalgo and R. Rodriquez, Journal of Physical Chemistry B 103 (1999) 10572.
8. C. Zandonella, Nature 410 (2001) 724.
9. M. Hirscher, M. Becher, M. Haluska, U. Dettlaff-Weglikowska, A. Quintel, G.S. Duesberg, Y.-M. Choi, P. Downes, M. Hulman, S. Roth, I. Stepanek and P. Bernier, Applied Physics A 72 (2001) 129.
10. C.C. Ahn, Y. Ye, V. Ratnakumar, C. Witham, R.C.Jr. Bowman and B. Fultz, Proceedings of the Battery Conference on Applications and Advances 14 (1999) 67.
11. M.G. Nijkamp, J.E.M.J. Raaymakers, A.J. van Dillen and K.P. de Jong, Applied Physics A 72 (2001) 619.
12. M. Endo, R. Saito, M.S. Dresselhaus and G. Dresselhaus, Carbon nanotubes: preparation and properties, (CRC Press, Boca Raton, 1997) p. 96.
13. T.C. Chieu, M.S. Dresselhaus and M. Endo, Physical Review B 26 (1982) 5867.
14. A. Bougrine, A. Dupont-Pavlovsky, A. Naji, J. Ghanbaja, J.F. Mareché and D. Billaud, Carbon 39 (2001) 685.
15. T.G. Ros, Ph. D. Thesis, Utrecht University (2001).
16. R.C. Weast, Handbook of Chemistry and Physics (CRC Press, Cleveland, Ohio, 1975).
17. T.G. Ros, A.J. van Dillen, J.W. Geus and D.C. Koningsberger, ChemPhysChem, acceped for publication.

5

Hydrogen Adsorption of K Intercalated Carbon Nanofibers

Abstract

In this chapter fishbone carbon nanofibers are intercalated with potassium. Their hydrogen storage capacity, morphology and structure are studied using H_2 physisorption, N_2 physisorption, TEM and XRD. XRD results show that the fibers are indeed intercalated and the d-spacing of a part of the graphitic fibers enlarges. The amount of hydrogen stored increases with the amount of K intercalated. Only part of the fibers are intercalated, which is probably related to the structure of the fibers, which contain small graphitic domains and a large number of defects.

5.1 Introduction

Hydrogen can be stored using physisorption. In chapter 2 we showed that for sufficient hydrogen storage capacity the adsorbent material has to contain a high volume of suitable micropores. We have also shown that small micropores (0.5-1.0 nm) probably store the highest amount of hydrogen. Intercalation of suitable materials into graphitic structures may create such a high microporous volume. Intercalation with alkali metals proceeds easily and ternary GICs containing hydrogen, argon and nitrogen exist positively. These can be formed by interaction of hydrogen with binary alkali GICs, such as potassium [1-3], rubidium [4,5] and cesium [4-6] graphite intercalated compounds. Obviously, the presence of the mentioned metals 'unlock' the space between the carbon layers by increasing the interlayer distance (see figure 5.1).

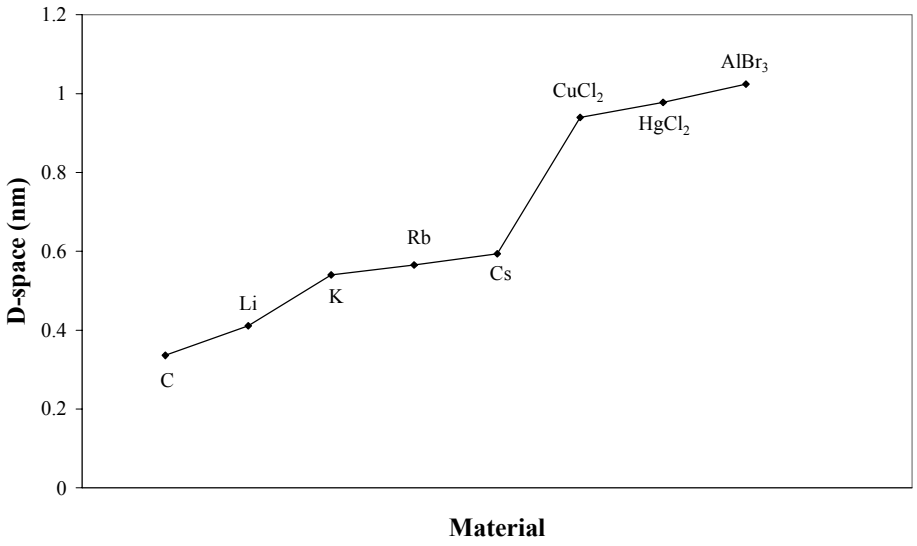

Figure 5.1 Resulting d-space of intercalated carbon compounds.

Upon intercalation of graphite, monolayers of reactant are inserted between the carbon sheets, which increase the interlayer distance. Interaction between the π system of the carbon layers and the intercalate layers results in either electron donation or electron acceptation by the reactant species. E.g. K-GICs are of the donor- and $FeCl_3$ of the acceptor-type. The concentration stage number *n* is defined as the ratio of carbon layers to reactant monolayers. In figure 5.2, intercalation compounds with different concentration stages are schematically represented. An increase in the c-axis of the unit cell, I_0, is obvious from this representation [7].

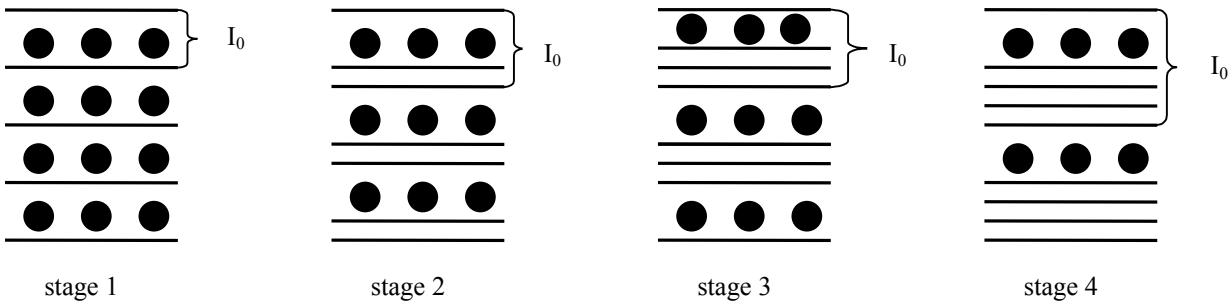

Figure 5.2 Structure of intercalation compounds with different stages.

5.2 Literature on K intercalation

The intercalation of graphite by alkali metals has been known since 1926 [8,9]. Graphite has been intercalated by Li, K, Cs and Rb, using several methods, such as the one-zone and two-zone method and liquid phase methods [10-14]. Also intercalation of alkali's and solvents or other compounds, such as K-THF [11] or K-$FeCl_3$ [15], K-NH_3 [16] and other options [17] are reported . It is also possible to intercalate hydrided potassium, KH into graphite [18-20].

It is well-known that K intercalated graphite adsorbs H_2 and a lot of research has been performed on the H_2 adsorption capacity of K-, Cs- and Rb-intercalated compounds [1-5,12,21-26]. Also the transport properties, such as resistance, of K intercalated compounds have been investigated [27]. K intercalated graphite has been mentioned as a getter compound to remove trace amounts of O_2 and H_2 from gasstreams [25]. In their review on hydrogen-alkali-metal-graphite ternary intercalation compounds in 1990 Enoki *et al*. [19] concluded that alkali-metal-graphite intercalation compounds absorb hydrogen in two ways: physisorption and chemisorption. Hydrogen uptake through the physisorption process occurs at temperatures below about 200 K in higher stage alkali-metal-GICs, where hydrogen molecules are stabilized to form a two-dimensional condensed phase in the galleries of the graphite sheets. The concentration of adsorbed hydrogen molecules is saturated at a ratio of H/K~4. The hydrogen physisorption shows a strong isotope effect and also a swelling effect on c-axis lattice expansion. In the case of hydrogen uptake through the chemisorption process, dissociated hydrogen species are stabilized in the intercalate spaces. The activity of the chemisorption increases in the order Cs < Rb < K. The introduction of hydrogen generates a charge transfer from the host alkali-metal-GICs to the hydrogen. The inserted two-dimensional hydrogen layer is suggested to consist of H^- ions with a weakly metallic nature.

In 1995, Klyamkin *et al*. [26] reported the interaction of potassium-graphite intercalation compounds with hydrogen at pressures up to 2000 atm. The maximum content of hydrogen in the samples was achieved at 78 K under pressures higher than 500 atm and it was close to the stoichiometry $KC_8H_{3.5-4}$.

Akuzawa *et al*. [3] reported the possibility to intercalate mesocarbon microbeads with potassium and then physisorb hydrogen at 77 K. All compounds, irrespective of their previous heat treatment temperature, physisorb hydrogen, but the amount is strongly dependent on this heat treatment temperature.

Since the appearance of single walled carbon nanotubes (SWNT) and catalytically synthesized carbon nanofibers (CNF) there has also been interest to intercalate these materials. Intercalation in single walled nanotubes can only be understood in the form of atomic dispersion of the metal between the tubes which are situated next to each other, because this are the only graphene sheets available to intercalate. This is indeed possible with Li [28-30]. It was also performed with K and the electronic structure and optical properties of potassium intercalated SWNT were studied by Pichler *et al*. [31]. Akuzawa *et al*. [3] reported intercalation of potassium in mesocarbon microbeads and subsequent H_2 physisorption. Furthermore Leroux *et al*. [32] reported the electrochemical insertion of lithium in carbon nanofibers. The material they intercalated consisted of a mixture of the fibers, carbon black and polyvinylidene fluoride. It is unclear from their report whether the lithium was actually intercalated into the fibers.

In 1996, Mordkovich *et al*. [33] reported the intercalation of multi walled nanotubes by K and $FeCl_3$. However, the TEM pictures shown suggest that the material forms large particles on the surface of the tubes, because the material 'comes out' of the tubes when exposed to air and can be removed with washing. The remaining tubes are still intact, which is highly unlikely after intercalation in a parallel multi walled carbon nanotube. Intercalation would destroy (parts of) the tubes. However, in 1997, they reported [34] the intercalation of $FeCl_3$ and K in bundles of multiwalled nanotubes using the one-zone method. Their XRD results show an enlargement of the d-spacing almost equal to that reported for graphite intercalated compounds. However, the fact that the intercalation can be reversed with washing, without destruction of the lattice, remains an enigma.

Scope of the chapter

In this chapter we study if the intercalation of carbon nanofibers with potassium increases the d-spacing and hydrogen adsorption capacity of the material in a similar way as it does with potassium intercalated graphite. Potassium intercalated carbon, however, is very sensitive towards oxygen and water. Intercalated K is atomically dispersed between the graphite planes. This material, when contacted with air, reacts violently to KO_2 and CO_2. This O_2 sensitivity makes it unfit to be used in commercial (mobile) applications. It is, however, suitable to perform research studies on. If successful, the intercalation may be performed with another material (see also chapter 6), which is less sensitive towards O_2. A large advantage of this material is that it can be synthesized easily and fast. The carbon nanofibers and potassium are contacted in an inert atmosphere and the temperature is raised to 200°C. The K melts and inserts between the graphite planes. After heating for 2 hours the intercalation is complete. The material can then be handled using standard inert atmosphere techniques.

To see if morphology and texture of the fibers had any influence on the intercalation behavior, several types of fibers were subjected to the same treatment. The results are compared. Also the hydrogen storage capacities of fishbone and parallel fibers were compared before and after intercalation treatments. The d-spacing and morphology changes of the material were studied with HR-TEM and XRD. The results of these experiments are described in this chapter.

5.3 Experimental

Fishbone carbon nanofibers (CNF-Eng) were produced in a fluidized bed (see chapter 3) at 570°C using catalytic decomposition of methane on the 60 wt% Ni on Al_2O_3 commercial catalyst from Engelhard (Ni 3288).

Parallel fibers (CNF-Hyp) were obtained from Hyperion. These are commercially available parallel carbon nanofibers which are grown from Fe. They were not subjected to any treatments to remove impurities before use.

Synthetic graphite was obtained from Fluka Chemika (Fluka Chemika Graphite 50870) and not subjected to any pretreatments before use.

Intercalation experiments were performed in a hydrogen adsorption apparatus (see figure 5.3). In this way the hydrogen adsorption capacity of the as synthesized material, which is very sensitive to air, could be determined immediately. The intercalation was performed by contacting the carbon nanofibers and the potassium in a helium atmosphere and heating up to 200°C, while mixing. In a typical experiment with untreated fishbone fibers a maximum 1.3% of the potassium could, in theory, react with the still present Al_2O_3. The potassium melts and intercalates between the graphite planes. When, after heating for 2 hours at this temperature the sample cools down the potassium remains between the planes. The same was performed for the intercalation of graphite, with the difference that the heating period was at least 48 hours to ensure that the potassium had been intercalated homogeneously over the whole sample. This is necessary because of the much longer graphite planes in graphite when compared to carbon fibers.

Transmission electron microscopy was performed using a Philips CM30UT electron microscope with a field emission gun as the source of electrons operated at 300 kV. Samples were mounted on a carbon polymer supported on a copper grid (Quantifoil®) by placing a few droplets of a suspension of ground sample in n-hexane on the grid, followed by drying at ambient conditions, all in an Ar glovebox. Samples were transferred to the microscope in a special vacuum-transfer sample holder under exclusion of air.

XRD patterns were recorded at room temperature with a Nonius PDS 120 powder diffractometer system equipped with a position-sensitive detector with a 2θ range of 120°. The radiation used was Co $K\alpha_1$ (λ=1.78897 Å). XRD patterns of intercalated samples were recorded with the same system. The intercalated fibers were brought into a suitable capillary in an inert atmosphere, which was afterwards sealed.

From the N_2 physisorption data, obtained with a Micromeritics ASAP 2400 apparatus at 77 K, the BET surface area, total pore volume and micropore volume were derived. Prior to the physisorption measurements, the non-intercalated fibers and graphite were evacuated at 300°C. When intercalated samples were studied with N_2 physisorption, they were evacuated at room temperature.

Hydrogen adsorption experiments were performed in a conventional static volumetric adsorption apparatus, made of Pyrex glass, which could be operated at hydrogen pressures of up to 1 bar. The apparatus is displayed in figure 5.3.

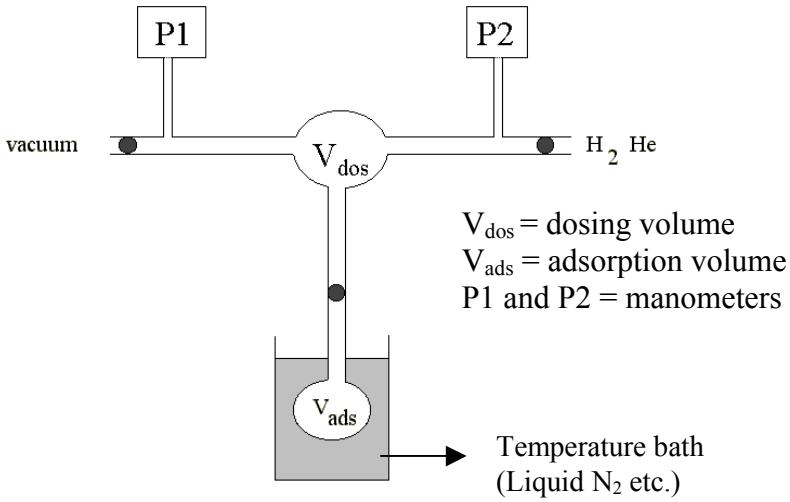

Figure 5.3 Static hydrogen adsorption apparatus up to 1 bar.

5.4 Results and discussion

5.4.1 XRD results of K intercalated fishbone fibers

The result of an intercalation experiment in which 0.8 g of as synthesized fishbone CNF was intercalated with 0.32 g K for 3 hours at 250°C in a helium atmosphere is shown in figure 5.4.

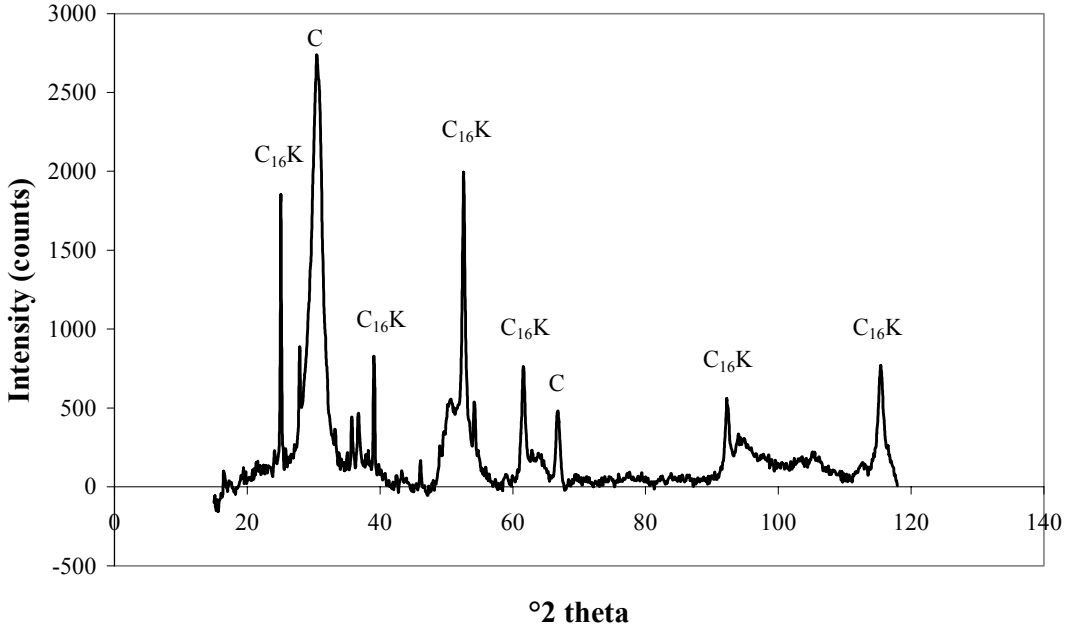

Figure 5.4 XRD pattern of fishbone CNF intercalated with K.

It is obvious that the carbon nanofibers are indeed intercalated and have enlarged their d-spacing. However, the material is not intercalated to C_8K, but rather to $C_{16}K$. From the still present graphite peaks at 30°, 50° and 66° 2θ it can be concluded that not all the fibers were intercalated. A significant amount of the added K is probably present between the fibers, possibly as very small K particles.

5.4.2 TEM results of potassium intercalated fishbone fibers

Fishbone fibers were intercalated with potassium, heated for 2 hours and then sealed and kept in an ampoule, sometimes up to several weeks. After transfer to a glove box, the samples for the electron microscope were prepared. In the microscope the presence of K was checked with EDX, which proved to be the case. Also the influence of the high intensity electron beam on the presence of K was checked with EDX. This was performed by checking the presence of K with EDX, then irradiating a spot with a very high intensity electron beam for several minutes. Afterwards the presence of potassium was again checked with EDX. The amount of K detected had not changed after this treatment. One sample ($C_{24}K$) was first studied with the EM and then removed from the microscope, subjected to air and then again studied. The 'oxidized' material looked a little bit less ordered when the morphology of the fibers was studied, but the distance and ordering of the graphite layers was the same as before.

The observed fibers are rather small, which is surprising because the samples are prepared by grinding the fibers and then distributing them over the grid, suspended in hexane. It is not expected that these fishbone fibers break by grinding. So the short fibers are an indication that the strength and integrity of at least some of the fibers is comprimised by the intercalation procedure.

In figures 5.5-5.11 potassium intercalated fibers, both fishbone and parallel, intercalated to a gross composition of C_8K, $C_{12}K$, $C_{16}K$, $C_{24}K$ are shown. These fibers do not show appreciable differences from non-intercalated fibers. From the images which are taken at high resolution, it is obvious that the d-spacing of the graphite planes in the fibers is still 0.34 nm. There are regions in the fibers where the d-spacing is larger, and also where it is smaller, but it ranges between 0.28 and 0.38 nm. This range is also found in as synthesized fibers (see also chapter 4). There is also no remarkable difference in d-spacing of highly intercalated fishbone fibers, such as C_8K or fibers intercalated to $C_{24}K$. Also the Hyperion fibers show a small range in d-spacing, as synthesized as well as intercalated to $C_{16}K$. The fibers show the same type of defects inside the fibers as before intercalation (see chapter 4).

The results of the TEM study show no systematic enlargement of the d-spacing. The XRD results show that a significant part of the fibers has not been intercalated and therefore does not show any enlargement of the d-spacing. Because with Electron Microscopy only a small part of the sample is studied it is possible that only non-intercalated parts were brought onto the grid and studied. On these parts it is still possible that K is present, between the fibers. It may also be possible that from the glovebox to the microscope the material had reacted slowly with air, de-intercalating the potassium. An explanation for the partial intercalation may be that fishbone fibers contain lots of defects inside the fibers and the graphite domains are usually quite small and angled upon each other. Lifting of the graphite planes in a system with a lot of those effects is more difficult.

When Hyperion carbon nanofibers are contacted with potassium, they do show adsorption behavior, which is similar to fishbone fibers. After intercalation, when the material is contacted with air, they react in the same way as the fishbone fibers. This is surprising, because it would be expected that these parallel fibers cannot be intercalated in the same way as the fishbone fibers. Because these parallel fibers are shaped as rigid hollow tubes, surrounding each other, intercalation between these graphite planes would have to cause destruction of the fibers, because the tubes cannot enlarge easily and accommodate potassium in between without destruction.

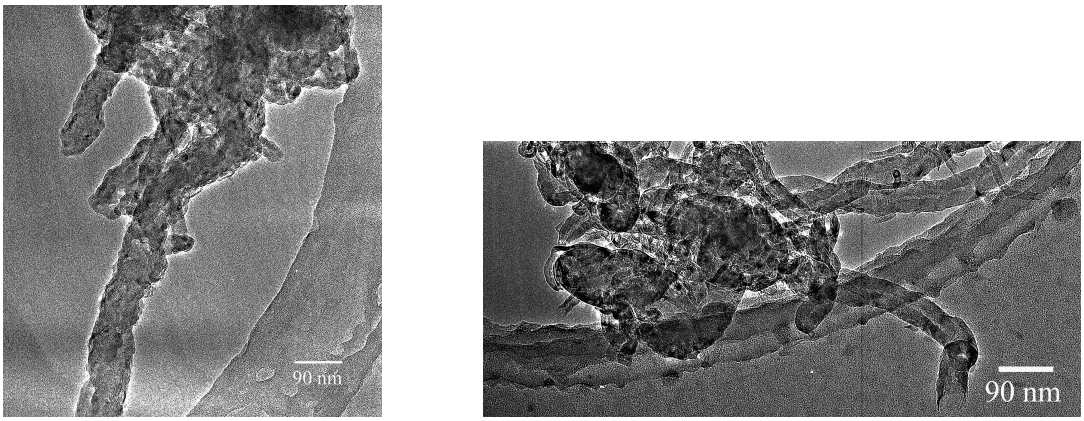

Figure 5.5 Potassium intercalated fishbone fibers, C_8K (left) and as synthesized fishbone fibers (right).

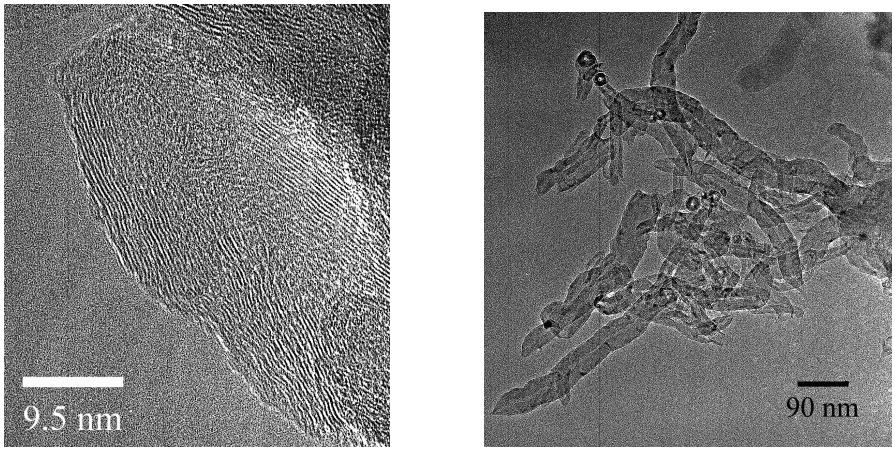

Figure 5.6 Potassium intercalated fishbone fibers, C_8K (left), and $C_{12}K$ (right).

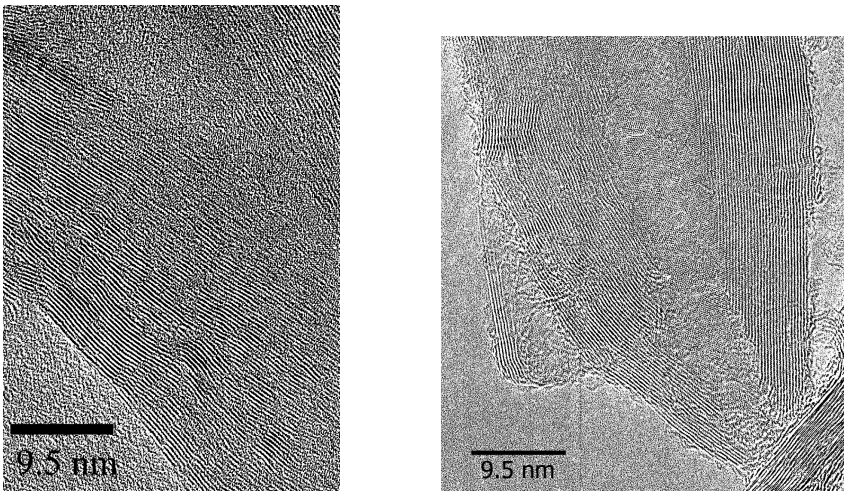

Figure 5.7 Potassium intercalated fishbone fibers, $C_{12}K$ (left) and an as synthesized fishbone fiber (right).

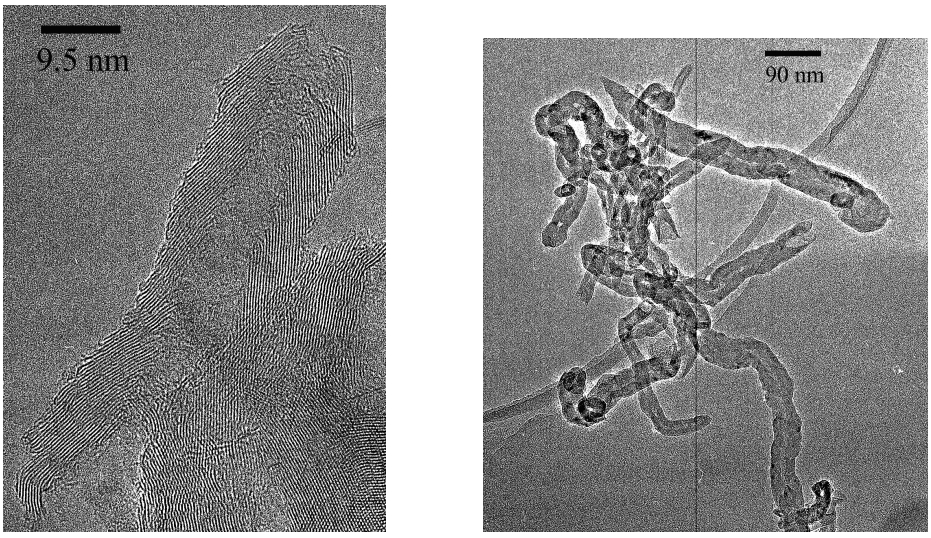

Figure 5.8 Potassium intercalated fishbone fibers, $C_{16}K$.

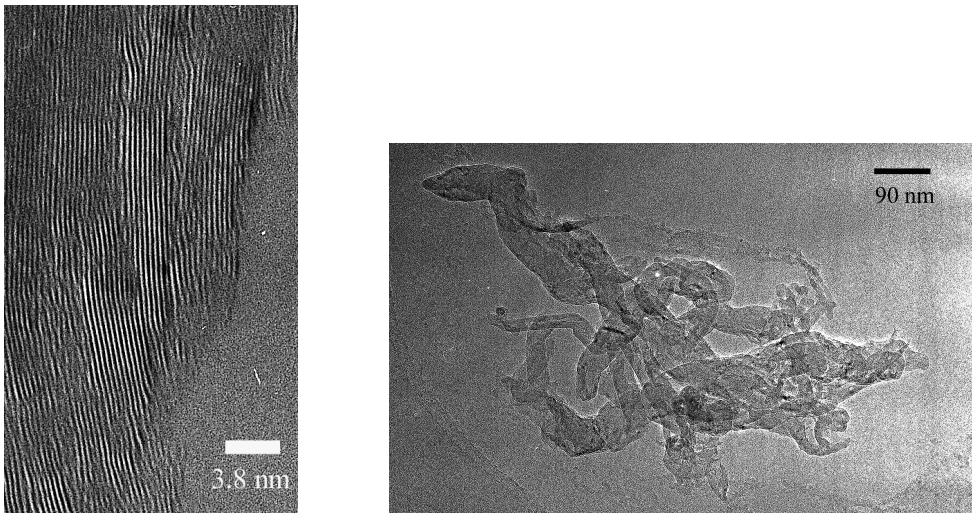

Figure 5.9 Potassium intercalated fishbone fibers, $C_{24}K$.

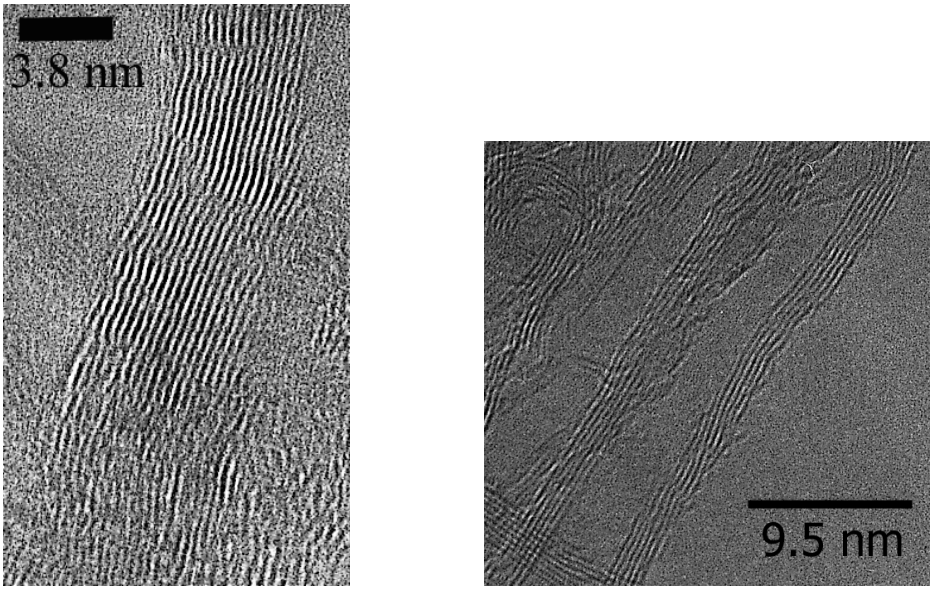

Figure 5.10 Potassium intercalated Hyperion fibers, $C_{16}K$ (left) and as synthesized Hyperion fibers (right).

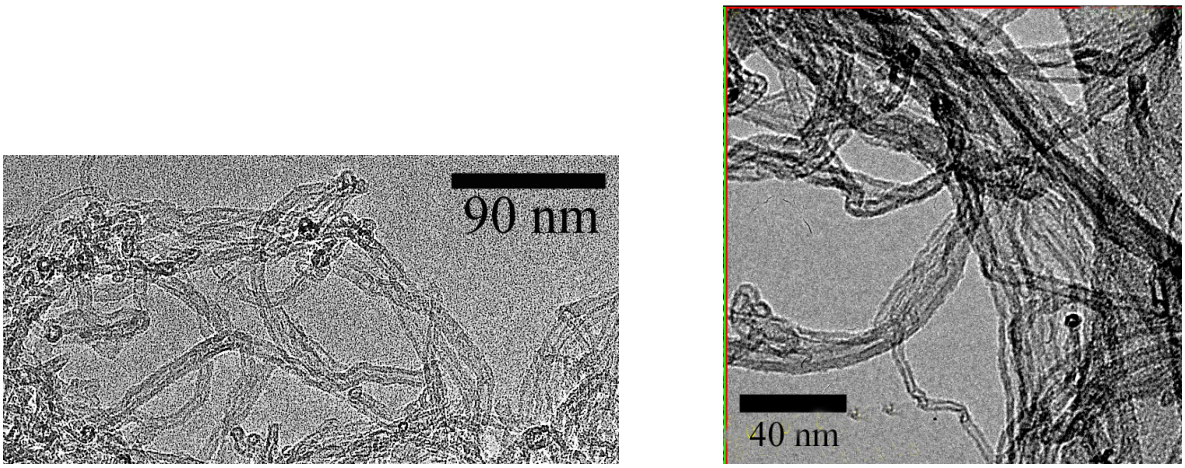

Figure 5.11 Potassium intercalated Hyperion fibers, $C_{16}K$ (left) and as synthesized Hyperion fibers (right).

5.4.3 N_2 physisorption results of K intercalated fibers and graphite

Because we hypothesized that an increased hydrogen storage could be the result of an increased micropore volume, the BET surface area and pore volume of the intercalated carbon nanofibers was compared with those of the as synthesized fibers. For transfer of the intercalated samples to the N_2 physisorption apparatus, without being subjected to air a schlenck techniques were used. Because the d-spacing of potassium intercalated graphite increases to 0.52 nm and this space also contains the graphite layer itself, it was already questionable whether N_2, which has a kinetic diameter of 0.41 nm, could penetrate between these graphite planes. By using intercalated graphite this was checked. It turned out

impossible to detect an enlargement of the micropore volume in intercalated graphite with N_2 physisorption. The intercalated graphite or fibers did not show any enlargement of the pore volume or BET surface area. After the N_2 physisorption measurements, the materials were contacted with air and all materials still showed large amounts of sample which violently reacted with air. This shows that there had not been any contamination with air, resulting in de-intercalation of K. It could therefore be concluded that N_2 is too large to penetrate between the intercalated graphite sheets.

5.4.4 H_2 adsorption capacity of K intercalated fishbone fibers

The H_2 storage capacity of fishbone carbon nanofibers has been determined for several stages of intercalated compounds. In table 5.1 the materials and their adsorption capacities are summarized.

Table 5.1 Hydrogen storage capacities of several K-intercalated fishbone carbon nanofibers at 77 K and 1 bar.

	H_2 storage capacity				
Sample	ml STP/$g_{adsorbent}$	ml STP/g_{carbon}	wt%	H/K	H/C
as synth.	10.4	10.4	0.10	-	0.01
$C_{24}K$	26.5	31.3	0.25	0.78	0.03
$C_{16}K$	65.6	80.2	0.60	1.40	0.07
$C_{12}K$	78.0	103.1	0.73	1.34	0.08
$C_{10}K$	53.8	74.0	0.50	1.24	0.08
C_8K	44.5	66.0	0.41	0.54	0.05
C_7K	100.8	162.5	0.99	1.27	0.11

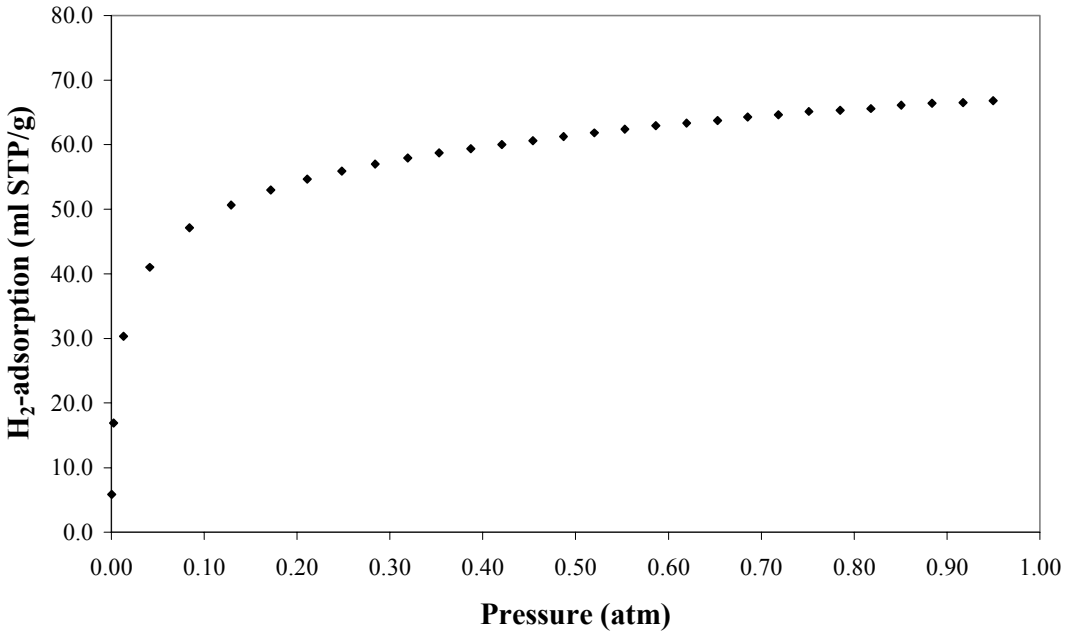

Figure 5.12 Hydrogen uptake of fishbone fibers, intercalated to $C_{16}K$ at 77 K.

The hydrogen uptake capacity of all these intercalated samples was tested repeatedly, each after 30 minutes of evacuation at 77 K. All samples were tested in at least 3 cycles, some in 6 cycles and still showed the same uptake capacity. The samples did not show any uptake at 193 and 298 K.

Tentatively, from the results can be concluded that most materials show hydrogen uptake related to the amount of K present, namely H/K ~1.3. This differs from the reported amount of H/K ~4. This can be explained because, firstly, we have not optimized this adsorption. Secondly, the structure and domain size of the CNF differs markedly from that of well-ordered graphite. Therefore, the structure of the intercalated compounds is also expected to be quite different. The XRD results showed that part of the fibers was not intercalated, and therefore, did not show an enlarged d-spacing. It is hard to determine how large this part is. It may be that the intercalated parts do adsorp H_2 with a H/K ratio of ~4. The samples for $C_{24}K$ and C_8K show a different uptake, which cannot be explained. We did not find chemisorption of the hydrogen, as was reported for K-GICs, because from the results it is clear that the adsorbed hydrogen is physisorbed. Therefore, it is thought that enlargement of the d-spacing and an increased micropore volume can be assumed significant to the hydrogen storage capacity enlargement of the K intercalated CNFs.

The heat of adsorption can be determined by measurement of adsorption isotherms at different temperatures. We have tried this by also measuring the adsorption of the K intercalated fibers at 193K (CO_2-aceton mixture) and at room temperature. In both cases the samples did not show any adsorption. These results prove the heat of adsorption to be ≤ 5 kJ/mol.

5.5 Conclusions

With XRD we have shown that intercalation of potassium in as synthesized fishbone nanofibers does increase the d-spacing of the fibers. It was also shown that part of the fibers is not intercalated and remains graphitic, with a d-spacing of 0.34 nm. Results of TEM experiments did not show an enlarged d-spacing. This may be the result of only non-intercalated parts being studied, or because of slow reaction with air and de-intercalation of K during insertion of the samples into the microscope. A lot of small carbon nanofiber parts is observed in the microscope, so the intercalation procedure seems to negatively affect the strength of the fibers.

Intercalation of potassium in carbon nanofibers does significantly increase the hydrogen storage capacity of these materials. The observed adsorption is physisorption and the intercalated fibers do not show any hydrogen storage capacity at 193 and 298 K. The H_2 adsorption has not been optimized. The amount of H_2 stored is different (H/K ~1.3) than the amount mentioned for K intercalated graphite (H/K ~4). This may turn out different when the intercalation is optimised. XRD results show that only part of the fibers is intercalated, so it may be that the H_2 adsorption capacity of the intercalated fibers is closer to H/K ~4.

It was shown that N_2 physisorption could not be used to show an enlarged BET surface area or micropore volume, because the N_2 molecule is too large to penetrate between the intercalated graphite sheets.

We have shown that intercalation of K increases the d-spacing of CNF and increases the H_2 adsorption capacity, similarly as can be performed with graphite. Because of the O_2 sensitivity of this material it is, however, not very suitable to use in mobile applications. However, use of another intercalant, which is less O_2 sensitive, may create a suitable H_2 adsorbent for mobile applications. In chapter 6 the intercalation of $FeCl_3$ in CNF and graphite and the effect on H_2 adsorption capacity of these materials is discussed.

Acknowledgements

We wish to acknowledge Dr. Patricia J. Kooyman of the National Center for High Resolution Electron Microscopy, Delft University of Technology, Delft for performing the electron microscopy investigations. We thank Marjan Versluijs for performing the XRD investigations. We wish to acknowledge John Raaymakers for performing the N_2 physisorption measurements.

References

1. T. Enoki, M. Sano and H. Inokuchi, Journal of Chermical Physics 78 (1983) 2017.
2. G.L. Doll and P.C. Ecklund, Physical Review B 36 (1987) 9191.
3. N. Akuzawa, T. Sakamoto, H. Fujimoto, T. Kasuu and Y. Takahashi, Synthetic Metals 73 (1995) 41.
4. G. Champetier, M. Colin and A. Hérold, C. R. Acad. Sc. Paris, t 269 Série C (1969) 1302.
5. G. Champetier, P. Lagrange, M.-H. Portmann and A. Herold, C. R. Acad. Sc. Paris, T. 283 série C (1976) 511.
6. C.J. Carlile, Physica B 491 (1998) 241.
7. D. Braga, A. Ripamonti, D. Savoia, C. Trombini and A. Umani-Ronchi, Journal of the Chemical Society Dalton (1979) 2026.
8. K. Fredenhagen and G. Cadenbach, Zeitschrift Fuer Anorganische Und Allgemeine Chemie 158 (1926) 249.
9. K. Fredenhagen and H. Suck, Zeitschrift Fuer Anorganische Und Allgemeine Chemie 178 (1929) 353.
10. D.E. Nixon and G.S. Parry, British Journal of Applied Physics (J. Phys. D.) 1 (1968) 291.
11. H. Selig and L.B. Ebert, Advances in Inorganic Chemistry and Radiochemistry 23 (1980) 281.
12. P.C. Ecklund, NATO ASI Series, Series B 148 (Intercalation Layered Materials) (1986) 309.
13. P. Sjovall, Surface Science 345 (1996) L39-L43.
14. Yu.N. Novikov and M.E. Vol'pin, Russian Chemical Reviews 40 (1971) 733.
15. O.El. Shazly, S.G. Tawfik, A.K. Ibrahim, I.H. Ibrahim and E.F.El. Wahidy, Journal of Materials Science 28 (1993) 5040.
16. J.K. Walters, N.T. Skipper and A.K. Soper, Chemical Physics Letters 300 (1999) 444.
17. A.J. Briard, C. Hérold, J.F. Mareché and P. Lagrange, Carbon, Letters to the Editor 38 (2000) 475.
18. H. Ogata, S. Miyajima, K. Matsutsuji and T. Enoki, Journal of Physical Chemistry and Solids 57 703.
19. T. Enoki, S. Miyajima, M. Sano and H. Inokuchi, Journal of Materials Research 5 (1990) 435.
20. D. Guerard and C. Takoundjou, Synthetic Metals 7 (1983) 43.
21. K. Watanabe, M. Soma, T. Onishi and K. Tamaru, Nature Physical Science 233 (1971) 160.
22. K. Watanabe, T. Kondow, T. Onishi and K. Tamaru, Chemistry Letters 2 (1972) 477.
23. T. Terai and Y. Takahashi, Carbon 22 (1984) 91.
24. G.L. Doll and P.C. Ecklund, Journal of Materials Research 2 (1987) 638.
25. K. Ichimura and M. Sano, Journal of Vacuum Science and Technology A 10 (1992) 543.
26. S.N. Klyamkin, V.A. Nalimova, K.N. Semenenko and A.A. Karih, Journal of Alloys and Compounds 231 (1995) 740.
27. L. Grigorian, G.U. Sumanasekera, A.L. Loper, S. Fang, J.L. Allen and P.C. Eklund, Physical Review B Condensed Matter and Materials Physics third series, volume 58 (1998) R4195-R4198.
28. G.T. Wu, C.S. Wang, X.B. Zhang, H.S. Yang, Z.F. Qi, P.M. He and W.Z. Li, Journal of the Electrochemical Society 146 (1999) 1696.

29. V.A. Nalimova, D.E. Sklovsky, G.N. Bondarenko, H. Alvergnat-Gaucher, S. Bonnamy and F. Béguin, Synthetic Metals 88 (1997) 89.

30. S. Suzuki, C. Bower and O. Zhou, Chemical Physics Letters 285 (1998) 230.

31. T. Pichler, M. Sing, M. Knupfer and M.S.F.J. Golden, Solid State Communications 109 (1999) 721.

32. F. Leroux, K. Méténier, S. Gautier, E. Frackowiak, S. Bonnamy and F. Béguin, Journal of Power Sources 81-82 (1999) 317.

33. M. Baxendale, V.Z. Mordkovich, S. Yoshimura and R.P.H. Chang, Physical Review B 56 (1997) 2161.

34. V.Z. Mordkovich, M. Baxendale, R.P.H. Chang and S. Yoshimura, Synthetic Metals 86 (1997) 2049.

6

$FeCl_3$ Intercalated Carbon Nanofibers and Graphite, Material Characteristics and Reduction Behavior

Abstract

We explored the perspectives for enhancement of adsorption of CNFs and graphite by intercalation of these carbon materials with $FeCl_3$, $FeCl_2$ and Fe^0. Iron(III)-chloride graphite intercalated compounds (GICs) were prepared using the one zone ampoule technique. The obtained GICs were studied with nitrogen physisorption, XRD, TGA, SEM and XPS. The conversion of $FeCl_3$-GICs into $FeCl_2$- and Fe-GICs by heating in N_2 and by reduction in H_2 appeared to be impossible. Thermal treatment nor reduction resulted in the desired GICs. Only de-intercalation of $FeCl_3$ was observed to occur, which partly deposited on the surface of the host lattice, in N_2 as $FeCl_2$, in H_2 as Fe^0. Our attempts to intercalate CNFs with $FeCl_3$ turned out to be fruitless. With the produced and pretreated $FeCl_3$-GICs no enhanced hydrogen adsorption capacity was effectuated.

6.1 Introduction

Already in the general introduction, chapter 1, we emphasized the potential of graphitic compounds, and notably of carbon nanofibers (CNFs), for hydrogen storage, provided that the space between the carbon layers can be made accessible for H_2 and adsorption and desorption takes place at a sufficiently high rate. Concerning the accessibility of the interlayer space of virginal graphite-like materials, Watanabe *et al*. [1] theoretically as well as experimentally showed that the formation of binary hydrogen-graphite intercalation compounds (H-GICs) is highly improbable. Their calculations indicated that H intercalation is much more difficult than the generation of atomic hydrogen, probably due to the lacking of energetically suitable p-orbitals with the hydrogen atoms. Also, convincing experimental evidence for direct intercalation of hydrogen molecules has never been produced [2,3].

In chapter 2 we showed that for sufficient hydrogen storage capacity the adsorbent material has to contain a high volume of suitable micropores. We have also shown that small micropores (0.5-1.0 nm) probably store the highest amount of hydrogen. We have shown in chapter 5 that intercalation of potassium into graphite and carbon nanofibers does increase the hydrogen storage capacity of these materials. These materials, however are not suitable as hydrogen storage materials, because of their high sensitivity to air. So, a suitable adsorbent material needs to be developed using less hazardous materials, which are more stable in air and do not react explosively when contacted with air. Therefore, in this chapter we will focus on one of the well known metal halide Graphite Intercalated Compounds (GICs), that of iron(III)-chloride and on that of iron(II)-chloride as possible hosts for hydrogen. We chose these intercalates for the following reasons:

1. A wide range of iron(III)-chloride GICs can simply be prepared and some authors claim that iron(II)-chloride GICs can be derived from these by cautious reduction, e.g., with hydrogen.
2. The binary iron(III)-chloride GICs are rather stable in air and even in aqueous suspension up to moderate temperatures. They are not poisonous and could be made abundantly available at low costs.
3. The layer distance in the $FeCl_3$-GIC (0.94 nm, see also figure 5.1) is close to optimal for accommodation of hydrogen molecules as is evidenced by Rzepka *et al*. [4] and Darkrim *et al*. [5] and Wang *et al*. [6].

The graphite compounds we used were synthetic graphite, activated graphites and several types of CNFs. Although the preparation of normal graphitic $FeCl_3$-GICs is rather simple, it was questionable whether the intercalation of $FeCl_3$ into CNFs would be successful as well. Literature on this subject is not unambiguous [7].

GICs of $FeCl_3$ have been the subject of intensive research for several decades. The synthesis of different stages of these compounds has been studied for many years, resulting in several successful preparation routes, such as the one zone and the two zone method and the use of a chlorine overpressure [8-11]. The characterization of $FeCl_3$ GICs has been performed with a multitude of different techniques, such as XRD, XPS, TEM, SEM, Raman, TGA and microstructural techniques [12-16].

Intercalation of graphite with $FeCl_3$ is achieved by heating graphite and dry $FeCl_3$ at 300°C in an evacuated glass tube for at least 24 hours. Thermodynamic calculations (see figure 6.1) show that under these conditions mainly Fe_2Cl_6 dimers in the gaseous phase are present. Insertion of these dimers in between the graphite sheets yields the desired $FeCl_3$-GIC. It can be observed from the results in figure 6.1 that part of the $FeCl_3$ decomposes to $FeCl_2$ and Cl_2 at around 250°C to 400°C.

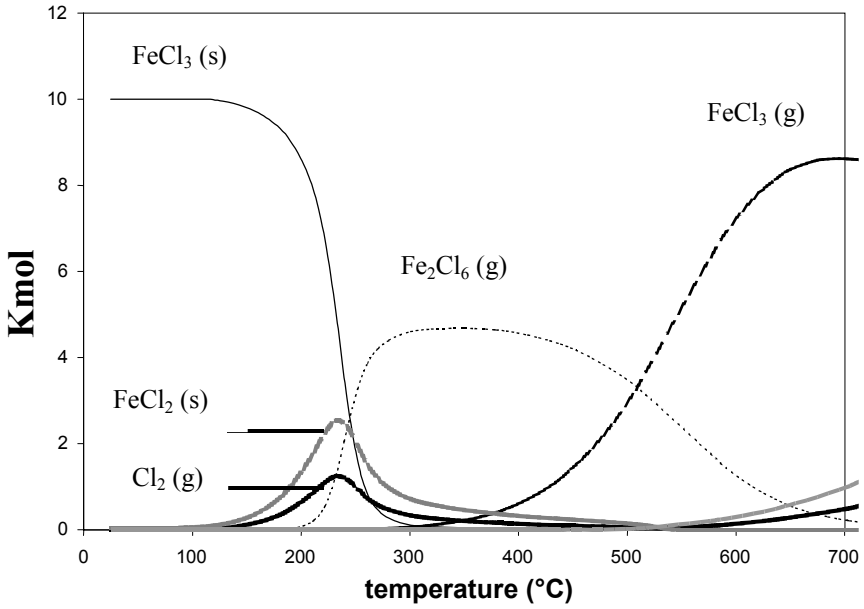

Figure 6.1 Equilibrium composition in a closed system containing 10 moles of $FeCl_3$ at 25°C and constant pressure in vacuum as a function of temperature, obtained using HSC3.

$FeCl_3$ itself crystallizes in a layered NiAs lattice, consisting of alternating Fe^{3+} and Cl^- layers. This structure is more or less maintained upon intercalation, resulting in a compound as schematically represented in figure 6.2. The carbon interlayer distance in $FeCl_3$-GIC, due to the larger ionic radii of the Cl^- ions, is 0.94 nm. As a side reaction, decomposition of $FeCl_3$ into $FeCl_2$ (s) and Cl_2 (g) may occur under reaction conditions. To suppress this reaction, a chlorine overpressure is sometimes applied during intercalation [17]. For $FeCl_3$-GICs stage 1 consists of C_6FeCl_3, stage 2 of $C_{12}FeCl_3$.

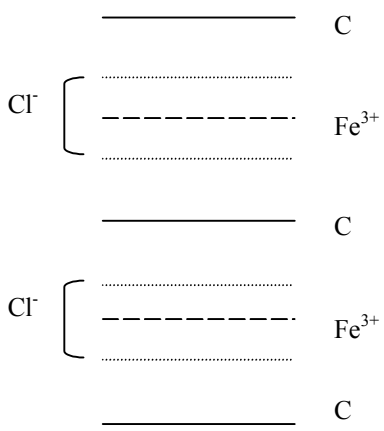

Figure 6.2 Lamellar structure of first stage $FeCl_3$-GIC.

When the extremely hygroscopic $FeCl_3$ crystals are exposed to air, rapid conversion to $FeCl_3.xH_2O$ and eventually hydrolyzed iron compounds takes place. The $FeCl_3$-GIC turns out to be much more stable in air. Probably the graphite layers shield the $FeCl_3$ layers from water. According to literature, long term exposure to air results in de-intercalation and hydrolysis of the intercalated $FeCl_3$ layers. The stability of the GIC is reported to depend on flake size and purity of the graphite used [18].

In this study carbon nanofibers were subjected to intercalation procedures as developed for graphite in order to intercalate $FeCl_3$ between the graphite planes. Because the CNFs are build up of graphitic planes, it was to be expected that intercalation would take place in the same way as in graphite. From literature it is well known that the perfection of the graphitic host lattice might significantly influence the intercalation process. We therefore pretreated some CNF samples at very high temperatures to explore this feature. For intercalation, carbon nanofibers as synthesized were used as well as heat treated samples of which the support, Al_2O_3, had been removed by boiling in HNO_3.

6.2 Literature results

To make these compounds suitable as absorbents for hydrogen, prerequisite of course remains that within the binary GICs enough space is left for the hydrogen. Because of the dense layered structure of iron(III)-chloride itself we anticipated that the density of large chloride ions might be too high to allow for hydrogen uptake to proceed. We therefore decided to examine whether reduction of the $FeCl_3$-GICs into $FeCl_2$-GICs is possible and leads to enhanced H_2 storage capacities. Literature on the reduction is scarce and not conclusive. A lot of effort has been put into the reduction or decomposition of the intercalated $FeCl_3$ to $FeCl_2$ and Fe^0, aiming to synthesize a compound which contains $FeCl_2$ or Fe^0, either atomically dispersed or in the form of small particles, between the graphite sheets [10,17,19,20]. Upon

intercalation with $FeCl_3$, the spacing between graphite sheets increases from 0.34 to 0.94 nm. Several authors claimed that reduction of the $FeCl_3$ layers in a $FeCl_3$ graphite intercalated compound (GIC) to $FeCl_2$ by thermal treatment does not influence the spacing between graphite layers. It is reported that the d-spacing in this $FeCl_2$-GIC remains 0.94 nm [14,16,21]. There is however no consensus and clarity on the nature and structure of the resulting compounds and on the processes that take place during such a reduction [21-25]. Several authors reported on the existence of so-called iron-graphite [17,21-25]. These compounds were believed to consist of alternating layers of graphite and metallic iron. In an attempt to prepare this material, Herein *et al*. [21] heated stage 1 $FeCl_3$-GIC in a H_2 atmosphere to achieve reduction of $FeCl_3$ to $FeCl_2$ or Fe^0 between the graphite layers. The $FeCl_3$-GIC samples were heated at a heating rate of 1°C/h to 500°C and characterized by XRD and SEM with EDX. At moderate temperatures of 250-300°C, reduction of the $FeCl_3$ layers to $FeCl_2$ was reported. Heating to 500°C resulted in the nearly complete de-intercalation and formation of three-dimensional Fe^0 particles on the external graphite surface.

The thermal behavior of stage 2 $FeCl_3$-GIC was studied *in situ* by Nagai *et al*. [14], using an analytical electron microscope. In their experiments, $FeCl_3$-GIC was heated in vacuum up to 400°C while electron diffraction (ED) patterns and electron energy loss spectra (EELS) were collected. They observed partial de-intercalation of $FeCl_3$ upon heating to 250°C and claimed that the remaining $FeCl_3$ between the graphite layers decomposed into $FeCl_2$ and Cl_2. At 400°C the chlorine gas, which up to that temperature remains in the GIC, is released which leads to a gradual conversion to $FeCl_2$-GIC.

Begin *et al*. [16] also claimed the formation of $FeCl_2$-GIC by thermal treatment of a $FeCl_3$-GIC. The changes in structure of a stage 1 $FeCl_3$-GIC upon heating in inert atmosphere were monitored using XRD. Samples were heated at a heating rate of 20°C/min up to 750°C. At 500°C two peaks appeared in the XRD pattern, which were attributed to the formation of $FeCl_2$-GIC. In the paper however, the exact positions of these peaks are not mentioned and they cannot be derived from the XRD patterns, as they were presented in a schematic way. The authors reported desorption of $FeCl_3$ from between the graphite sheets between 350°C and 550°C. TGA analysis was performed while heating the $FeCl_3$-GIC at different heating rates (5, 10, 20°C/min). Desorption proved to be more complete with increasing heating rate. Crystallinity of the graphite used was also found to be of influence on the desorption process. A $FeCl_3$-GIC prepared from monocrystalline graphite showed less desorption than polycrystalline graphite $FeCl_3$ intercalation compounds.

Research described in this chapter is aimed at the preparation of $FeCl_3$-GICs, using the method developed by Kalucki [8]. After synthesis and characterization we attempted to prepare $FeCl_2$ or Fe^0 intercalated materials by thermal decomposition of $FeCl_3$ between the layers and by reduction of the $FeCl_3$-GIC with H_2. This chapter describes the results of these experiments and the subsequent analyses performed with SEM, XRD, TPR, BET, XPS and TGA. Also the H_2 storage capacity of the prepared products was measured.

6.3 Experimental

Fishbone carbon nanofibers (CNF-Eng) were produced in the fluidized bed (see chapter 3) at 570°C using catalytic decomposition of methane over the 60 wt% commercial catalyst from Engelhard (Ni 3288). To remove exposed Ni (< 2.3 wt% after fiber growth) and Al_2O_3 (< 1.5 wt% after fiber growth), 10 grams of the as synthesized fibers were refluxed for 2 hours in 100 ml boiling concentrated HNO_3. Subsequently the fibers were washed with water and dried for 16 hours at 120°C.

A pretreatment in HNO_3 leads to oxidation of the surface of the fibers, creating for instance carboxyl and carbonyl groups [26]. To prevent their interference with the chemistry at high temperatures the oxygen containing groups were largely removed by heating the samples at 800°C for 4 hours in a nitrogen flow (CNF-Eng-pt).

We also used commercially available parallel fibers (CNF-Hyp, Hyperion), which are grown from Fe. They were not subjected to any pretreatments to remove impurities.

Carbon nanofibers of the parallel type (CNF-Par) were produced by catalytic decomposition of syngas, a mixture of CO and H_2, over Ni/Al_2O_3 catalysts. The Ni/Al_2O_3 catalyst with 20 wt% Ni metal loading was synthesized by a deposition-precipitation technique. Alumina (Alon-C, Degussa) was suspended in an acidified (pH=3) aqueous solution of nickel nitrate (0.086 M, Across, 99%). Ammonia (0.5 M) was injected for two hours at room temperature under vigorous stirring until the pH had reached a value of 8.5. Next, the suspension was filtered and the residue was washed, dried at 120°C and calcined at 600°C in stagnant air for three hours. Parallel carbon nanofibers were synthesized in small quantities in a fully automated micro-flow system. For the growth of parallel carbon nanofibers, 100 mg of the calcined precursor of the 20 wt% Ni/Al_2O_3 catalyst was reduced at 700°C in 20% H_2/Ar (flow rate 100 ml/min.) in a micro-flow reactor for two hours. Then, the temperature was decreased to 600°C and synthesis gas (20% CO and 7% H_2 in Ar, flow rate 100 ml/min.) was passed through the reactor during 10 hours. After reaction, about 0.5 g of parallel fibers were collected [26].

The fibers were heat treated at 1600 and 2000°C (CNF-Eng-1600, CNF-Eng-2000, CNF-Hyp-2000, CNF-Par-2000). All samples were kept at the desired temperature for 30 minutes in an Ar atmosphere. Details of the heat treatment can be found in chapter 4, section 4.2.

Synthetic graphite was obtained from Fluka Chemika (Fluka Chemika Graphite 50870) and not subjected to any pretreatments before use. In the remainder of this chapter this material will be simply referred to as ‘graphite’.

Activated graphites were obtained from Lonza. These materials have a significant micropore volume (0.3 and 0.5 ml/g), which is the result of a specific activation treatment. They are referred to as AG-100 and AG-300. To prevent the interference of oxygen-containing groups on the surface with the intercalation mechanism these groups were largely removed by heating the samples at 800°C for 4 hours in a nitrogen flow (AG-100-pt and AG-300-pt).

All GICs were prepared using the method developed by Kalucki [8]. A weighed amount of $FeCl_3$ (Aldrich, 97%) was transferred, using standard nitrogen bag techniques, into an ampoule already containing a weighed amount of graphite or CNFs. Typically 0.75 g carbon, 2 g $FeCl_3$ and an ampoule of ~15 ml were used. After mixing the two components the ampoule was evacuated, sealed and heated up to 300°C and kept at this temperature for 72 hours in case of the graphite samples. With the CNF samples the ampoules were kept at 300 or 400°C for periods ranging from 3 days to 3 weeks. After the heating period the ampoule was cooled to room temperature, opened and after which the samples were suspended in a mixture of HCl and water in a volume ratio of 1:1 and swirled for 2 hours to ensure that no residual $FeCl_3$ remained on the external surface. After washing the suspension was filtered, using a Büchner funnel, and dried at 120°C for 16 hours in air.

Heat treatments in a flow of pure N_2 or in a flow of 20% H_2 in N_2 were performed in a standard fixed bed reactor at temperatures in the range of 250°C to 600°C. Various details of the treatments are depicted in table 6.1.

Table 6.1 Temperature programs applied for reduction and heat treatment of $FeCl_3$ intercalated graphites.

325°C		550°C	
Temperature interval	Heating rate/ dwell time	Temperature interval	Heating rate/ dwell time
20-150°C	300°C/hr	20-175°C	300°C/hr
150-325°C	5°C/hr	175-550°C	120°C/hr
325°C	1 hr	550°C	1 hr

XRD patterns were recorded at room temperature with a Nonius PDS 120 powder diffractometer system equipped with a position-sensitive detector with a 2θ range of 120°. The radiation used was Co $K\alpha_1$ (λ=1.78897 Å).

TPR measurements were performed in a Thermoquest TPDRO 1100. Weighed samples of about 50 mg were exposed to 5% H_2 in Ar (total flow 20 ml/min). The temperature was raised with 5°C/min up to 1050°C. The consumption of hydrogen was measured with a hot wire detector.

Scanning Electron Microscopy was performed with a Philips XL30 FEG apparatus, equipped with an EDX facility.

N_2 physisorption data were obtained with a Micromeritics ASAP 2400 apparatus. From the results the BET surface area, total pore volume, micropore volume and t-surface were derived.

H_2 adsorption measurements at 77 K up to a pressure of 1 bar were performed with a Micromeritics ASAP 2010 or in a conventional static adsorption apparatus, made of Pyrex glass. For more details about the Pyrex adsorption apparatus see chapter 5.

The XPS data were obtained with a Vacuum Generators XPS system, using a CLAM-2 hemispherical analyzer for electron detection. Non monochromatic Al(K_α) X-ray radiation was used for exciting the photo electron spectra using an anode current of 20 mA at 10 keV. The pass energy of the analyzer was set at 20 eV. The survey scan was taken with a pass energy of 100 eV.

TGA analyses were carried out on a Netzsch STA-429 thermobalance. Samples of approximately 20-100 mg were heated in a flow of Ar or a flow of 5% H_2 in Ar at a heating rate of 300°C/h up to 850°C.

6.4 Results and discussion

6.4.1 Intercalation experiments in graphite and carbon nanofibers.

In a typical intercalation experiment, 0.75 g carbon, 2.0 g of $FeCl_3$ and an ampoule of ~15 ml were used. The $FeCl_3$ was transferred using standard nitrogen bag techniques into the ampoule, which already contained the weighed amount of graphite or CNFs. After mixing the two components the ampoule was evacuated, sealed and heated up to 300°C and kept at this temperature for several days. After the ampoule was cooled to room temperature it was opened, after which a chlorine smell was often detected. After synthesis, the GIC was always washed to remove excess $FeCl_3$ present on the surface.

In figure 6.3 representative XRD diffractograms of a stage 1 $FeCl_3$ intercalation in graphite and of carbon nanofibers treated with $FeCl_3$ are shown. It is obvious that with the nanofiber sample no intercalate had been formed, because the (d_{002}) peak does not shift to lower 2θ values. This shift to lower 2θ values is indicative of the enlargement of the d-spacing which results from the intercalation of $FeCl_3$ between the graphite planes.

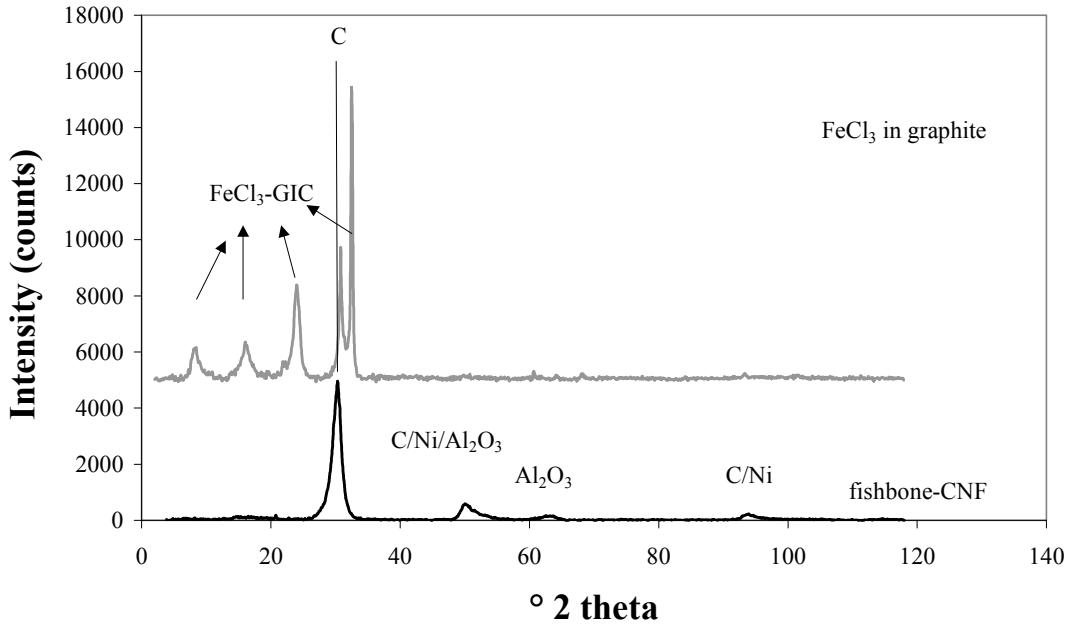

Figure 6.3 XRD pattern of $FeCl_3$ intercalated graphite and a fishbone CNF sample which has undergone the same treatment.

In table 6.2 the d-values of the most important reflections of graphite and stage 1 and 2 $FeCl_3$-GIC are shown. Intercalated carbon nanofibers should show the same enlargement of the d-spacing, from 0.336 to 0.941 nm for the (d_{002}) reflection.

Table 6.2 Most important reflections of graphite and $FeCl_3$ intercalated graphite, stage 1 and 2, d-values and intensities.

Sample	d-values (Å)/intensity (%)					
graphite	3.36/100	2.03/50	1.678/80	1.158/50	0.994/40	0.829/40
stage 1 $FeCl_3$-GIC	10.9/30	9.41/65	7.50/25	4.67/100	3.33/20	3.13/80
stage 2 $FeCl_3$-GIC	12.8	6.43	4.30	3.33		

In figure 6.4 the XRD results of two carbon nanofibers treated with $FeCl_3$ and subsequently washed are shown. A heat treated fishbone fiber and a pretreated fiber which has been heated with $FeCl_3$ in an ampoule for 7 days at 400°C are shown. It is obvious that the materials have not been intercalated, because they do not show any peaks typical for intercalation. The only peaks visible can be assigned to graphite, Ni or Al_2O_3 present in the fibers.

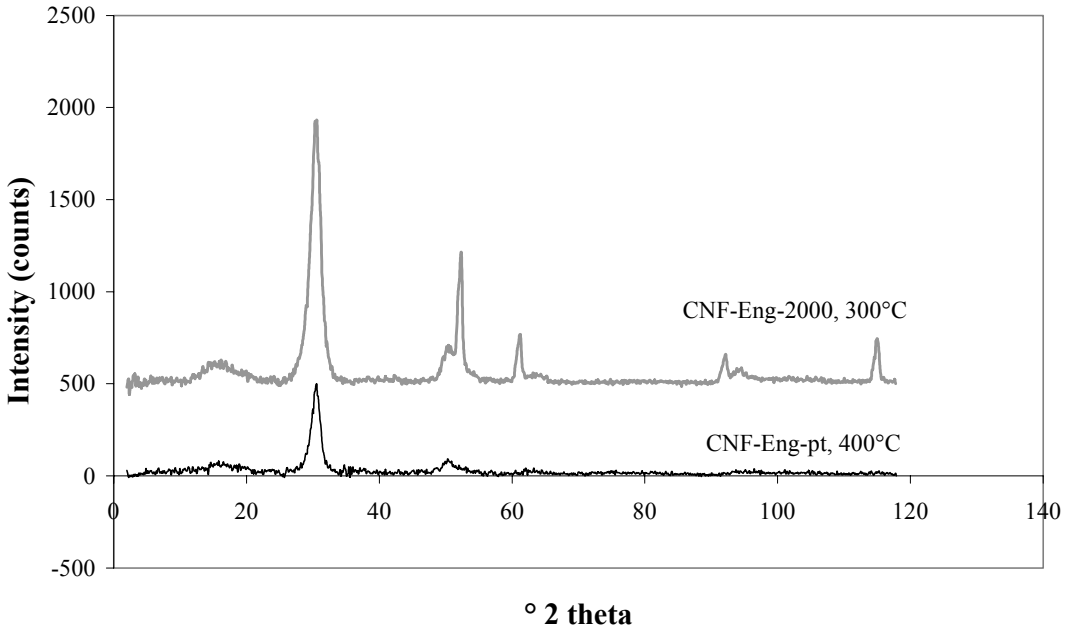

Figure 6.4 XRD-results of fishbone fibers treated with $FeCl_3$.

The XRD results of all intercalation experiments with the carbon nanofibers are summarized in table 6.3.

Table 6.3 Results of the intercalation experiments of carbon nanofibers with $FeCl_3$.

Sample	Temperature (°C)	Reaction time (days)	Most intense XRD peak (d-value)	Intercalation (yes/no)
CNF-Eng	300	3	3.4	No
CNF-Eng	400	3	3.4	No
CNF-Eng	300	7	3.4	No
CNF-Eng	300	21	3.4	No
CNF-par	300	3	3.4	No
CNF-Hyp	300	3	3.4	No
CNF-Eng-pt	300	3	3.4	No
CNF-Eng-pt	400	7	3.4	No
CNF-Eng-1600	300	3	3.4	No
CNF-Eng-2000	300	3	3.4	No
CNF-Par-2000	300	3	3.4	No
CNF-Hyp-2000	300	3	3.4	No

Only with ordered graphite $FeCl_3$-GICs can be obtained. Thus, CNFs show a deviating behavior towards intercalation from that of normal graphite. This difference may be explained with different theories. The size of the graphite domains of the fibers may be too small to stabilize the intercalation compound. The graphite planes of graphite are more extended than those of fishbone fibers (see also the results described in chapter 4). It might be reasonable to assume that a minimum plane or domain size is needed to bring about the stability of the GIC compound. In order to check this proposition, graphite fibers with diameters between 200 and 1000 nm were grown from unsupported Ni particles and subjected to the intercalation procedure. Also with these thick fibers, intercalation failed to occur. A HRTEM study revealed, however, that also these thick fibers consisted of many small graphitic domains, not larger than the small fishbone fibers grown from the small supported Ni particles.

To find other arguments for this hypothesis, activated graphites, obtained from Lonza, were also subjected to the same intercalation pretreatment. These materials have a significant micropore volume, which is the result of a specific activation treatment. The high pore volume of these materials suggests that, compared to untreated graphite, the graphitic domains are much smaller. In table 6.4 the characteristics of the as synthesized materials are given. The results of the intercalation experiments of the activated graphites are summarized in table 6.5.

Table 6.4 Characteristics of the as synthesized Lonza graphites.

Sample	Most intense XRD peak (d-value)	BET surface area (m^2/g)	Total pore volume (ml/g)
AG-100	3.4	119	0.3
AG-100-pt	3.4	111	0.2
AG-300	3.4	287	0.5
AG-300-pt	3.4	292	0.5

Table 6.5 Results of the intercalation experiments of Lonza graphites with $FeCl_3$.

Sample	Temp (°C)	Reaction time (days)	Most intense XRD peak (d-value)	BET surface area (m^2/g)	Total pore volume (ml/g)	Intercalation (yes/no)
AG-100	300	3	3.34 & 4.67	51	0.2	yes
AG-100-pt	300	3	3.34 & 4.67	71	0.2	yes
AG-300	300	3	3.34	280	0.5	no
AG-300-pt	300	3	3.34	280	0.5	no

From the above results it can be deceived that only with samples with a specific surface area smaller than 300 m^2/g intercalation (or partial intercalation) proceeds, which is strong evidence for our hypothesis that the extend of the graphite planes influences the stability of the intercalation compound. Further research, for instance with graphites with intermediate sized domains is necessary to draw more quantitative conclusions.

Another and perhaps an additional explanation for the deviating intercalation behavior of the nanofibers may be found in the higher energy that is needed to increase their d-spacing. In graphite the carbon atoms in the flat planes are strongly bound, but in the c-direction the material is only stabilized by relatively weak Van der Waals forces. It is therefore quite easy for a layer structured compound, like $FeCl_3$, to penetrate between the graphite planes and lift these. This is shown by the large range of materials, e.g. $CuCl_2$, $CuBr_2$, K, Rb, Cs etc., that can be intercalated in graphite [10,11]. In CNFs, however, the planes may be connected to each other in the center of the tube and many planes are connected in the bulk of the fibers via the large number of defects present there. In chapter 4 we showed evidence of these 'bulk' defects, both in as-synthesized and in heat treated fibers. These connections may make it impossible for the (Fe_2Cl_6) intercalating species to lift up the planes sufficiently to allow intercalation and formation of a stable compound. This rigidity of the structure is quite different from that of normal graphite and could very well explain the behavior of the CNFs with regard to intercalation. To examine whether these aforementioned defects affect the intercalation behavior of the fibers negatively the fibers were subjected to heat treatment up to 2000°C in order to reduce the amount of defects. Details of the experiments and results are included in chapter 4. Since we found that heat treatment up to 2000°C only influenced the surface of the fibers and did not affect the bulk structure it is not surprising that with the heat treated fibers intercalation of $FeCl_3$ failed to occur too.

In 1996, Mordkovich *et al*. [7] reported the intercalation of multiwalled nanotubes by K and $FeCl_3$. However, the TEM pictures of the heated samples shown suggest that only large particles of the added components were present on the surface of the tubes, because the material 'comes out' of the tubes when exposed to air and can be removed with washing. The remaining tubes are still intact, which is highly unlikely after intercalation in a parallel multi walled carbon nanotube.

Endo *et al*. reported [27] that it is possible to intercalate vapor grown fibers after heat treatment at 2900°C for 30 minutes. It is known that after treatment at that temperature the material shows characteristics of well-organized graphite.

Because of the negative results with respect to the intercalation of CNFs we decided to continue our investigation with intercalated well-ordered graphite materials. From thermodynamic calculations (see section 6.1, introduction) it is obvious that $FeCl_3$ decomposes to $FeCl_2$ and Cl_2 when heated to 300°C. So it was decided to use this approach to create $FeCl_2$ intercalated graphite. This would possibly create a microporous structure between the graphite planes.

6.4.2 TGA and TPR results

The thermograms of stage 1 $FeCl_3$-GICs in H_2 and N_2 atmosphere are, as shown in figure 6.5, almost identical up to about 400°C. For both a weight loss of 17% is measured. Upon further heating, the weight of the sample heated in N_2 remains more or less constant to 600°C, before falling to 55% of the original weight at 800°C. XRD measurements (see section 6.4.4) show almost complete de-intercalation of $FeCl_3$-GIC samples after heat treatment at 550°C. The first weight loss step in both atmospheres may be attributed to de-intercalation of the $FeCl_3$ from between the graphite sheets. Part of this $FeCl_3$ is evaporated and taken away in the gas stream. Some remains at the surface and is decomposed to $FeCl_2$ and Cl_2. The thus formed Cl_2 also desorbs from the surface of the sample. The $FeCl_3$ evaporation was also observed as the $FeCl_3$ material condensed again on the colder surfaces of the set-up. In the nitrogen atmosphere the second weight loss step between 600 to 800°C can be attributed to the desorption of the de-intercalated $FeCl_2$ species from the surface of the graphite. For the reduction, performed in a H_2 containing atmosphere, part of the de-intercalated $FeCl_3$ is reduced to $FeCl_2$ before it can evaporate from the surface and eventually on to Fe^0. The formed HCl evaporates from the surface, causing the weight loss between 400 and 600°C. The formed iron particles remain on the graphite flakes. This explains the higher remaining weight of the reduced sample, when compared to the sample heated in N_2.

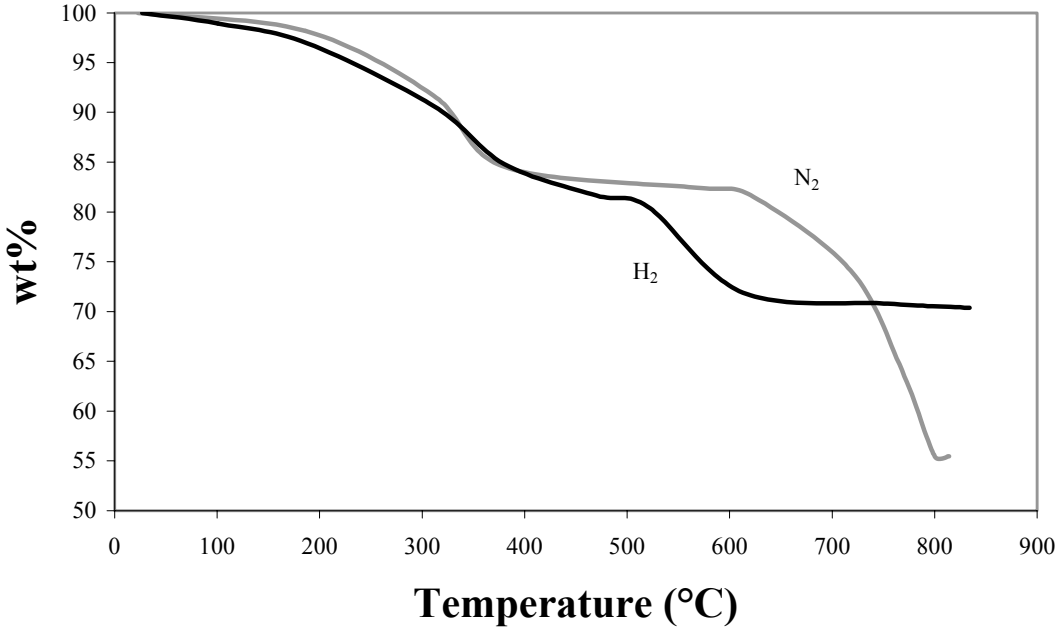

Figure 6.5 TGA curves $FeCl_3$ GIC in N_2 and H_2 atmosphere.

An unexpected observation with the sample in H_2 flow is the lack of weight loss above 600°C. Probably, even after metal formation the graphite matrix is stable in H_2 flow up to 800°C. Also with TPR measurement of the sample obviously H_2 consumption approaches again to zero at 800°C and H_2 consumption up to that temperature we can ascribe to a stepwise reduction of the originally intercalated $FeCl_3$ phase.

From the thermograms as shown in figure 6.5 we can conclude that quantitative interpretation from the total amount of H_2 consumption with TPR (figure 6.6) should take into account that part of the de-intercalated $FeCl_3$ is removed from the reactor with the gas stream. Nevertheless, in view of the pattern of the course of the H_2 consumption we are convinced that up to 325°C reduction of $FeCl_3$ to $FeCl_2$ proceeds and next, beyond 400°C further reduction of $FeCl_2$ to Fe^0 takes place, which reaction is completed at ~800°C. Thus, the TPR results nicely agree with the TGA results. Based on above observation we decided to further characterize samples of the stage 1 $FeCl_3$-GIC after treatment in N_2 at 325°C in order to prepare stage 1 $FeCl_2$-GIC. Also stage 1 $FeCl_3$-GIC samples were reduced using H_2 at 550°C, a temperature at which most of the $FeCl_2$ phase is reduced to Fe^0.

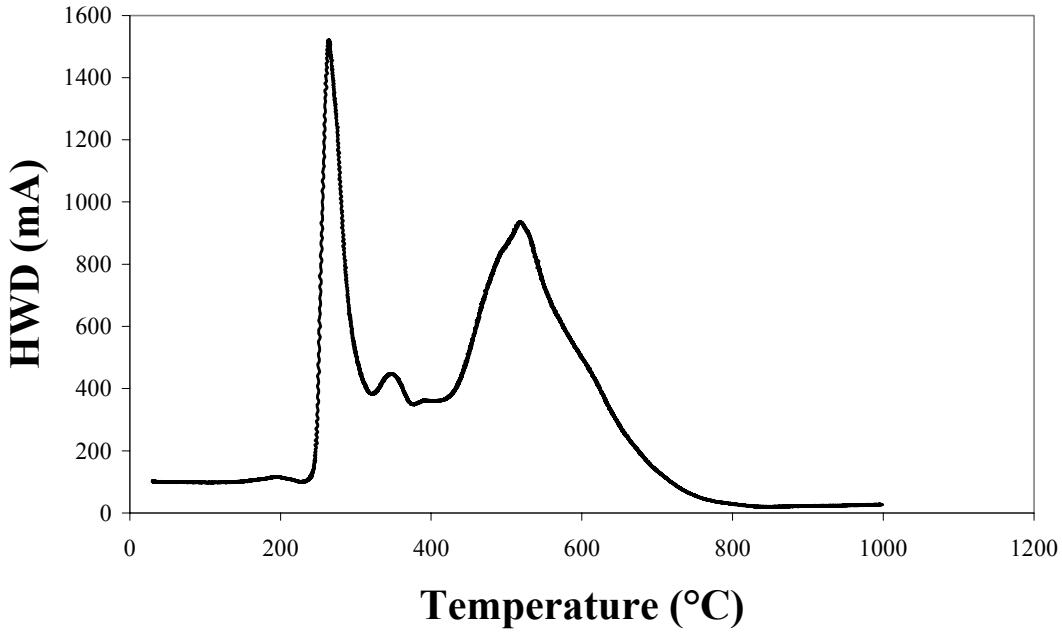

Figure 6.6 TPR profile of a stage 1 $FeCl_3$ intercalated graphite.

For further characterization, SEM, TEM and XPS were used. There we must stress that for analysis the heat treated samples were exposed to air during transport and, undoubtedly $FeCl_3$, $FeCl_2$ and Fe^0 present have become hydrolyzed and/or oxidized before measurement.

6.4.3 SEM results of $FeCl_3$ intercalation in graphite

Untreated and $FeCl_3$ intercalated graphite samples were studied with SEM to find out to what extent intercalation has effect on the morphology of the sample.

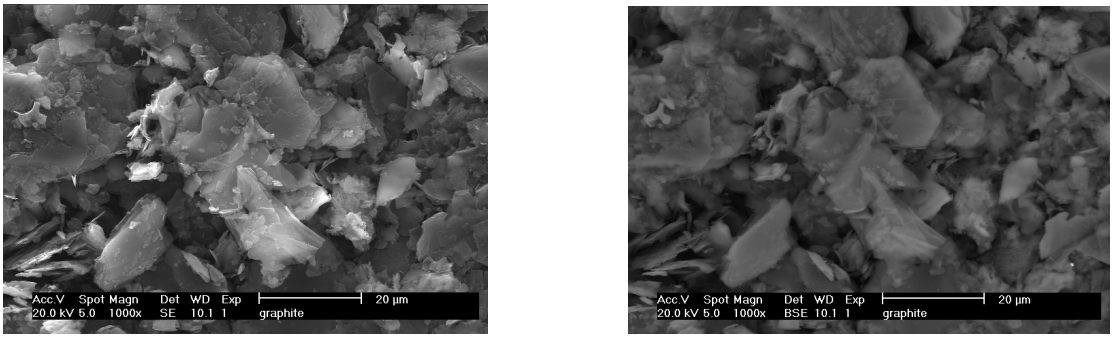

Figure 6.7 Scatter- (left) and backscatter- (right) image of untreated Fluka Chemika graphite.

From figure 6.7 it is obvious that the size distribution of the graphite flake size is broad. The graphite flakes range from 1 to 20 µm and are up to 1 µm thick. From backscatter images and EDAX analysis it is concluded that there are no heavy element impurities present in the graphite.

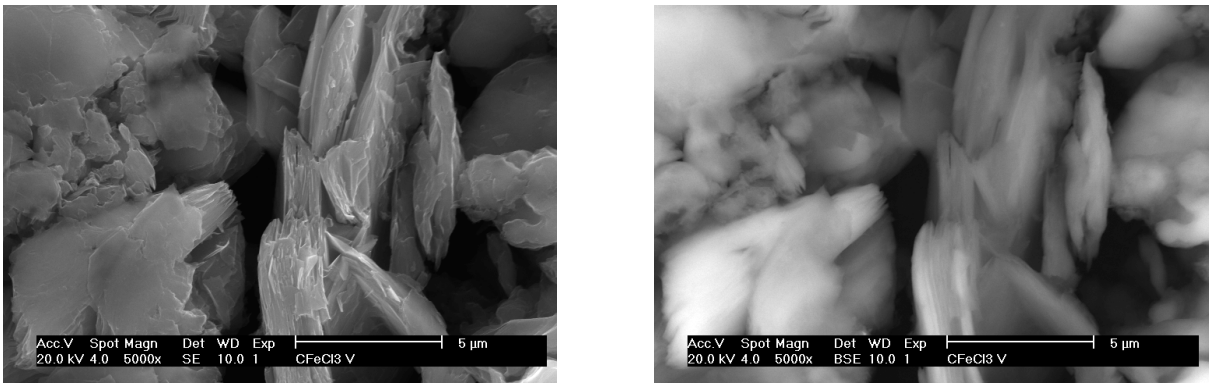

Figure 6.8 Scatter- (left) and backscatter- (right) image of stage 1 $FeCl_3$ intercalated graphite.

In figure 6.8 it is visible that in the intercalated samples regions are present, which do not differ much from untreated graphite. However, in figure 6.9 it is shown that there are regions where the mesoscopic structure of the graphite flakes has been affected. There are significant cracks in the surface, which run parallel to the graphite planes. The backscatter-image and EDAX analysis (see figure 6.10) show that in all samples $FeCl_3$ is distributed homogeneously.

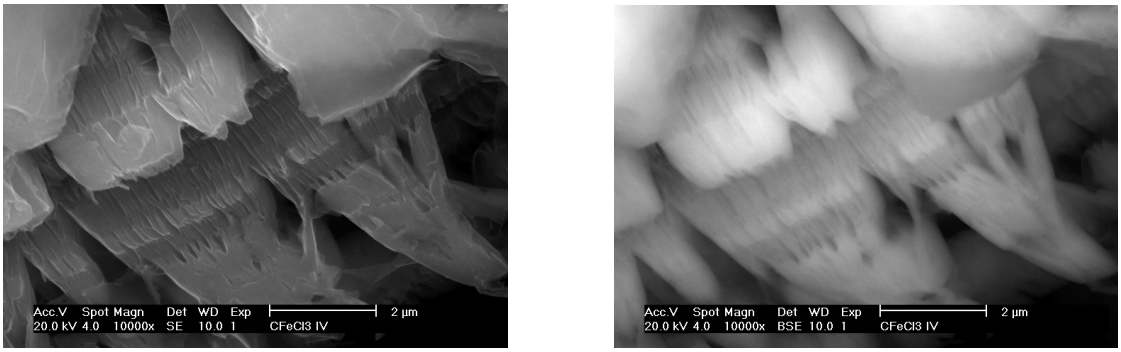

Figure 6.9 Scatter (left) and backscatter (right) image of exfoliated stage 1 $FeCl_3$ intercalated graphite.

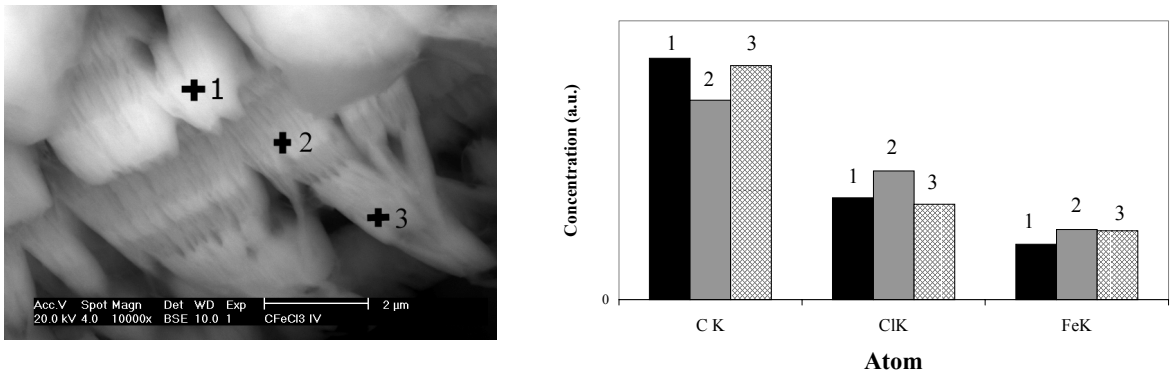

Figure 6.10 Qualitative EDAX analysis of $FeCl_3$ intercalated graphite.

The cracks in the GICs are a well-known result of the stress caused by the expansion of the space between the graphite planes, brought about by intercalation. This process is called exfoliation [12].

6.4.4 Heat treatment in N_2 of $FeCl_3$ intercalated graphite

As we stated earlier, heat treatments at 325°C could result in the formation of a $FeCl_2$-GIC. However, it turns out that when the intercalated graphites are heated in nitrogen at 325°C, de-intercalation of the $FeCl_3$ phase takes place. SEM images show large amounts of small particles on the surfaces of the graphite flakes. With XRD these particles are identified as Fe_2O_3, which results from $FeCl_2$ particles, which have been contacted with air. Probably, de-intercalation takes place via the edges of the graphite planes, because the highest concentration of particles can be found there (see figures 6.11 and 6.12).

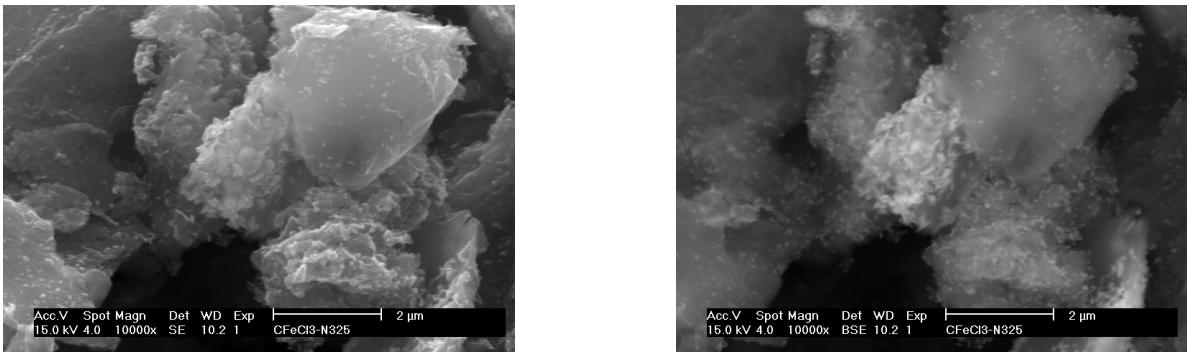

Figure 6.11 Scatter (left) and backscatter (right) image of $FeCl_3$ intercalated graphite, heat treated at 325°C.

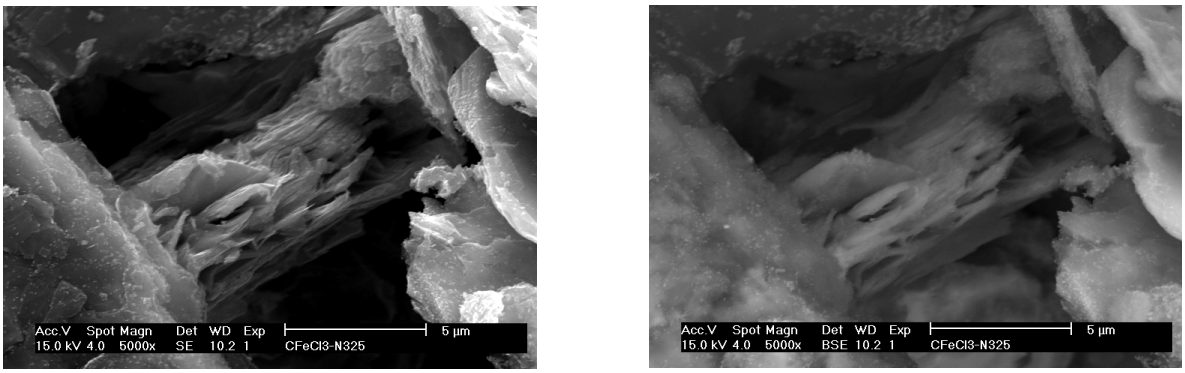

Figure 6.12 Scatter (left) and backscatter (right) image of $FeCl_3$ intercalated graphite, heat treated at 325°C.

When the GICs are heat treated at 325°C and subsequently washed in HCl the particles as present in the unwashed sample had disappeared (see figures 6.13 and 6.14).

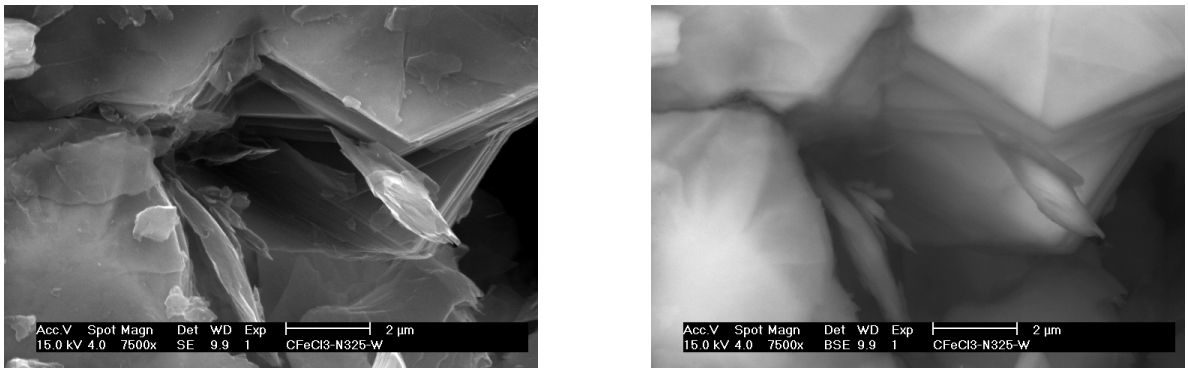

Figure 6.13 Scatter (left) and backscatter (right) image of $FeCl_3$ intercalated graphite, heat treated in N_2 at 325°C and subsequently washed.

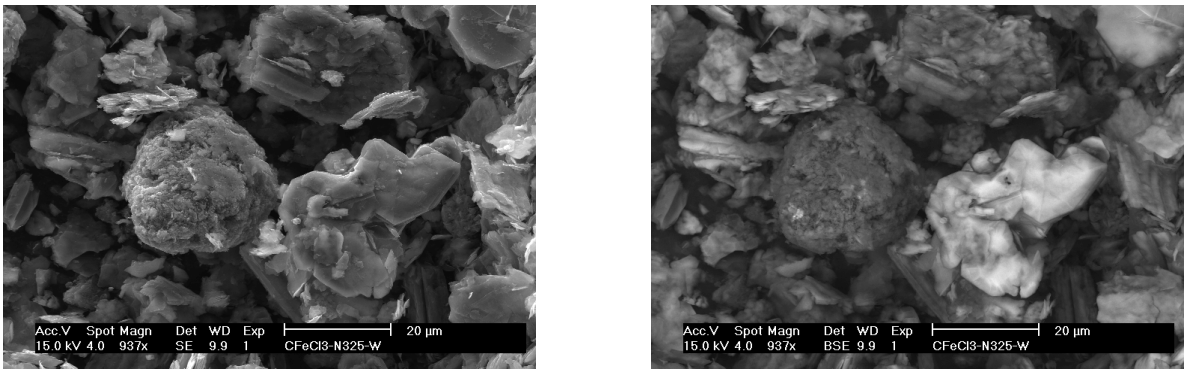

Figure 6.14 Scatter (left) and backscatter (right) image of $FeCl_3$ intercalated graphite, heat treated in N_2 at 325°C and subsequently washed.

Obviously, after heat treatment in N_2 at 550°C, the iron containing phase, which comes out between the planes is completely covering the edges of the graphite planes, in the shape of a large slab. From the backscatter images (figures 6.15 and 6.16) it is suggested that no $FeCl_3$ has remained in the graphite.

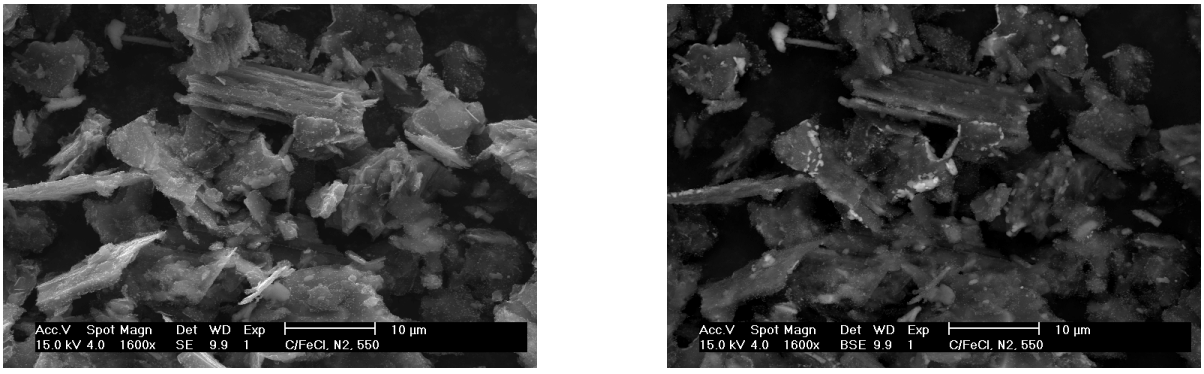

Figure 6.15 Scatter (left) and backscatter (right) image of $FeCl_3$ intercalated graphite after heat treatment at 550°C.

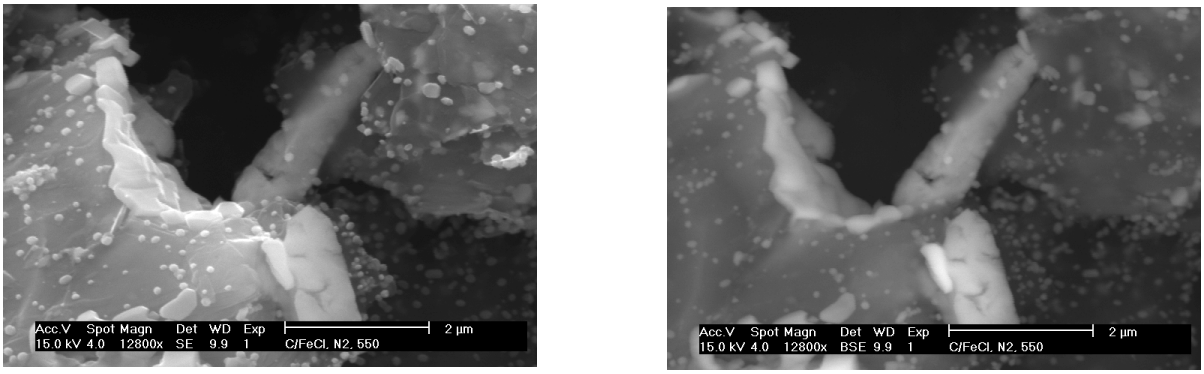

Figure 6.16 Scatter (left) and backscatter (right) image of $FeCl_3$ intercalated graphite after heat treatment at 550°C.

XRD patterns (figure 6.17) were collected on both as synthesized and washed samples. The XRD results are in agreement with the changes observed with the SEM. The peaks of a stage 1 and a stage 2 $FeCl_3$ intercalated graphite are summarized in table 6.2.

For the intercalated graphites heat treated in N_2 at 325°C, roughly the same is observed as with electron microscopy, namely the partial de-intercalation of $FeCl_3$ from the graphite planes. The stage 1 peaks diminish and disappear, stage 2 peaks appear and the intensity of the unreacted graphite slightly increases. Furthermore, also Fe_2O_3 peaks appear. After washing, some of these peaks have disappeared, but some remain, indicating that the washing procedure does not remove all the de-intercalated $FeCl_3$ and/or Fe_2O_3 particles from the surface. It is also clear that there is still $FeCl_3$ left after this treatment, because there are still peaks present, which are attributed to the intercalated species.

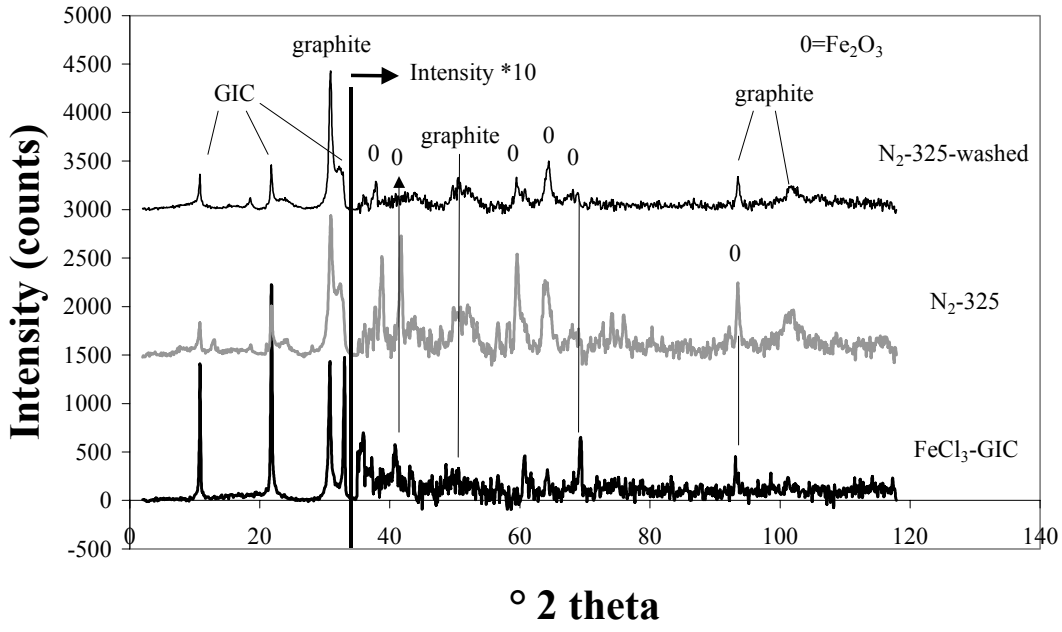

Figure 6.17 XRD patterns of $FeCl_3$ intercalated graphite, and this material heat treated in N_2 at 325°C, before and after washing.

At 550°C, almost all $FeCl_3$ has de-intercalated from the graphite as was also concluded from the TGA and SEM results. The $FeCl_3$ and Fe_2O_3 peaks remain, especially on the as synthesized sample. The heat treated and washed sample is almost completely graphitic, with only very small peaks remaining that can be attributed to $FeCl_3$ intercalated GIC.

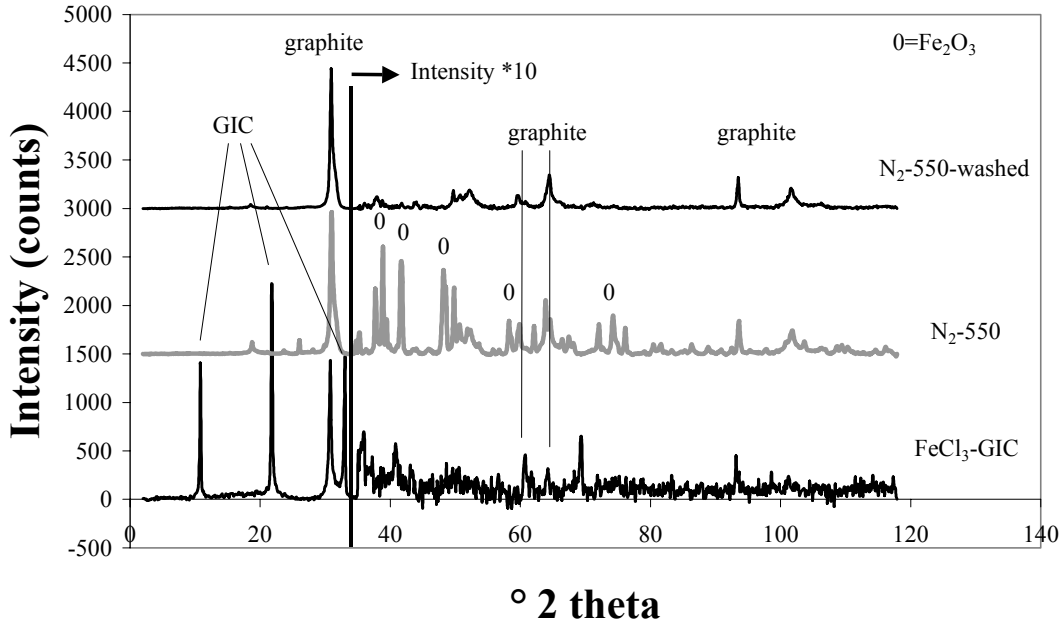

Figure 6.18 XRD patterns of $FeCl_3$ intercalated graphite, and this material heat treated in N_2 at 550°C, before and after washing.

Because XPS is a surface sensitive technique it was used to asses the structure of the species present at or near the surface. Literature data on expected binding energies of Fe- and Cl-species are collected in table 6.7.

Table 6.7 Handbook results of the peak positions of Fe and Cl in $FeCl_3$ compounds [28].

Compound	Fe-position (eV)	Cl-position (eV)
Fe(0)	706.8	-
$FeCl_2$	710.3	198.6
$FeCl_3$	711.1	198.8

It is obvious from figure 6.19 that after heat treatment at 325°C and subsequent washing Fe remains on the surface. All samples show also the characteristic 'Fe_2O_3 peak' at 725 eV. This can be explained with the reaction of the $FeCl_3$ or $FeCl_2$ species with H_2O from the air. This obviously takes place when the $FeCl_3$ material is outside the graphite planes, after reduction at 325°C, but it also takes place at the exposed edges of the intercalated material. According to XRD results these materials were stable for a very long time in air, but these XPS results show that surface oxidation takes place to some extent.

The same Fe_2O_3 peak can be observed in the other samples, however because the intensity of the peaks is much lower, this is not so distinct. Since these materials have also been subjected to O_2 and H_2O containing environments it is also expected to observe the effects of reactions with these compounds.

After washing and after heat treatment at 550°C, the intensity of the Fe- and Cl-signal diminishes, because a lot of the surface of the graphite is no longer 'covered' with $FeCl_3$ or Fe- and Cl-containing compounds. The presence of the typical Fe_2O_3 bump is the result of reactions with O_2 and H_2O from the air.

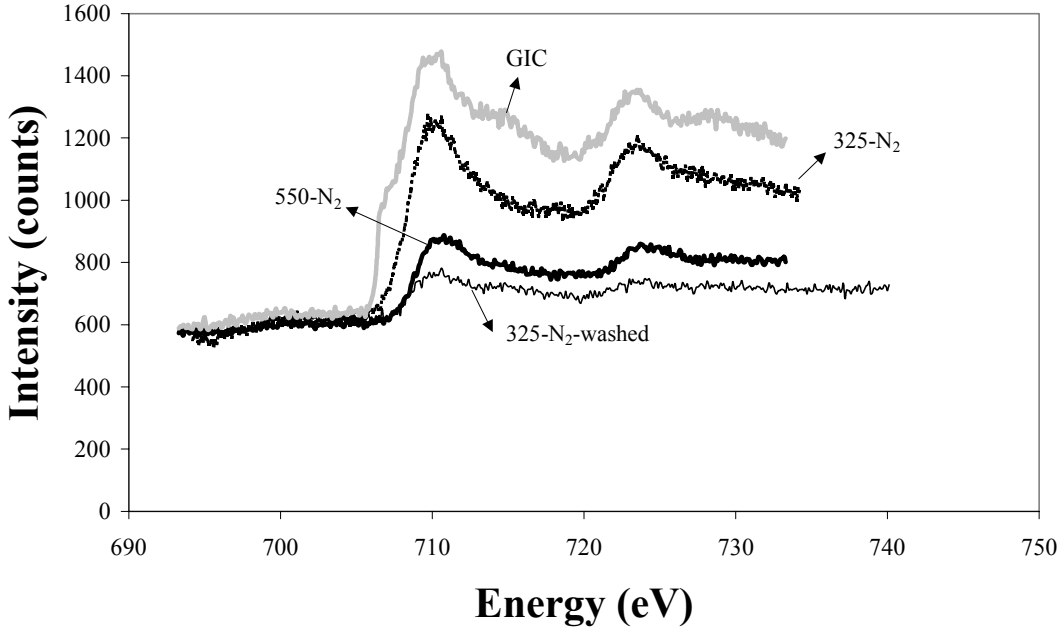

Figure 6.19 XPS results of the $FeCl_3$ GIC materials heat treated in N_2 at 325 and 550°C, eV range containing the Fe-signal.

In table 6.8 the intensities of the Fe- and Cl-signals are compared. The shape of the Fe-peaks makes it difficult to determine the surface area. From the results it is obvious that the heat treated materials have largely reacted with O_2 and H_2O, because the relative intensities of the Cl-peaks are much lower than with the untreated samples. It is clear that the Fe_2O_3 bump, which makes the surface area of the Fe-peak very undefined, causes the GIC-sample to not display the Fe/Cl ratio consistent with $FeCl_3$.

The positions of the peaks were corrected on the C-peak, but because of the broad shape of especially the Fe-peaks, an error of about 1 eV in the peak position is assumed. So from the peak positions it can be concluded that the present species are either Fe^{2+} or Fe^{3+}.

Table 6.8 Ratio of Fe and Cl from the surface of the XPS peaks of the reduced intercalated $FeCl_3$ in graphite samples.

Sample	Fe surface area (a.u.)	Cl surface area (a.u.)	I_{Cl}/I_{Fe}	I_{Fe}/I_C	I_{Cl}/I_C
$FeCl_3$-GIC	2941	827	2.07	0.06	0.13
N_2-325	4313	690	0.69	0.08	0.05
N_2-325-washed	851	331	1.68	0.01	0.03
N_2-550	1234	281	0.98	0.02	0.03

Table 6.9 Peak positions of Fe and Cl of the reduced $FeCl_3$ in graphite samples.

Sample	Corrected Fe peak (eV)	Corrected Cl peak (eV)
$FeCl_3$-GIC	710 ± 1	199
N_2-325	710 ± 1	198
N_2-325-washed	710 ± 1	198
N_2-550	711 ± 1	199

6.4.5 Reduction of $FeCl_3$ intercalated graphite

The GICs were reduced with H_2 at 325°C in hope to reduce intercalated $FeCl_3$ to $FeCl_2$ or Fe^0 in between the graphite planes.

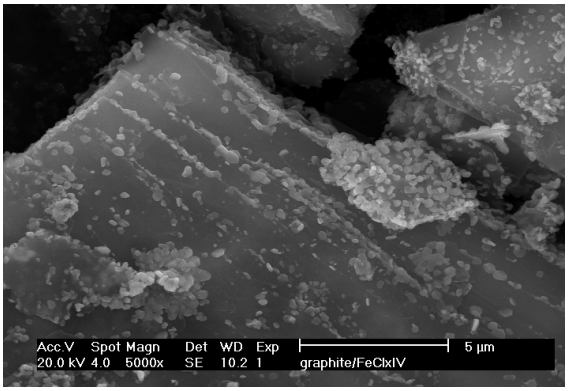

Figure 6.20 SEM image of stage 1 $FeCl_3$ intercalated graphite after reduction with H_2 at 325°C.

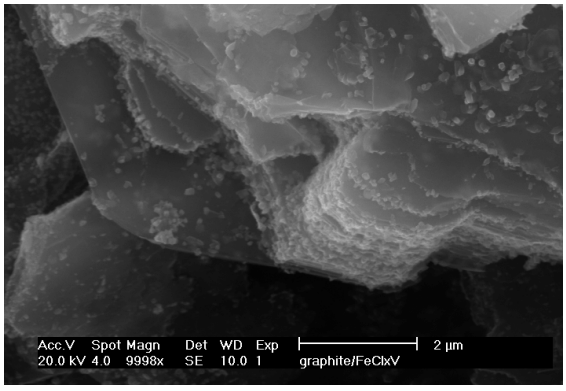

Figure 6.21 SEM image of stage 1 $FeCl_3$ intercalated graphite after reduction with H_2 at 325°C.

In figure 6.20 a SEM image of the resulting material is shown. On the graphite surface small, oxidized $FeCl_2$ particles have appeared. These particles were not observed before the reduction treatment and are therefore the direct result of this reduction treatment. It is obvious that part of the $FeCl_3$ de-intercalates with this treatment. From figures 6.20, 6.21 and 6.22 it is obvious that the de-intercalation mostly takes place via the edges of the graphite planes, because the highest concentration of particles is localized there.

The backscatter image in figure 6.22 clearly shows that the $FeCl_3$ particle distribution is not homogeneous any more after the reduction treatment.

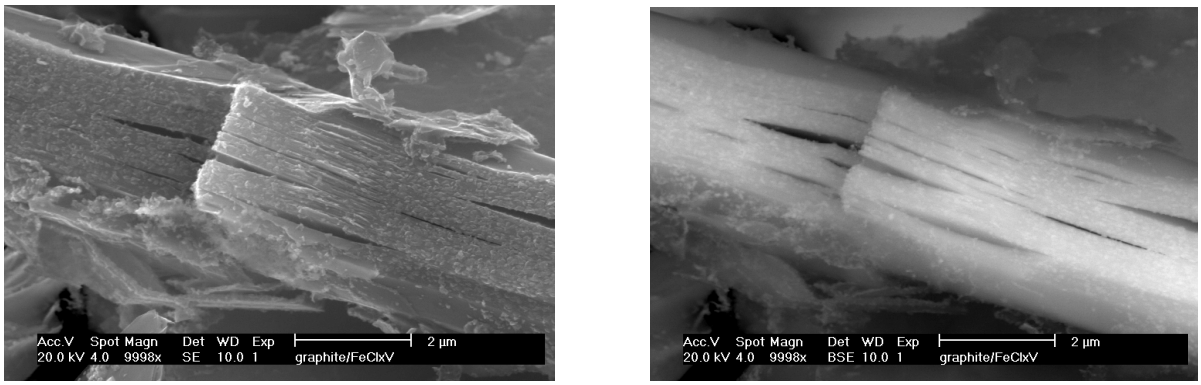

Figure 6.22 SEM image and backscatter-image of stage 1 $FeCl_3$ intercalated graphite after reduction with H_2 at 325°C, close up of edges decorated with $FeCl_3$ particles.

When the $FeCl_3$ intercalated graphite is reduced at 325°C and subsequently is washed with HCl, the $FeCl_3$ particles disappear from the surface and the edges of the graphite. The graphite structure of course still shows evidence of exfoliation (figure 6.23).

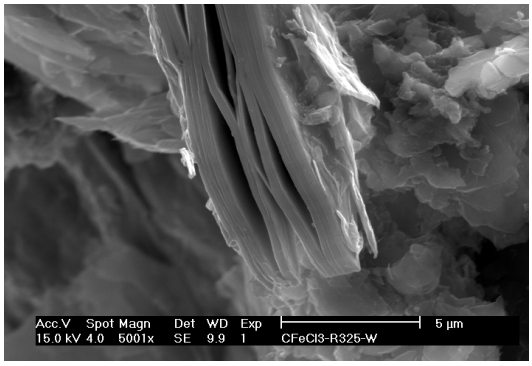

Figure 6.23 SEM image of $FeCl_3$ intercalated graphite, reduced at 325°C and washed.

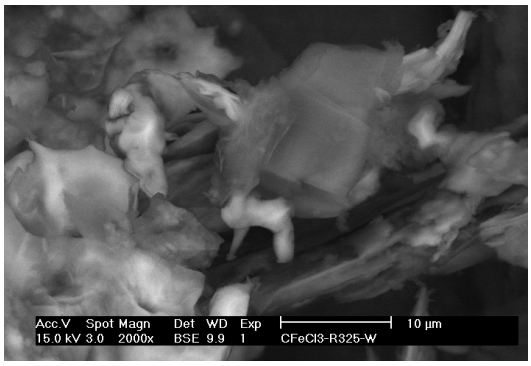

Figure 6.24 $FeCl_3$ intercalated graphite reduced at 325°C and subsequently washed.

The backscatter image shown in figure 6.24 shows that in some parts of the reduced and washed intercalated graphite heavy elements are still present, and that in other parts the de-intercalation is quite complete.

The XRD peaks of a stage 1 and a stage 2 compound were summarized in table 6.2. After reduction at 325°C the peaks of the stage 1 compound have diminished and the peaks of the second stage compound have enlarged (figure 6.25). This demonstrates that during the reduction treatment at 325°C de-intercalation takes place. The appearance of peaks of Fe_2O_3 originates from $FeCl_2$ which remained at the edges during de-intercalation. During exposure to air $FeCl_2$ oxidized and hydrolyzed which, ultimately, results in the formation of Fe_2O_3. After washing these peaks have disappeared. Because very small peaks remain, it can be concluded that not all the $FeCl_3$, $FeCl_2.xH_2O$ or Fe_2O_3 is removed with the washing procedure.

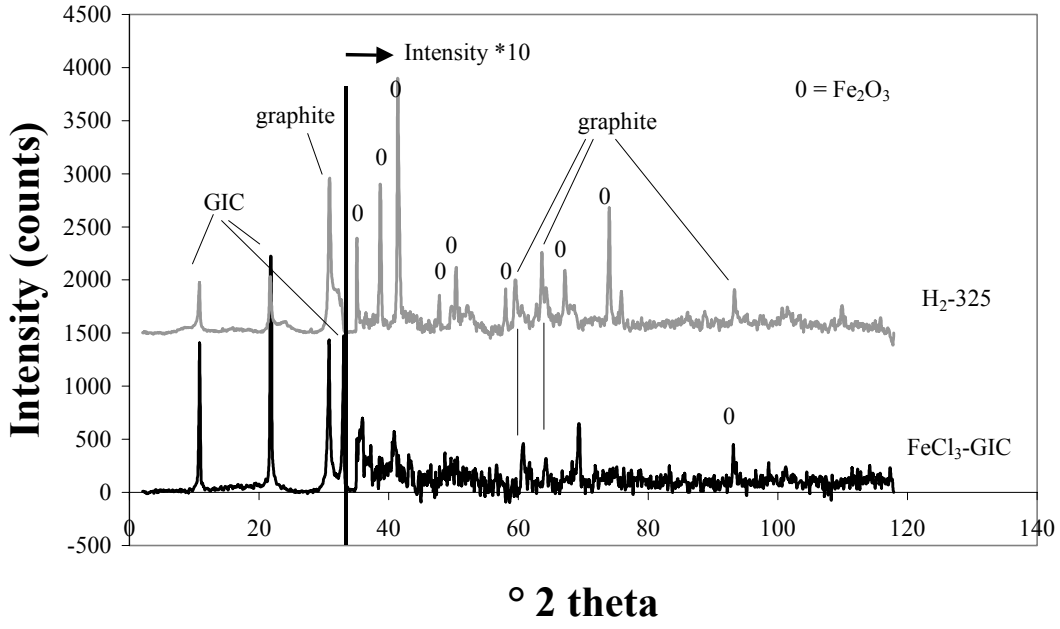

Figure 6.25 XRD patterns of $FeCl_3$ intercalated graphite, and this material reduced at 325°C.

XPS was used to asses the structure of the species present on the surface. It is obvious from figure 6.26 that after reduction at 325°C and subsequent washing not much Fe remains on the surface. Originally small $FeCl_3$ particles sintered to much larger particles, which cover a smaller part of the graphite surface area than the intercalated graphite, which was molecularly spread in between the graphite planes and in this way covered almost the complete graphite surface. After washing the intensity lowers even more, because most of the sintered particles are removed (see also SEM and XRD results). The samples that do show the presence of Fe also show the obvious Fe_2O_3 peak at 725 eV as we also observed with the heat treated sample. This peak results from the reaction of $FeCl_3$ or $FeCl_2$ species with H_2O from the air, which takes place when the $FeCl_3$ material is outside the graphite planes and at the exposed edges of the intercalated material.

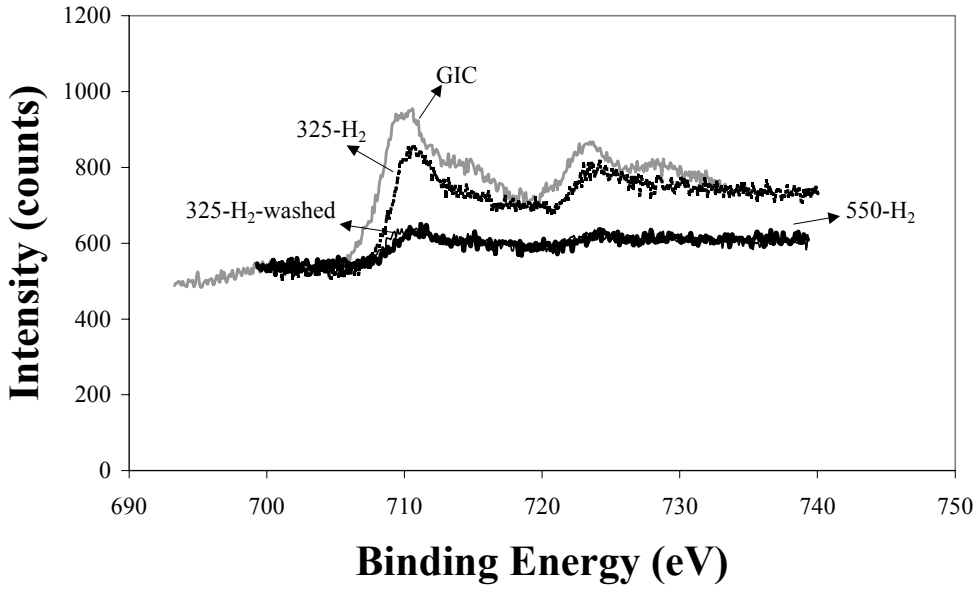

Figure 6.26 XPS results of the starting GIC and materials reduced at 325°C and 550°C, eV range containing the iron signal.

After reduction at 550°C large particles are visible next to the graphite. Most of the $FeCl_3$ has de-intercalated from the graphite and has subsequently been reduced to Fe^0 as can be concluded from the related XRD pattern shown in figure 6.28. The iron is now visible as large, facetted particles next to the graphite flakes (see figure 6.27). The reduction at 550°C is much more complete than at 325°C, but unfortunately intercalated $FeCl_3$ is not reduced to intercalated $FeCl_2$ or Fe^0. $FeCl_3$ is first de-intercalated and next (partly) reduced to $FeCl_2$ and/or Fe^0.

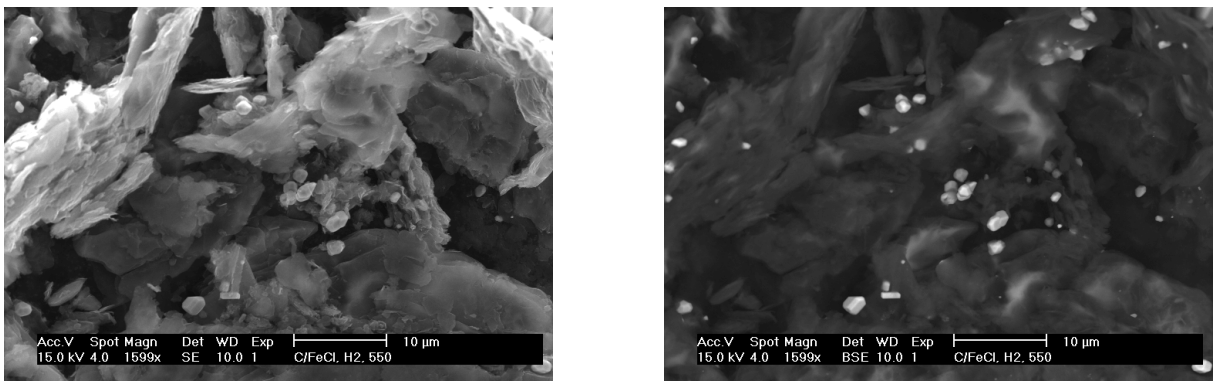

Figure 6.27 Scatter- (left) image and backscatter- (right) image of stage 1 $FeCl_3$ intercalated graphite after reduction with H_2 at 550°C.

Study of the backscatter image (see figure 6.27) shows that there are still small parts in the material which contain heavy elements inside the graphite flakes. This demonstrates that after reduction at 550°C domains remain with intercalated iron or iron chloride.

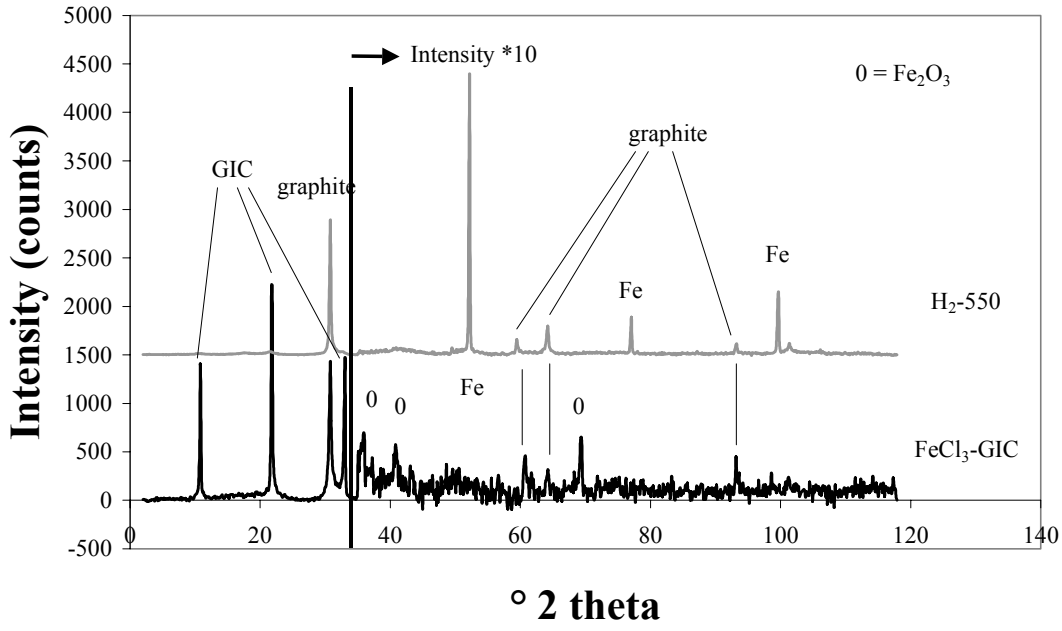

Figure 6.28 XRD patterns of $FeCl_3$ intercalated graphite, and this material reduced at 550°C.

The XRD patterns of the GIC reduced at 550°C show the disappearance of the stage 1 or stage 2 peaks, reappearance of the graphite peaks and the appearance of Fe^0 peaks. These peaks have a small width, which is consistent with the large reduced and sintered Fe^0 particles we observed in the SEM images. Also, in this diffractogram it can be seen that almost all $FeCl_3$ has de-intercalated from the graphite, because the intensity of the intercalation peaks has diminished considerably and the graphite peak at d=0.336 nm has increased to the most intense peak in the XRD pattern again. This shows that the material consist of graphite, with large Fe^0 particles between the graphite flakes. There are no peaks present in this pattern, or in the pattern of the $FeCl_3$ reduced at 325°C, that could be attributed to Fe^0 or $FeCl_2$ intercalated between the graphite planes.

The XPS results are summarized in tables 6.10 and 6.11. In table 6.10, the ratios of the corrected intensities of the Fe- and Cl-peaks are compared. As with the heat treated samples, the shape of the Fe-peaks makes it difficult to determine the surface area. This is very apparent from the material, which is reduced at 550°C, because it shows a high Cl/Fe ratio, which is inconsistent with SEM and XRD results, which show the presence of Fe^0 particles. However, since these cover only a very small amount of the surface, the resulting Fe peak is very small, as can be observed in figure 6.26.

Table 6.10 Ratio of Fe and Cl from the surface of the XPS peaks of the reduced intercalated $FeCl_3$ in graphite samples.

Sample	Fe-surface area (a.u.)	Cl-surface area (a.u.)	I_{Cl}/I_{Fe}	I_{Fe}/I_C	I_{Cl}/I_C
$FeCl_3$-GIC	2941	827	2.07	0.06	0.13
H_2-325	1775	335	1.39	0.03	0.05
H_2-325-washed	382	140	2.70	0.01	0.08
H_2-550	538	251	3.45	0.01	0.02

Table 6.11 Peak positions of Fe and Cl of the reduced $FeCl_3$ in graphite samples.

Sample	Corrected Fe peak (eV)	Corrected Cl peak (eV)
$FeCl_3$-GIC	710 ± 1	199
H_2-325	710 ± 1	199
H_2-325-washed	711 ± 1	199
H_2-550	710 ± 1	199

In table 6.7 the literature peak positions of $FeCl_2$ and $FeCl_3$ peaks were given. Also for these samples the broad nature of the peaks makes it impossible to draw definite conclusions from the obtained peak positions. The measured peak positions from the reduced samples are summarized in table 6.11. The results show again that on the surface Fe^{3+} and Fe^{2+} are present.

6.4.6 N_2 physisorption results and H_2 adsorption measurements

The BET surface area of the normal graphite is extremely low, below 10 m^2/g, and an extremely small mesopore volume is detected. With the various $FeCl_3$-GICs, as prepared and washed, no significant enlargement of BET surface areas and pore volumes was measured. Even the with SEM observed cracks and holes, which are the results of the intercalation of the $FeCl_3$ in the graphite and are referred to as exfoliation, did not bring about any measurable increased physisorption of nitrogen at 77 K.

The reduced samples and the reduced-washed samples lacked any extension of their pore volume too. This is consistent with the stage theory, which states that the space between two host layers is or completely occupied or completely empty (see figure 5.2).

Of all these materials, the hydrogen adsorption capacities were measured and compared to those of untreated graphite, to check whether intercalation and subsequent treatment had any influence on the adsorption capacities. The adsorption capacity of graphite is extremely low. Nevertheless, intercalation and all subsequent treatments did not have any measurable influence on the hydrogen adsorption capacity of these materials, i.e. the capacities remained very low, in the order of a few ml (STP)/$g_{adsorbent}$.

6.5 Conclusions

We did not succeed in synthesizing $FeCl_3$ intercalated CNFs. With the well-ordered graphite samples intercalation of $FeCl_3$ proceeded smoothly. The deviating behavior of CNFs and activated graphite material shows that the domain size of the CNF may be too small to produce stable intercalated compounds. In the CNF samples, the specific structure of the fibers with bulk defects may also make intercalation very difficult. We, nevertheless, further explored the concept of creating adsorption sites for hydrogen within the graphitic lattice using normal graphite samples intercalated with $FeCl_3$.

Using TGA, SEM, XRD and XPS we demonstrated that thermal treatment nor reduction of the $FeCl_3$-GICs resulted in $FeCl_2$-GICs or Fe^0-GICs. Only de-intercalation of $FeCl_3$ proceeds. In inert atmospheres, part of it remains at the graphite surface in the form of $FeCl_2$ up to about 400°C. When contacted with air, this material is oxidized or hydrolyzed. At high temperatures $FeCl_2$ evaporates from the surface also. In hydrogen, up to 325°C the $FeCl_3$ de-intercalated from the graphite is deposited as small $FeCl_2$ particles on the edges and basal planes of the graphite. When the material is reduced at 550°C the $FeCl_3$ de-intercalates and reduces via $FeCl_2$ to Fe^0.

The untreated, nor the heat-treated and the reduced samples show any enhanced hydrogen adsorption capacity.

Further research may involve intercalation with other metal halogenides, which can be reduced more easily, e.g. $CuCl_2$. Also catalyzed reduction, using finely distributed Pt on the graphite surface, may make reduction possible below the temperature of de-intercalation of the intercalated species. In that way, the reduction may take place between the graphite planes and a micropore volume may be created.

Acknowledgements

The intercalation in carbon nanofibers was based on the experimental work executed by Ruud Branderhorst within the framework of his graduate research project. The study on intercalation and reduction of $FeCl_3$ in graphite was based on the experimental work executed by Jaap Bergwerff within the framework of his graduate research project. We wish to acknowledge Ad Mens for the performing the XPS measurements and dr. Onno Gijzeman for the discussions concerning the XPS data. We thank Marjan Versluijs for performing the SEM measurements.

References

1. M. Watanabe, M. Tachikawa and T. Osaka, Electrochimica Acta 42 (1997) 2707.
2. C. Zandonella, Nature 410 (2001) 724.
3. M. Hirscher, M. Becher, M. Haluska, U. Dettlaff-Weglikowska, A. Quintel, G.S. Duesberg, Y.-M. Choi, P. Downes, M. Hulman, S. Roth, I. Stepanek and P. Bernier, Applied Physics A 72 (2001) 129.
4. M. Rzepka, P. Lamp and M.A. de la Casa-lillo, Journal of Physical Chemistry B 102 (1998) 10894.
5. F. Darkrim and D. Levesque, Journal of Chemical Physics 109 (1998) 4981.
6. Q. Wang and J.K. Johnson, The Journal of Physical Chemistry B 103 (1999) 277.
7. M. Baxendale, V.Z. Mordkovich, S. Yoshimura and R.P.H. Chang, Physical Review B 56 (1997) 2161.
8. K. Kalucki and A.W. Morawski, Reactivity of Solids 4 (1987) 269.
9. E. Stumpp, Materials Science and Engineering 31 (1977) 53.
10. H. Selig and L.B. Ebert, Advances in Inorganic Chemistry and Radiochemistry 23 (1980) 281.
11. P.C. Ecklund, NATO ASI Series, Series B 148 (Intercalation Layered Materials) (1986) 309.
12. Y. Soneda and M. Inagaki, Solid State Ionics 63-65 (1993) 523.
13. Ya.V. Zubavichus, Yu.L. Slovokhotov, L.D. Kvacheva and Yu.N. Novikovk, Physica B 208-209 (1995) 549.
14. K. Nagai, H. Kurata, S. Isoda and T. Kobayashi, Journal Pf Physcial Chemistry Solids 53 (1992) 883.
15. M. Asano, T. Sasaki, T. Abe, Y. Mizutani and T. Harada, Journal of Physical Chemistry Solids 57 (1996) 787.
16. D. Begin, F.G. Alain. E. and J.F. Mareche, Journal of Physical Chemistry Solids 57 (1996) 849.
17. D. Braga, A. Ripamonti, D. Savoia, C. Trombini and A. Umani-Ronchi, Journal of the Chemical Society Dalton (1979) 2026.
18. R. Schlögl and W. Jones, Journal of the Chemical Society of Dalton Trans. (1984) 1283.
19. D. Braga, A. Ripamonti, D. Savoia, C. Trombini and A. Umani-Ronchi, Journal of the Chemical Society Dalton Letters (1981) 328.
20. D. Braga, A. Ripamonti, D. Savoia, C. Trombini and A. Umani-Ronchi, Journal of the Chemical Society, Chemical Communications 18 (1978) 927.
21. D. Herein, T. Braun and R. Schlogl, Carbon 35 (1997) 17.
22. D.J. Smith, R.M. Fisher and L.A. Freeman, Journal of Catalysis 72 (1981) 51.
23. R. Erre, A. Messaoudi and F. Beguin, Synthetic Metals 23 (1998) 493.
24. G. Bewer, N. Wichman and H.P. Boehm, Materials Science and Engineering 31 (1977) 73.
25. A. Mastalir, Z. Kiraly, I. Dekany and M. Bartok, Colloids and Surfaces A: Physicochemical and Engineering Aspects 141 (1998) 397.
26. T.G. Ros, Ph. D. Thesis, Utrecht University (2001).
27. M. Endo, R. Saito, M.S. Dresselhaus and G. Dresselhaus, Carbon nanotubes: preparation and properties, (CRC Press, Boca Raton, 1997) p. 96.

28. C.D. Wagner, W.M. Riggs, L.E. Davis, J.F. Moulder and G.E. Muilenberg, Handbook of X-ray photoelectron spectroscopy (Perkin-Elmer Corporation Physical Electronics Division, Eden Prairie, Minnesota, USA, 1979).

7

Summary and Concluding Remarks

This thesis describes our research on adsorbent systems for hydrogen storage for small-scale, mobile applications. Hydrogen storage is a key element in the change-over from the less efficient and polluting internal combustion engine to the pollution-free operating hydrogen fuel cell. In general, hydrogen can be stored pressurized, liquefied, absorbed in metals and physisorbed on a suitable material (adsorbent). All of these options are being investigated extensively, but with none a breakthrough has been effectuated. Our analysis was, weighing the advantages and disadvantages of the different options, that storage by physisorption might be the most promising one. We therefore decided to focus our efforts on a further exploration of this alternative.

Probably, storage by physisorption has the highest energy efficiency, even when such a system has to be kept at a low temperature of 77 K. Uptake and release of hydrogen can be fast and easily effectuated with relatively small pressure and/or temperature changes. Because the non-specificity of the interaction, the amount of adsorbed hydrogen will, at set temperature and pressure, mainly be related to the specific surface area, notably due to pore structure and pore diameter, and less to the chemical nature of the adsorbent material. This opens the opportunity to choose a material, which is abundantly available, not toxic by itself and safe when used. Complying with these arguments and taking into account the know-how and expertise of our research group in the field of production and design of (catalyst) support materials including graphitic carbon nanofibers (CNFs), we concentrated on various carbon materials.

Activated carbons contain many different types of carbon structures that provide a variety of environments for hydrogen bonding and promising results were already reported in the literature, especially with materials exhibiting a large micropore volume [1]. On the other hand, in graphite-like carbons potentially the highest micropore volume is present, provided that the space between the graphite layers can be made accessible for hydrogen. We therefore extensively explored the suitability of graphitic carbon materials, notably of CNFs.

Our results presented in **chapter 2** demonstrate that a large storage capacity for hydrogen by physisorption under the chosen conditions (77 K, 1 bar) is only obtained with adsorbents containing a large volume of micropores with a suitable diameter. Although with zeolite-like materials the chance to define an optimal pore diameter seems realistic, their unavoidably limited micropore volume makes their applicability less likely. With activated carbons a more optimistic perspective can be offered. Their micropore volume can probably be increased to a value above 1 ml/g, while by increasing the storage pressure or by tuning the pore diameter the storage capacity can be raised up to the targets set for mobile applications. Because of the various sizes and shapes of the micropores in activated carbon it is as yet impossible to comment in detail on the optimum pore size and shape. Preliminary results indicate that pores of 0.5-1.0 nm in diameter are more beneficial than those of 1.0-2.0 nm. High adsorption capacities should be obtained with carbon materials with a high volume of these suitable pores.

In their recent critical survey on the suitability of hydrogen storage materials for mobile applications Schlapbach and Zuttel [2], using our results, confirm our conclusion that further exploration of storage by physisorption is worthwhile, but whether a hydrogen storage material will emerge, remains open question.

Our further research efforts we focused on inclusion of hydrogen in graphite-based structures, *i.e.*, in normal graphite and notably in CNFs. As said, these structures could accommodate large amounts of hydrogen if the space between the graphite planes can be made accessible for hydrogen. Especially of CNFs we cherished great ambitions. Although, in view of many literature reports and our own experience, direct loading with hydrogen is not possible, we estimated research on the formation of ternary hydrogen GICs as very sensible.

In order to study large quantities of graphite-based adsorbent materials large amounts of fishbone carbon nanofibers had to be produced. Therefore a method was developed to produce 10-20 grams of homogeneous CNFs, as described in **chapter 3**. This method comprises growth in a fluidized bed reactor using a commercially available 60 wt% Ni on Al_2O_3 catalyst. It was shown that the resulting fiber granules were able to withstand the forces of the fluidized bed for a limited period of time. Adjusting the gas flow to keep the fluidization profile intact during growth proved unnecessary. It was shown that the catalyst used was also very well able to withstand the attrition forces of the fluidized bed. The high Ni loading of the catalyst gave high fiber yields. The fibers had diameters between 20 and 90 nm, with most fiber diameters between 40 and 70 nm. This is probably caused by the Ni particle

size distribution. Therefore, if a very narrow diameter distribution of the fibers is desired, this catalyst is less suitable. From XRD experiments we found that after reduction of the catalyst for 2 hours at 700°C nickel particles are present with a mean diameter between 9 and 12 nm. After 30 minutes of fiber growth, the mean nickel diameter had increased to 15-16 nm. This shows that during the first stage of the growth the Ni particles enlarge under influence of the growth process, *e.g.* carbide formation and/or methane dissociation. Nevertheless, the mean diameter of the observed Ni particles remains significantly smaller than the average fiber diameter (between 20 and 90 nm) and with this that of the Ni particles present in the fibers, implying that further Ni sintering occurs prior to growth. We have found no indications for structural differences between fibers grown in our fluidized bed and fibers grown in a fixed bed set-up. The microscopic structure as well as the macroscopic structure (specific surface area and pore volume) are comparable. The shape of the macroscopic aggregates of CNFs resembles the shape of the original catalyst particles.

This fluidized bed process is the first step in the possible scale up to commercial production of CNFs. Such a process would make carbon nanofibers available for low prices, allowing their application as catalyst support materials. To bring down the production costs of carbon nanofibers to 10 US$/kg or less a number of important improvements have to be achieved with respect to the presented lab-scale set-up. In the first place a process should be developed that comprises recycling of methane. Furthermore, the development of a catalyst with a very high activity for fiber growth should be pursued, which would allow a short cycle time of adding new catalyst and harvesting grown fibers in a continuous process. Also the amount of fibers grown per gram of Ni should be enhanced. Considerable engineering challenges remain to develop a full-scale commercial process for the catalytic growth of carbon nanofibers.

Because of its expected influence on the inclusion processes we profoundly studied, with several techniques, the degree of perfection of the microstructure of the fibers as synthesized and after heat treatment up to 2000°C. The results of this research are presented in **chapter 4**. In this chapter the microscopic structure of fishbone and two types of parallel carbon nanofibers as synthesized and after heat treatment at 2000°C were studied with several techniques. The fishbone nanofibers were shown from TEM analysis to display a significant amount of defects, such as two planes coinciding to one, bending planes, planes more or less parallel to the fiber axis and plane ends parallel to the fiber surface. After heat treatment at 1600°C and 2000°C the fibers showed a similar number of bulk defects. The planes terminated no longer parallel to the surface of the fiber, however, but protruded from the surface, as if they had straightened out. The BET surface areas of these materials has diminished, possibly caused by a decreased surface roughness. To gain more insight into this phenomenon more research is needed. The parallel and Hyperion carbon fibers contain the same amount and types of defects and also have connecting graphite planes inside the channels. TEM analyses did not show a diminished amount of defects after heat treatment and the BET surface area of these materials did not change either.

Thermo Gravimetric Analysis shows that oxidation of heat-treated fibers starts at a higher temperature than that of untreated fibers, closer to the onset temperature of graphite oxidation. Because defects at the surface of the fiber are the most logical candidates for the start of the oxidation, the heat treatment must have diminished the amount of these surface defect sites. These results suggest that the fibers have increased their surface aromaticity. IR results are consistent with TEM and TGA results. The surfaces of the fishbone and parallel fibers have become much more aromatic. For the fishbone fibers this can also be seen clearly from protruding graphite planes (TEM). For the parallel fibers this is not well observed with TEM, but TGA and IR show a decrease of aliphatic carbon. The results for Hyperion fibers are less consistent. From IR and TEM results the material does not seem to be affected much, but TGA shows an increase in oxidation temperature.

It can be concluded that although the surfaces of the fibers are affected by heat treatment at 2000°C for 30 minutes, the bulk of the fibers is not. To influence the defects inside the fibers higher temperatures and longer treatment times are needed.

In **chapter 5** carbon nanofibers were intercalated with potassium. With XRD we have shown that intercalation of potassium in as synthesized fishbone nanofibers increased the d-spacing of the fibers. It was also shown that part of the fibers is not intercalated and remains graphitic, with a d-spacing of 0.34 nm. Results of TEM experiments did not show an enlarged d-spacing. This may be the result of only non-intercalated parts being studied, or because of slow reaction with air and resulting de-intercalation of potassium during insertion of the samples into the microscope. A lot of small carbon nanofiber parts were observed in the microscope, so the intercalation procedure seemed to negatively affect the integrity of the fibers.

Intercalation of potassium in carbon nanofibers significantly increases the hydrogen storage capacity of these materials. Typically, at 77 K and 1 bar the uptake of hydrogen upon intercalation of potassium increases from 10 to 160 ml (STP)/g_{carbon}. The observed adsorption was reversible at that temperature, whereas the intercalated fibers did not show any hydrogen storage capacity at 193 and 298 K. The H_2 adsorption has not been optimized. The amount of hydrogen stored is different (H/K ~1.3) than the amount mentioned for K intercalated graphite (H/K ~4). This may turn out different when the intercalation is optimized. XRD results show that only part of the fibers were intercalated, so it may be that the H_2 adsorption capacity of the intercalated fibers is closer to H/K ~4.

It was shown that nitrogen physisorption could not be used to show an enlarged BET surface area or micropore volume, because the N_2 molecule is too large to penetrate between the intercalated graphite sheets.

We have shown that intercalation of K increases the d-spacing of CNFs as well as increases the H_2 adsorption capacity, similar to graphite. Because of the oxygen sensitivity of this

material it is however not very suitable for use in mobile applications. However, use of another intercalate which is less sensitive to oxygen may provide a suitable H_2 adsorbent for mobile applications.

In **chapters 6** we describe the formation of binary iron-chloride GICs. Intercalation of $FeCl_3$ in carbon nanofibers turned out to be impossible. Variation of the temperature and heating time did not influence the results. Also different pre-treatments of the fibers, varying from removal of the Ni and Al_2O_3 still present in the fibers, to heat treatments up to 2000°C, did not result in intercalation of $FeCl_3$ into carbon nanofibers. This may be caused by the much smaller graphitic domains of carbon nanofibers, when compared to graphite and activated graphite. It can also be caused by the inhibition of these materials to increase their d-spacing sufficiently. In CNFs the planes may be connected in the center of the tube and also planes are internally connected via defects in the fibers. These connections within the planes may inhibit the Fe_2Cl_6 intercalating species to lift up the planes sufficiently to allow intercalation and formation of a stable compound. This rigidity of the structure is quite different from graphite and could very well explain the deviating behavior of the CNFs with regard to intercalation. Heat treatment at 2000°C did not change the behavior of the carbon nanofibers with regard to intercalation. Treatment at higher temperature (3000°C) is probably needed to sufficiently change the character of the fibers to allow intercalation.

Subsequently, intercalation experiments were performed with well-ordered graphite to check our hypothesis of increased hydrogen storage capacity upon micropore formation. It was very well possible to intercalate graphite with $FeCl_3$. The intercalated graphite did not show an enhanced hydrogen adsorption capacity, however, which can be blamed on the total filling of the graphite with the intercalate, leaving no room for H_2 to adsorb between the graphite planes. To create more space, attempts were made to reduce intercalated $FeCl_3$ to $FeCl_2$ or Fe^0 remaining situated between the graphite planes. Using TGA, SEM, XRD and XPS we demonstrated that thermal treatment nor reduction of the $FeCl_3$-GICs resulted in $FeCl_2$-GICs or Fe^0-GICs. Only de-intercalation of $FeCl_3$ proceeds. In inert atmospheres, part of this $FeCl_3$ remained at the graphite surface in the form of $FeCl_2$ up to about 400°C. When contacted with air, this material was oxidized or hydrolyzed. At high temperatures $FeCl_2$ evaporated from the surface. In hydrogen, up to 325°C, the $FeCl_3$, de-intercalated from the graphite was deposited as small $FeCl_2$ particles on the edges and basal planes of the graphite. When the material is reduced at 550°C the $FeCl_3$ de-intercalates and reduces *via* $FeCl_2$ to Fe^0.

The untreated, nor the heat-treated and the reduced samples show any enhanced hydrogen adsorption capacity.

Further research may involve intercalation with other metal halogenides, which can be reduced more easily, *e.g.* $CuCl_2$. Also catalyzed reduction, using finely distributed Pt on the graphite surface, may facilitate reduction below the temperature of de-intercalation of the intercalated species. In that way, the reduction may take place between the graphite planes and a micropore volume may be created.

The work described in this thesis has provided valuable information about the demands on hydrogen adsorbents and the structure and modification of carbon nanofibers. The results contribute to a better understanding of the material demands we place on hydrogen adsorbents. Furthermore we have gained a more fundamental understanding of the structure of carbon nanofibers and the possibilities and impossibilities of their modification. This study describes the importance of the presence of small (diameter below 1 nm) micropores for high hydrogen adsorption capacities of adsorbents. The possibility to synthesize large, homogeneous batches of carbon nanofibers using a fluidized bed system has also been described. It was shown that fishbone, as well as parallel carbon nanofibers contain a large amount of defects, on the surface of the fiber, as well as inside in the fibers. Furthermore it was shown that heat treatments at 2000°C in an inert atmosphere increase the aromatic character of the surface of the fibers, whereas these heat treatments have no influence on the amount and nature of the defects inside the fibers.

It has been described that intercalation of $FeCl_3$ in carbon nanofibers did not proceed and intercalation of $FeCl_3$ in graphite did not enlarge the micropore volume and hydrogen storage capacity of the resulting material. Subsequent treatment of the intercalated graphite to produce $FeCl_2$ intercalated graphite, which would enhance the micropore volume of these materials, did not enlarge the hydrogen storage capacity of the resulting materials. Intercalation of potassium in carbon nanofibers did significantly increase the hydrogen storage capacity of this material as was previously shown with graphite. Unfortunately, the amounts of adsorbed hydrogen are not enough to meet the DOE target and it remains unclear whether improvements can be made by using other fibers or other hydrogen storage pressures. Additionally, the resulting material is not very suitable for vehicular use, since it is very sensitive to air. The atomically dispersed potassium reacts violently when contacted with air, oxidizing the potassium and carbon, erupting in flames and sparks. This is not a very desirable property for a material to be used in vehicles, where there is always the possibility of collision and penetration of the tanks.

We would like to end with concluding that further exploration of hydrogen storage by physisorption is worthwhile, although it remains an open question whether a suitable hydrogen storage material will ultimately evolve from, these efforts.

References

1. A.J. Kidnay and M.J. Hiza, Advances in Cryogenic Engineering 12 (1967) 730.
2. L. Schlapbach and A. Zuttel, Nature 414 (2001) 353.

Samenvatting

In dit proefschrift staat het onderzoek naar de ontwikkeling van een geschikt adsorbens voor waterstofopslag voor kleinschalige mobiele toepassingen centraal. Het beschikbaar komen van een dergelijk systeem is noodzakelijk om vervanging van de inefficiënte en vervuilende interne verbrandingsmotor door de meer efficiënte H_2/O_2 brandstofcel mogelijk te maken. Waterstof kan worden opgeslagen als gas onder hoge druk en als vloeistof bij lage temperatuur. Een andere mogelijkheid is waterstof op te slaan door absorptie in bepaalde metalen en legeringen en door fysisorptie aan een geschikt adsorptie middel bij lage temperatuur. Hoewel er aan deze alternatieven intensief onderzoek werd en wordt verricht, heeft dit tot nu toe voor geen enkele daarvan tot een doorbraak geleid.

Wel is duidelijk dat opslag door middel van fysisorptie bij een temperatuur niet lager dan 77 K het meest efficiënt zou zijn. Opname en afgifte van waterstof verlopen in dit geval snel door het aanleggen van kleine temperatuur- en/of drukverschillen. Door de niet-specifieke aard van de interactie zal de opname capaciteit bij gegeven condities meer van de grootte van het specifieke oppervlak en vooral van het microporie volume en niet van de aard van dit materiaal afhangen. Hierdoor wordt het wellicht mogelijk een materiaal te kiezen dat ruim voorradig, niet giftig en veilig te gebruiken is. Deze voorwaarden en de beschikbare expertise op het gebied van de vormgeving en productie van katalysatordragers heeft ons doen besluiten het onderzoek te concentreren op het ontwikkelen van een geschikt adsorptiemiddel op basis materialen bestaande uit koolstof.

Actieve kolen bevatten veel verschillende koolstofstructuren, met een ruime variatie aan omgevingen om geadsorbeerd waterstof te stabiliseren. Met monsters met een hoog microporievolume zijn veelbelovende resultaten beschreven in de literatuur [1]. Daar tegenover staat dat potentieel in grafitische koolstofstructuren wellicht het hoogste microporie

volume te vinden is, indien de ruimte tussen de grafietlagen beschikbaar gemaakt kan worden voor waterstof. Om die reden hebben we de mogelijkheden van grafitische materialen uitgebreid bestudeerd, in het bijzonder die van grafitische kooldraden.

Onze resultaten beschreven in **hoofdstuk 2** tonen aan dat een hoge opslagcapaciteit voor waterstof door middel van fysisorptie bij de gekozen condities (77 K, 1 bar) slechts gerealiseerd kan worden met adsorbentia met een groot volume aan microporiën met een geschikte diameter. Hoewel met zeolieten de kans om een optimale poriediameter te kunnen realiseren groot lijkt, maakt het relatief geringe microporievolume hun toepasbaarheid minder waarschijnlijk. Voor actieve kolen zijn de vooruitzichten optimistischer. Het microporievolume van deze materialen kan waarschijnlijk tot 1 ml/g of meer vergroot worden. Door verhoogde druk bij opslag en / of een meer optimale afstemming van de poriediameter kan de opslagcapaciteit van waterstof mogelijk opgevoerd worden en het doel dat gesteld is voor mobiele toepassingen (720 ml (STP)/g) gehaald worden. Vanwege de variatie in vorm en diameter straal van de microporiën in actieve kolen is het nu echter nog onmogelijk om de details van een optimum van beide variabelen te voorspellen. Voorlopige resultaten tonen aan dat poriën met een diameter tussen 0.5 en 1.0 nm per volume-eenheid meer waterstof opslaan dan die met een diameter tussen 1.0 en 2.0 nm. In hun recent verschenen analyse bevestigen Zuttel en Schlapbach [2], gebruikmakend van onze resultaten, onze conclusie dat verder onderzoek naar opslag door middel van fysisorptie interessant is, maar dat het de vraag blijft of een systeem voor opslag van waterstof gevonden of geproduceerd kan worden op basis van actieve kool. Over de opname van H_2 in grafitische structuren, zoals met name CNFs, laten de genoemde auteurs zich niet uit.

Zoals geschreven, zouden deze structuren grote hoeveelheden waterstof kunnen opslaan, mits de ruimte tussen de grafietlagen toegankelijk gemaakt kan worden. Hoewel uit metingen van ons en anderen blijkt dat het onmogelijk is om kooldraden direct met waterstof te beladen, meenden we dat onderzoek naar de opname van H_2 in een GIC met een tweede component die voor H_2 toegankelijk is, zinvol was.

Aangezien in het onderzoek grote hoeveelheden kooldraden nodig waren is, zoals in **hoofdstuk 3** beschreven, een methode ontwikkeld om per “batch” 10 tot 20 gram draden met reproduceerbare eigenschappen te groeien. We kozen voor een wervelbed reactor en een commercieel verkrijgbare Ni op Al_2O_3 katalysator (60 wt% Ni). We toonden aan dat de gevormde kooldraadkluwens slijtage in het wervelbed gedurende een beperkte tijd weerstaan. De hoge nikkelbelading van de katalysator zorgt voor een hoge opbrengst aan kooldraden met diameters tussen 20 en 90 nm, de meeste tussen 40 en 70 nm. Deze diameterverdeling wordt waarschijnlijk veroorzaakt door de deeltjesgrootteverdeling van de Ni-deeltjes. Indien een zeer nauwe diameterverdeling van de draden gewenst is, is deze katalysator dan ook minder geschikt. Uit Röntgendiffractie experimenten is gebleken dat na reductie van de katalysator gedurende 2 uur bij 700°C, de Ni-deeltjes een gemiddelde diameter van 9 tot 12 nm hebben. Na 30 minuten groei van kooldraden blijkt de gemiddelde diameter groter te zijn geworden: 15-16 nm. Dit toont aan dat de nikkeldeeltjes gedurende het eerste deel van de draadgroei

groter worden onder invloed van dat groeiproces. Nader onderzoek zal moeten uitwijzen welk mechanisme hieraan ten grondslag ligt. Echter, de gemiddelde diameter van de na 30 minuten groei geobserveerde Ni deeltjes blijft significant kleiner dan de gemiddelde diameter van de draden (tussen de 20 en 90 nm) en daarmee kleiner dan de Ni deeltjes aanwezig in de draden. Er zijn geen aanwijzingen gevonden voor structurele verschillen tussen kooldraden die gegroeid zijn in het wervelbed en draden gegroeid in een vast bed. Zowel de microscopische als de macroscopische structuur (specifiek oppervlak en porievolume) zijn vergelijkbaar. De vorm van de macroscopische deeltjes is vergelijkbaar met die van de originele katalysatordeeltjes.

Dit wervelbedproces is een eerste stap in de opschaling naar een commercieel (continu) proces. Hiermee zullen kooldraden beschikbaar komen tegen lage kosten, waardoor ze toegepast kunnen worden als katalysatordragers. Om de productiekosten van kooldraden tot maximaal 10 US$/kg te beperken moet het gepresenteerde proces op een aantal punten verbeterd worden. In de eerste plaats moet een proces ontworpen worden, waarin niet-omgezet methaan terugvoerd wordt naar de reactor. Tevens moet er een katalysator ontwikkeld worden met een zeer hoge groei-activiteit, waardoor een korte cyclus van toevoegen van nieuwe katalysator en oogsten van gegroeide draden mogelijk wordt. Ook moet de opbrengst van draden per gram Ni verhoogd worden. Om een commercieel katalytisch groeiproces van kooldraden te realiseren dient dus nog veel onderzoek verricht worden.

De mate van perfectie van de gegroeide draden na behandeling bij hoge temperatuur is uitgebreid bestudeerd, aangezien verwacht werd dat de invloed ervan op het intercalatieproces groot zou zijn. Dit onderzoek wordt besproken in **hoofdstuk 4**. In dit hoofdstuk wordt de microscopische structuur van visgraatkooldraden en twee typen parallelle kooldraden bestudeerd met behulp van verschillende technieken, zowel direct na groei als na behandeling bij 2000°C. Uit TEM analyses van de visgraatkooldraden blijkt dat deze een significante hoeveelheid defecten bevatten, bijvoorbeeld twee grafietlagen samengroeiend tot één en gebogen lagen. Opmerkelijk is dat in een visgraatkooldraad gebieden voorkomen waarin de grafietlagen evenwijdig aan de as liggen. Ook eindigen veel visgraatlagen liggend op (parallel aan) het oppervlak. Na behandeling bij 1600 en 2000°C vertonen de draden een vergelijkbare hoeveelheid defecten. De lagen eindigen echter niet meer parallel aan het oppervlak, maar steken uit, alsof ze zich gestrekt hebben. Uit ons onderzoek blijkt ook dat parallele draden hetzelfde aantal en soort defecten bevatten als visgraatdraden. TEM-analyse toont geen verminderde hoeveelheid defecten na de behandeling bij hoge temperatuur aan.

Met TGA-metingen toonden we aan dat bij hoge temperatuur behandelde draden bij een hogere temperatuur oxideren dan onbehandelde draden. De starttemperatuur van de oxidatie ligt dichter bij die van grafiet. De temperatuurbehandeling heeft de hoeveelheid oppervlaktedefecten verminderd, waardoor de oxidatie pas bij hogere temperatuur kan beginnen. IR-resultaten ondersteunen deze conclusie. De oppervlakken van de visgraat- en parallele draden zijn meer aromatisch geworden. Bij de visgraatdraden is dit ook duidelijk zichtbaar door de rechte en daardoor van het oppervlak uitstekende einden van de grafietvlakken. Voor de parallelle draden is dit niet duidelijk uit de TEM-resulaten, maar de IR-resultaten tonen een duidelijke vermindering van aliphatische koolstof aan. De IR- en TEM-resulaten tonen geen grote veranderingen in het materiaal, maar uit TGA blijkt wel een toename in oxidatietemperatuur.

Er kan geconcludeerd worden dat alleen het oppervlak van de draden verandert door behandeling bij 2000°C gedurende 30 minuten. Om meer invloed uit te kunnen oefenen op de defecten in de draden zijn hogere temperaturen en langere behandelingstijden noodzakelijk.

In **hoofdstuk 5** zijn kooldraden geïntercaleerd met kalium. Met Röntgendiffractie is aangetoond dat intercalatie van kalium in kooldraden de d-afstand tussen de grafietlagen inderdaad laat toenemen. Ook is aangetoond dat een deel van de draden niet geïntercaleerd wordt en grafitisch blijft, met een d-afstand van 0.34 nm. In de TEM-analyse werd geen toegenomen d-afstand waargenomen. Dit kan het resultaat zijn van slechts bestuderen van niet-geïntercaleerde delen of wellicht door langzame reactie met lucht en deïntercalatie van kalium gedurende het inbrengen van het monster in de microscoop. Er werden veel korte delen van draden waargenomen, hetgeen erop wijst dat intercalatie een negatief effect heeft op de sterkte van de draden.

Intercalatie van kalium in kooldraden verhoogt de capaciteit voor waterstofopslag van deze materialen significant. Bij 77 K en 1 bar neemt de opslag van waterstof bij intercalatie met kalium toe van 10 naar 160 ml (STP)/$g_{koolstof}$. De geobserveerde adsorptie bij 77 K is zwak en de geïntercaleerde draden vertonen geen adsorptie bij 193 en 298 K. De opslag werd niet geoptimaliseerd. De hoeveelheid waterstof die opgeslagen wordt ten opzichte van kalium is anders dan de hoeveelheid die in de literatuur genoemd wordt voor kalium geïntercaleerd grafiet (H/K ~4). Dit zou kunnen veranderen indien de adsorptie geoptimaliseerd wordt. Röntgendiffractie toont aan dat slechts een deel van de draden geïntercaleerd is, dus het zou kunnen dat de H_2 opslagcapaciteit van de draden die wel geïntercaleerd zijn dichter bij H/K ~4 ligt.

Er is aangetoond dat N_2-fysisorptie geen geschikte techniek is om, na intercalatie met kalium, een vergroot BET oppervlak of microporievolume aan te tonen, aangezien het stikstofmolecuul te groot is om tussen de geïntercaleerde grafietlagen te passen.

We hebben aangetoond dat door intercalatie van K de d-afstand van de grafietlagen in de kooldraden groter wordt en de waterstofopslagcapaciteit toeneemt, vergelijkbaar met de resultaten die gerapporteerd worden voor grafiet. Door de zuurstofgevoeligheid van dit materiaal is het echter niet erg geschikt voor mobiele toepassingen. Intercalatie van kooldraden met een ander materiaal, dat minder gevoelig is voor zuurstof zou wellicht wel een geschikt adsorbens voor opslag van waterstof voor mobiele toepassingen kunnen vormen.

In **hoofdstuk 6** beschrijven we de vorming van binaire ijzer-chloride GICs. Intercalatie van $FeCl_3$ in kooldraden bleek onmogelijk. Variatie van de temperatuur en duur van verwarmen hadden geen invloed op de resultaten. Ook resulteerden verschillende voorbehandelingen van de draden, variërend van verwijdering van het in de draden na groei nog aanwezige Ni en Al_2O_3, tot behandelingen bij 2000°C, niet in intercalatie van $FeCl_3$. Dit kan veroorzaakt worden door de veel kleinere grafietdomeinen van kooldraden, waardoor geen stabiele verbinding gevormd kan worden. Het kan ook veroorzaakt worden door de onmogelijkheid van deze materialen om hun d-afstand voldoende te vergroten dat $FeCl_3$ er tussen past. In kooldraden kunnen de grafietlagen verbonden zijn in het midden van de draad en zijn lagen tevens intern verbonden via de defecten in de draden. Deze verbindingen in het midden kunnen het onmogelijk maken voor de intercalerende Fe_2Cl_6 verbinding om de lagen voldoende op te tillen om intercalatie toe te staan en een stabiele verbinding te vormen. Mogelijk kan dit het afwijkende gedrag van kooldraden met betrekking tot intercalatie verklaren. Warmte behandeling bij 2000°C heeft geen invloed op het niet-intercaleren van kooldraden. Waarschijnlijk is hiervoor een behandeling bij nog hogere temperatuur (3000°C) nodig om het karakter van de draden voldoende te veranderen om intercalatie mogelijk te maken.

Vervolgens zijn intercalatie-experimenten uitgevoerd met grafiet om onze hypothese van microporievorming en toegenomen capaciteit voor waterstofopslag te testen. Het bleek zeer goed mogelijk om grafiet te intercaleren met $FeCl_3$. Het geïntercaleerde grafiet vertoonde geen toegenomen capaciteit voor waterstofopslag, hetgeen verklaard kan worden door aan te nemen dat de ruimte tussen grafietlagen volledig gevuld wordt door $FeCl_3$, waardoor geen ruimte voor waterstof overblijft. Om meer ruimte te creëren werd geprobeerd het geïntercaleerde $FeCl_3$ om te zetten of te reduceren naar $FeCl_2$ en Fe^0 tussen de grafietlagen. Gebruikmakend van TGA, TEM, SEM, XRD en XPS hebben we laten zien dat noch thermische behandeling noch reductie van de $FeCl_3$-geïntercaleerde verbindingen resulteert in $FeCl_2$-geïntercaleerde verbindingen of Fe^0 tussen de grafietlagen. Er treedt alleen deïntercalatie van $FeCl_3$ op. In inerte atmosfeer tot ongeveer 400°C blijft een deel van dit $FeCl_3$ achter op het grafietoppervlak. Indien dit $FeCl_3$ in contact komt met lucht oxideert of hydrolyseert het materiaal. Bij hogere temperaturen verdampt alle $FeCl_3$ van het oppervlak. In waterstof deïntercaleert $FeCl_3$ tot ongeveer 325°C en ontleedt in kleine $FeCl_2$ deeltjes op de randen en basale vlakken van het grafiet. Als het materiaal bij 550°C gereduceerd wordt dan deïntercaleert het $FeCl_3$ en wordt het via $FeCl_2$ omgezet naar Fe^0.

De onbehandelde, noch de in inert behandelde, noch de gereduceerde monsters vertonen een toegenomen opslagcapaciteit voor waterstof.

Verder onderzoek kan intercalatie met andere metaalhalogeniden behelzen, welke gereduceerd worden onder mildere condities, zoals bijvoorbeeld $CuCl_2$. Ook gekatalyseerde reductie, waarbij gebruik gemaakt wordt van fijn verdeeld Pt op het grafiet oppervlak, kan reductie bij lagere temperatuur dan de deïntercalatie-temperatuur mogelijk maken. Op die manier kan reductie van de geïntercaleerde verbinding wellicht wel plaatsvinden tussen de grafietvlakken en kan er microporievolume gevormd worden.

Het onderzoek beschreven in dit proefschrift heeft waardevolle informatie opgeleverd over de eisen die gesteld worden aan adsorbentia voor de opslag van waterstof en over de structuur en modificatie van kooldraden. De resultaten dragen bij aan een beter begrip van de materiaaleisen die we stellen aan materialen voor waterstofopslag. Verder hebben we een dieper inzicht gekregen in de structuur van kooldraden en de mogelijkheden en onmogelijkheden van hun modificatie. Deze studie beschrijft het belang van de aanwezigheid van kleine (< 1 nm) microporiën in adsorbentia om hoge capaciteiten voor waterstofopslag te halen. Ook is de mogelijkheid beschreven om grote hoeveelheden homogene kooldraden te groeien in een wervelbedreactor. Er is aangetoond dat zowel visgraat- als parallele kooldraden veel defecten bevatten, zowel op het oppervlak als in de draad. Verder is aangetoond dat temperatuurbehandelingen bij 2000°C onder inerte atmosfeer een toename in het aromatische karakter van het oppervlak van de draden geven, maar dat deze behandelingen geen invloed hebben op de hoeveelheid en aard van de defecten in de draden.

Er is aangetoond dat intercalatie van kalium in kooldraden de waterstofopslagcapaciteit significant laat toenemen, net zoals bij grafiet. De intercalatie van $FeCl_3$ in kooldraden is niet gelukt en door intercalatie van $FeCl_3$ in grafiet nemen het microporievolume en de waterstofopslagcapaciteit van het materiaal niet toe. Ook vervolgbehandelingen van het materiaal om $FeCl_2$ geïntercaleerd grafiet te produceren hebben het microporievolume niet laten toenemen.

We willen graag eindigen met concluderen dat verder onderzoek naar opslag van waterstof door middel van fysisorptie van belang is. Het blijft echter de vraag of een geschikt opslagmateriaal gevonden zal worden.

Referenties

1. A.J. Kidnay en M.J. Hiza, Advances in Cryogenic Engineering 12 (1967) 730.
2. L. Schlapbach en A. Zuttel, Nature 414 (2001) 353.

Samenvatting voor leken

In de afgelopen vier jaar hebben mensen mij vaak, als ze hoorden dat ik een promotie-onderzoek deed, gevraagd of dat niet saai was, vier jaar lang aan hetzelfde werken. Mijn antwoord was altijd dat ik het zag als een reis. Een reis waarbij je verschillende bestemmingen bezocht en steeds weer van richting veranderde. Maar saai was het nooit, want de bestemming en de manier van reizen waren steeds weer anders. In dit hoofdstuk mijn poging om deze reis te beschrijven voor mensen die geen ervaring hebben met de bestemmingen die ik aan heb gedaan en geen kennis over de middelen waarmee ik heb gereisd.
Ik zal in dit stuk vaak spreken over wij. Dat is geen pluralis majestatis, maar omdat je zulk onderzoek nu eenmaal niet alleen doet. Ik heb altijd samengewerkt met mijn begeleiders (Jos van Dillen, co-promotor) en Krijn de Jong (promotor), met studenten die in het kader van een bijvak of afstuderen een poosje met mij samenwerkten en collega's. Daarom dus wij!

De wereldvoorraad ruwe aardolie is eindig. Daarnaast heeft het gebruik van benzine voor voertuigen een aantal belangrijke nadelen. Bij de verbranding van benzine in de motor om de auto voort te bewegen worden enkele ongewenste stoffen uitgestoten. De efficiëntie van de interne verbrandingsmotor is tevens bijzonder laag. Van de 100 eenheden energie die in ruwe aardolie aanwezig zijn in de bron zijn bij het tanken nog 80 eenheden over (dus na oppompen, vervoer naar de raffinaderij, omzetting in de raffinaderij naar benzine en vervoer van de bezine naar de pomp). Daarvan worden in de motor maar *10* eenheden energie gebruikt voor de voortbeweging. De rest wordt omgezet in warmte. Een veel schoner en efficiënter systeem kan gevormd worden door gebruik te maken van een brandstofcel op waterstof en vervolgens aandrijving door middel van een elektromotor. De efficiëntie van dit systeem is veel hoger en er wordt slechts water uitgestoten. Het benodigde waterstof kan gemaakt worden door water te electrolyseren tot waterstof en zuurstof. Dit kan uitgevoerd worden met zonnecellen. Deze brandstof kan in ieder geval niet op raken, aangezien de cyclus oneindig herhaald kan worden. Idealiter zou de vorming van het waterstof uitgevoerd moeten worden op een plaats waar veel zonlicht beschikbaar is. De gevormde waterstof kan dan vandaar verspreid worden naar tankstations. Echter, om op waterstof te kunnen rijden moeten we er op veilige wijze voldoende van mee kunnen nemen in onze auto. Dat is niet eenvoudig, aangezien waterstof rondom kamertemperatuur en bij normale luchtdruk een gas is. Benzine is een vloeistof en dus veel dichter. Indien je waterstof in de gasfase bij kamertemperatuur mee zou willen nemen moet je een enorme ballon aan je auto hangen. Niet praktisch en niet veilig dus. Daarom moeten we een truukje bedenken om waterstof mee te kunnen nemen in onze auto. We stellen veel eisen aan zo'n systeem. Het moet voldoende waterstof op kunnen slaan om een redelijke afstand te kunnen rijden (vergelijkbaar met huidige auto's op 1 tank benzine), het moet veilig zijn, niet te duur, niet te volumineus (want dan past het niet in de auto), niet te zwaar (want dan gaat de auto weer veel meer energie verbruiken), de materialen die gebruikt worden moeten niet te exotisch zijn (want het moet gemaakt kunnen worden voor in principe alle auto's ter wereld) en het moet sterk zijn (want het moet tegen alle bewegingen van de auto kunnen). Als laatste moet het geen extra gevaar opleveren indien het materiaal bij een aanrijding buiten de auto komt, oftewel het mag niet heftig reageren met lucht en het mag niet giftig zijn.

Ruwweg zijn er 4 mogelijkheden om waterstof op te slaan voor toepassingen in voertuigen. Waterstof kan vloeibaar gemaakt worden, kan samengedrukt worden, kan opgeslagen worden in een metaal (chemisorptie) en kan opgeslagen worden op een materiaal met een hoog oppervlak (fysisorptie). De genoemde methoden hebben allemaal nadelen. Om waterstof vloeibaar te maken moet je het afkoelen tot 20 K, hetgeen -253°C is, 20 graden boven het absolute nulpunt. Dit kost vreselijk veel energie. Ook samendrukken kost veel energie. Daarnaast zijn voor beide genoemde systemen hele dure tanks nodig, die de kosten van een auto flink zouden verhogen. Het opslaan in metalen gaat heel makkelijk, maar het waterstof er weer uit halen kost ook veel energie. Tevens zijn dit erg zware systemen, waardoor de auto meer energie gaat verbruiken bij het rijden. Het opslaan op een materiaal met een hoog oppervlak lijkt het minste energie te kosten. Weliswaar moet je hiervoor ook naar lage temperaturen (vanaf ongeveer -200°C), maar er is wellicht wel een licht en goedkoop materiaal te maken. Deze optie van waterstofopslag zijn wij dus nader gaan onderzoeken.

In de eerste plaats hebben we gekeken naar de algemene eisen waaraan een materiaal moet voldoen om veel waterstof op te kunnen slaan. Hiervoor hebben we een aantal materialen geselecteerd die flink van elkaar verschillen in vorm en oppervlaktestructuur. Sommige materialen waren heel vlak, anderen bestonden uit kleine bolletjes, anderen uit lange, dunne cylinders en anderen uit een soort gatenkaas, met veel kleine poriën. Wij dachten namelijk dat waterstof misschien wel graag in die kleine poriën wilden zitten. Dat bleek ook zo te zijn. Waterstof heeft een voorkeur voor hele kleine poriën. Hoe meer van zulke poriën een materiaal bevat, hoe meer waterstof erin opgeslagen kan worden. Theoretisch bestaat dus het beste materiaal voor opslag van waterstof uit heel veel kleine poriën naast elkaar met hele dunne wandjes ertussen. Zo'n materiaal kan het beste opgebouwd worden uit koolstof, aangezien dit hele dunne wanden kan vormen en dus voor een lager gewicht en in kleiner volume evenveel poriën kan vormen als andere materialen, die ingewikkeldere en dikkere wanden moeten vormen. We hebben toen van een groot aantal materialen bekeken hoeveel kleine poriën ze hadden, hoe groot die poriën precies waren en hoeveel waterstof daar in ging zitten. Het meeste waterstof ging zitten in de materialen met de kleinste poriën, 0.5-1.0 nm ($1 * 10^{-9}$ m). Er zijn ook mensen die met computers aan dit soort systemen gerekend hebben en uit hun berekeningen was gekomen dat je de meeste waterstof op kon slaan in een materiaal met poriën van ongeveer 1 nm. Dat komt dus aardig overeen met onze resultaten.

Nu weten we dus wat we moeten maken of vinden, namelijk een materiaal, bestaande uit koolstof met poriën van ongeveer 1 nm groot. Tevens moet het materiaal sterk zijn, niet giftig en liefst goedkoop. We denken aan grafiet (dat wat in je potlood zit). Dat zijn allemaal koolstoflagen bovenop elkaar. We weten dat je tussen die lagen andere materialen kunt stoppen die de koolstoflagen verder uit elkaar drukken. Normaal is de ruimte van het midden van de ene koolstoflaag naar het midden van de volgende 0.34 nm. We weten dat als we sommige materialen tussen die lagen stoppen (dat noemen we intercaleren) dat de afstand van de ene laag naar de volgdende dan opgerekt wordt tot 0.52 nm (als we er kalium in stoppen) of zelfs tot 0.94 nm (als we er ijzer(III)chloride in stoppen). Alleen is grafiet helaas niet erg sterk. Dat weet je wel, aangezien je er mee kunt schrijven en het als smeermiddel kunt gebruiken. Dat komt namelijk omdat je de verschillende lagen van grafiet zo van elkaar kunt wrijven, want die zijn niet zo stevig aan elkaar gebonden. Zo'n laag onderling is wel weer heel sterk, net zo sterk als diamant! Maar omdat het dus niet zo sterk is, is grafiet niet zo geschikt om in auto's te gebruiken. Gelukkig zijn er varianten van grafiet en één daarvan

noemen we kooldraden. Dat zijn hele dunne, lange draden, opgebouwd uit grafietlagen. De draden zijn zo dun dat je ze met het blote oog niet kunt zien. Ze hebben een diameter van ongeveer 55 nm. De draden zijn veel sterker dan grafiet, omdat ze of opgebouwd zijn uit gestapelde frietzakken of uit cylinders in elkaar (beginnend met een hele dunne en steeds dikker wordend naar buiten toe). Je kunt de grafietlagen dan niet meer zo van elkaar wrijven. Deze kooldraden zijn dus wel sterk, licht en heel veilig (want ze bestaan voornamelijk uit grafiet en dat is niet giftig). Ze zijn alleen nog niet heel ruim voorradig.

Om te zorgen dat de kooldraden uiteindelijk ook ruim beschikbaar zouden kunnen komen en omdat we veel van de materialen nodig hadden voor het onderzoek hebben we een proces gemaakt waarmee we redelijk eenvoudig grote heoveelheden draden konden maken. We maakten de draden al lang zelf, maar altijd in kleine hoeveelheden, waardoor je of heel zuinig moest zijn met experimenteren, of heel vaak nieuwe draden moest maken. We hebben een systeem gebouwd waardoor je in één keer 10 keer zo veel kon maken. Dat was een grote vooruitgang. Deze kooldraden maken wij door over hele kleine deeltjes (zo'n 55 nm) van een metaal (meestal nikkel) heel zuiver aardgas te leiden. Dat aardgas ontleedt op het nikkel in waterstof en koolstofatomen. Het waterstof verdampt weer, maar het koolstof zit graag bij het nikkel en kruipt erin. Daardoor kan er weer nieuw aardgas ontleden en die koolstoafatomen lopen ook het nikkel in. Het eerdere koolstof wordt naar beneden door het deeltje gedrukt en aan de andere kant van het deeltje gekomen vormt het een mooie grafietplaat. Bij een nikkeldeeltje vormt het meestal frietzakken, die achter elkaar opstapelen en zo een draad vormen. Zo'n kooldraad noemen we een visgraatkooldraad, aangezien het skelet van de draad een visgraatstructuur heeft als je erdoorheen kijkt met de electronenmicroscoop. Soms vormt het lange buizen in elkaar en dan heet het een parallele draad.

Uit eerder onderzoek wisten we dat de temperatuur een grote invloed had op het groeien van kooldraden. Door de temperatuur te veranderen kunnen verschillende soorten (visgraat en parallelle) kooldraden gegroeid worden. Dus het systeem dat we gebouwd hebben is ontworpen om de temperatuur zo gelijk mogelijk te houden tijdens het groeien. Tevens is het zo ontworpen dat dit eenvoudig overgenomen kan worden als er op nog veel grotere schaal gegroeid gaat worden (industriële schaal). Daarnaast is het met dit systeem hopelijk mogelijk om de kooldraden continu te groeien, dat wil zeggen dat je aan één kant gegroeide kooldraden uit de reactor haalt en aan de andere kant nieuwe kleine nikkeldeeltjes toevoegt die dan weer kunnen gaan groeien. De reactie, het groeien van de draden zou dan niet tussendoor stopgezet hoeven worden. Dat zou ideaal zijn voor een industrieel proces. Om dit te kunnen verwezenlijken is extra onderzoek nodig.

Vervolgens hebben we de gemaakte kooldraden uitgebreid bestudeerd door ze te vergelijken met eerder gegroeide draden en door ze te bekijken in een electronenmicroscoop. Een electronenmicroscoop is vergelijkbaar met een lichtmicroscoop in dat je op monsters kunt kijken en dan het oppervlak kunt bekijken (dat noemen we een SEM, een Scanning Electron Microscope) of dat je hele dunne plakjes maakt en dan door je monsters heen kunt kijken (een TEM, een Transmission Electron Microscope). Aangezien deze microscopen 'kijken' door middel van electronen (die heel klein zijn) kun je ook hele kleine dingen bestuderen. Een electronenmicroscoop kan ongeveer deeltjes van 1 nm van elkaar onderscheiden. Hele goede microscopen kunnen zelfs nog kleinere deeltjes zien. Die hebben we gebruikt om naar de kooldraden te kijken. De microscoop is zo goed dat je de verschillende vlakken in het grafiet

(die dus op 0.34 nm afstand van elkaar zitten) kunt zien. Toen we de kooldraden bestudeerden hebben we ontdekt dat de in het nieuwe systeem gegroeide draden hetzelfde zijn als eerder gegroeide draden. Maar we dachten altijd dat kooldraden uit heel mooie, nette grafietvlakken bestonden, net zoals grafiet zelf. Dat bleek niet zo te zijn. Het onderzoek met de transmissie electronenmicroscoop liet ons zien dat in de visgraatkooldraden ook veel parallelle draden zaten en veel draden waarvan stukken parallel waren. Ook bleken veel grafietlagen niet mooi recht te lopen, maar hobbelig te zijn, of te splitsen in twee lagen en verderop weer samen te komen. De uiteinden van de grafietlagen aan de buitenkant van de draad waren ook vaak gebogen. Aangezien we vermoedden dat al deze onregelmatigheden en afwijkingen van het grafietrooster invloed zouden kunnen hebben op de mogelijkheid om materialen tussen de lagen te stoppen, wilden we kijken of we de kooldraden konden 'grafitiseren'. Dat wil zeggen, ze verhitten tot hele hoge temperaturen, waardoor de grafietlagen rechter zouden worden en het aantal afwijkingen minder zou worden. Uit beschrijvingen van anderen hadden we begrepen dat je vanaf 1600°C invloed op de draden kon uitoefenen. Vanaf 2000°C zou je duidelijke veranderingen binnen de grafietlagen waar moeten nemen en bij 3000°C zou je een zeer nette grafietstructuur moeten krijgen met prachtige rechte lagen. Nu is het niet eenvoudig om een oven te vinden die zulke temperaturen haalt, zeker niet aangezien in de oven natuurlijk ook absoluut geen zuurstof mocht komen, want dan zouden de draden bij deze hoge temperatuur allemaal wegbranden. Gelukkig kon Philips Lighting Components ons helpen.

We hebben de visgraatdraden bij 1600 en 2000°C verwarmd en parallelle draden bij 2000°C. Daarna hebben we de materialen weer bekeken. We konden direct waarnemen dat er in de afstand tussen de lagen niets veranderd was en het materiaal niet opeens veel netter was. Dat hadden we ook niet verwacht, want dan moest je nog 1000°C hoger verwarmen. Met de electronenmicroscoop zagen we meteen dat er *in* de draden nog net zoveel fouten en onregelmatigheden en afwijkingen zaten bij beide soorten draden als voor het verhitten. Maar we zagen ook meteen dat bij de visgraatdraden de einden van de draden niet meer krom waren, maar recht uitstaken, van de draden af. Bij de parallelle draden konden we geen verschillen zien met de electronenmicroscoop. Maar met twee andere technieken wel. We hebben gekeken bij welke temperatuur de draden gaan reageren met zuurstof, door ze langzaam op te warmen in zuurstof op een balans, een apparaat dat het gewicht meet. We weten dat het materiaal reageert als het gewicht verandert. Door dat punt bij alle draden voor en na behandeling met elkaar te vergelijken en te vergelijken met het punt waarop grafiet begint te reageren konden we zien dat alle verhitte materialen meer op grafiet waren gaan lijken. De temperatuur waarop reactie met lucht begon lag namelijk dichter bij de temperatuur van de grafietreactie naarmate het materiaal meer was verhit. Met een andere techniek hebben we gekeken wat voor soort chemische groepen er op het oppervlak van de draden zitten. Dit hebben we bekeken voor en na verhitting en na verhitting waren er minder groepen die wijzen op gebogen grafietlagen en meer groepen die wijzen op nette grafietlagen. Dat komt dus overeen met de resultaten van de andere technieken. We hebben uiteindelijk vastgesteld dat er in de draden veel onregelmatigheden zitten en dat we daar invloed op uit konden oefenen door de draden te verhitten. Voor invloed op de grafietlagen aan het oppervlak is verhitten tot 1600 tot 2000°C voldoende. Voor invloed op de grafietlagen *in* de draden zijn hogere temperaturen nodig.

Nadat we zo veel grote hoeveelheden draden konden maken en goed wisten hoe ze eruit zagen hebben we geprobeerd om poriën te maken die geschikt zijn voor waterstofopslag. Dit hebben

we gedaan door een metaal, kalium, tussen de grafietlagen van de visgraatkooldraden te stopen (dat heet intercaleren). Op deze manier worden de lagen uit elkaar gedrukt en ontstaat er ruimte tussen. We zijn begonnen met kalium omdat het niet zo moeilijk te intercaleren is en we ook ervaring daarmee hadden. Tevens wisten we uit rapportages van anderen dat grafiet waar kalium in gestopt was meer waterstof opsloeg dan onbehandeld grafiet. Het nadeel van het systeem is echter dat het zeer brandbaar is. Kalium reageert heftig met water (vergelijkbaar met het jullie misschien welbekende natrium), het gaat namelijk branden. Om in een auto te gebruiken is het dus zeker niet geschikt, aangezien het niet veilig zou zijn bij aanrijdingen als er lucht bij zou komen. Aangezien het makkelijk te maken is, hebben we het wel bestudeerd als modelsysteem. Je maakt het door de materialen bij elkaar te voegen, te zorgen dat er geen zuurstof bij zit en bij kan komen, verwarmen, roeren, een paar uur wachten, af laten koelen, klaar! Om te voorkomen dat het materiaal zou reageren met zuurstof maakten we het in het apparaat waarin we ook konden bepalen hoeveel waterstof het materiaal op wilde nemen. Al snel bleek dat het tussen de platen stoppen van kalium er inderdaad voor zorgt dat de kooldraden veel meer waterstof op gaan slaan. Zonder kalium slaan ze ongeveer 10 ml H_2 per gram kooldraden op. Met kalium toegevoegd neemt dit toe tot 160 ml H_2 per gram kooldraden, 16 keer zoveel dus! We hebben dus laten zien dat net als bij grafiet ook bij kooldraden de hoeveelheid waterstof die opgeslagen wordt toeneemt indien kalium tussen de grafietlagen wordt gestopt. Tevens hebben we laten zien dat het waterstof maar zwak gebonden is. Dat deden we door na het opslaan van waterstof al het waterstof uit het systeem te pompen en vervolgens weer opnieuw waterstof op te slaan. Indien er precies dezelfde hoeveelheid waterstof telkens weer opnieuw kon worden opgeslagen was zeker dat er geen waterstof achterbleef omdat het sterk gebonden was.

Het feit dat het materiaal zo makkelijk met zuurstof reageert maakte het moeilijk om het te bestuderen. Bij veel technieken worden de materialen blootgesteld aan lucht. Maar aangezien we graag zeker wilden weten dat de afstand tussen de platen inderdaad veranderd was, groter was geworden, hebben we daar met drie technieken naar gekeken. De eerste is Röntgendiffractie. Hierbij wordt met röntgenstraling gekeken of er ordening in het materiaal zit. Die ordening uit zich in pieken, die aangeven op welke afstand tussen de atomen er herhaling in het materiaal zit. Hiermee konden we zien of de herhaling, die voor het ertussen stoppen van kalium op 0.34 nm zat nu op 0.52 nm terug te vinden was. Dat bleek zo te zijn voor een deel van de draden. Een ander deel was niet veranderd. Het kalium gaat dus niet in alle draden tussen de platen zitten. Ook met een hele goede electronenmicroscoop hebben we weer naar de draden gekeken. Hiervoor moesten de geïntercaleerde draden gemaakt worden, vervoerd in luchtdichte glazen houders en daarna in een zuurstofvrije kast op het houdertje gelegd en dan snel naar de microscoop. Helaas was in de microscoop geen duidelijk verschil te zien met draden waar geen kalium in zat. Wij denken dat het overbrengen toch niet helemaal goed is gegaan en het kalium met lucht heeft gerageerd. Het was helaas niet mogelijk om het nog anders te proberen. Uiteindelijk hebben we ook nog gekeken of het oppervlak van het systeem groter was geworden. Als je grotere poriën maakt in een systeem moet het oppervlak groter worden. Ook hier hebben we geen verandering gemeten. Dit kunnen we verklaren omdat het molecuul dat we gebruiken om te kijken hoe groot het oppervlak is, het meetmolecuul, te dik is om in de gevormde poriën te passen. Dit hebben we gecontroleerd door te proberen het molecuul in grafiet te stoppen waar kalium in zat. Daar paste het ook niet, dus is het logisch dat het ook bij de kooldraden niet lukte. Uiteindelijk hebben we vastgesteld dat het kalium niet in alle draden gaat zitten. Dat komt waarschijnlijk

omdat de draden zo veel minder regelmatig zijn dan grafiet. Kalium kan gewoon niet overal tussen omdat de grafietlagen niet overal opgelicht kunnen worden. Wel hebben we aangetoond dat kalium tussen de platen zit en dat dit ervoor zorgt dat er meer waterstof kan worden opgeslagen, die ook eenvoudig weer verwijderd kan worden, door kleine temperatuur- en of drukverschillen.

Nadat we dit aangetoond hadden wilden we graag een materiaal maken waarbij de poriën groter waren en dat niet zo heftig reageerde met lucht. Een geschikt materiaal om tussen de platen te stoppen is ijzer(III)chloride. De afstand tussen de grafietlagen wordt dan 0.94 nm en het reageert niet heftig met lucht. Het tussen de platen stoppen van ijzer(III)chloride is iets ingewikkelder dan bij kalium, je stopt het bij elkaar, mengt, verlaagt de druk, sluit het systeem af, verwarmt gedurende enkele dagen, afkoelen en klaar! Helaas is het niet gelukt om het materiaal in kooldraden te stoppen. We hebben alles geprobeerd, langer verwarmen, andere temperaturen, verschillende soorten kooldraden en ook de kooldraden met een netter, meer grafietachtig oppervlak, die verhit waren tot 1600 en 2000°C. Niets hielp. Het ijzerchloride wilde niet tussen de grafietlagen van de kooldraden gaan zitten. Waarschijnlijk komt dit omdat de kooldraden zoveel onregelmatiger zijn. De platen kunnen niet allemaal goed opgelicht worden.

Omdat het met kooldraden niet lukte hebben we verder gewerkt met grafiet. Dit is niet sterk genoeg voor toepassing in auto's, maar wel geschikt als modelsysteem. Nadat we het ijzer(III)chloride tussen de platen gestopt hadden hebben we dit gecontroleerd door te kijken met Röntgenstraling of de herhaling zich nu op 0.94 nm bevond. Dit bleek inderdaad het geval. Het goede materiaal was gevormd. Helaas sloeg het niet meer waterstof op en was het oppervlak ook niet groter geworden. We konden niet zien dat er extra poriën gevormd waren. Het ijzer(III)chloride drukt de platen uit elkaar en gaat ertussen zitten, maar daarmee is alle ruimte tussen de platen ook weer gevuld. Om toch ruimte beschikaar te maken hebben we bedacht dat het ijzerchloride kleiner gemaakt kan worden door het om te zetten naar van ijzer(III)chloride (dus per ijzer atoom drie chloor atomen) naar ijzer(II)chloride (per ijzer atoom twee chloor atomen) of zelfs naar ijzer, dus zonder chloor atomen. Indien dit tussen de grafietlagen zou blijven zitten zou er veel ruimte voor waterstof ontstaan. Deze omzettingen hebben we geprobeerd te doen door het materiaal te verwarmen, waardoor het gaat ontleden van ijzer(III)chloride naar ijzer(II)chloride en chloor en door het te laten reageren met waterstof. Dan reageert ijzer(III)chloride naar ijzer(II)chloride en HCl en vervolgens naar ijzer en nog twee HCl. Om te kunnen reageren moesten de materialen echter wel verwarmd worden en het bleek dat het ijzer(III)chloride eerst weer tussen de grafietlagen uitkwam en dan pas reageerde. Het lukte niet om de reactie tussen de platen te laten plaatsvinden. Met allerlei technieken hebben we de materialen en de op het oppervlak ontstane deeltjes bekeken, maar er bleken geen poriën gevormd te worden of achter te blijven en er kon geen extra waterstof opgeslagen worden in dit systeem. Als we een materiaal kunnen vinden dat wel tussen de grafietlagen blijft zitten en dan omgezet kan worden en zo poriën maakt dan is dat zeker een geschikt materiaal om waterstof in op te slaan.

Al met al is het dus niet gelukt om een geschikt systeem te maken om waterstof in op te slaan. Wel weten we beter hoe zo'n systeem eruit moet zien en hebben we ook vreselijk veel geleerd over kooldraden. Dus het is zeker niet voor niets geweest!

Dankwoord

Dit onderzoek heb ik gelukkig niet in mijn eentje uitgevoerd. Veel mensen hebben bijdragen geleverd, zaken uitgelegd, me geholpen en me gemotiveerd. Ik hoop dat ik de mensen die ik nu ga bedanken mijn dank en waardering gaandeweg voldoende heb getoond toon en dit dankwoord dus eigenlijk overbodig is, maar het is ook wel erg leuk om het allemaal eens op te schrijven.

Ik wil beginnen met mijn promotor, Krijn de Jong. Krijn, ik wil je bedanken voor je positieve en steeds motiverende houding. Ik heb vreselijk veel geleerd van jouw kritische vragen over mijn resultaten en je vernieuwende kijk op de zaken. Dat langzamerhand enkele van mijn hypothesen ook in jouw presentaties opdoken vond ik leuk om mee te maken.
Jos van Dillen, mijn co-promoter is van onschatbare waarde geweest om mee te denken in de dagelijkse voortgang van het onderzoek, om mijn hart te luchten als iets niet lukte, om nieuwe mogelijkheden te bedenken en de laatste paar maanden om een enorme stapel lees- en corrigeerwerk door te worstelen. Dat wij behoorlijk verschillend denken en redeneren heeft het boekje juist erg veel duidelijker gemaakt en ik heb ontzettend veel van je geleerd. Jos, je bent een oneindige vat vol spannende onderzoeksideeën. Door de aard van dit onderzoek is een groot aantal van je ideeën nooit uitgevoerd en dat is jammer. Gelukkig zijn er genoeg nieuwe "kooldraadmensen" bijgekomen die hopelijk nog enkele van je mooie ideeën wel uitvoeren.
Harry, 2^{e} begeleider, dank voor het samen denken over bepaalde berekeningen en de uitgebreide (wetenschappelijke) discussies die we vaak gehad hebben. Jammer dat het klussen in jullie nieuwe huis samenviel met mijn drukke schrijfperiode, maar om het goed te maken zal ik in je nieuwe keuken snel eens rijst komen strooien!

Ook bij Shell, die mijn onderzoek financierden, had ik het gevoel dat ik altijd aan kon kloppen voor overleg, adviezen en hulp. Daarvoor wil ik Hans Geerlings en Heiko Oosterbeek bedanken. Het was altijd heel motiverend om een bespreking te hebben met jullie, die zo'n heel andere kijk op de zaak hebben. Jullie kritische houding en enthousiasme over het project waren erg prettig. Op deze plek mag ik zeker Herman Kuijpers niet vergeten, die mij op zeer kundige wijze begeleid heeft bij mijn eerste schreden in waterstof-opslag-land!

Onno, dank voor de hulp met het uitwerken van de XPS data van $FeCl_3$ in grafiet. Het was leerzaam om daar samen aan te rekenen en over te brainstormen. Ad Mens, dank voor de XPS metingen en de laatste BET-metingen (spannend, belangrijk en brandbaar!). Fred, dank voor je TGA-metingen, het snelle bestellen van chemicaliën en hulp bij het verwisselen van zo'n enorme CO-fles. Ad van der Eerden, we hebben niet echt samengewerkt, maar ik wil van de gelegenheid gebruik maken me te verontschuldigen voor het feit dat het me steeds weer lukte om in onze gesprekken een opmerking over je leeftijd te maken. Ik deed het *echt* niet expres!
Marjan, dank voor de XRD-ondersteuning en veel dank voor het vele SEM-werk. Samen genoten we van "mooie plaatjes" en we hebben heel wat interessante foto's geschoten van

gapende gaten, motorblokken, Jan Hagel en ander spannends. Johnnieboy, heel veel dank voor ontzettend veel BET-metingen, TPR-werk en H_2–opslag metingen. Vrijwel alle metingen van hoofdstuk 2 zijn van jouw hand. Daarnaast dank voor veel discussies, veel muziek en veel videos. Ik had gehoopt dat IK je nog wel op mijn feestje kon krijgen en dat ik dat niet meer kan proberen voor elkaar te krijgen doet pijn. Ik zal een colaatje drinken op jou.

Mannen van de glasblazerij (Igno, Wim, Wil, Maarten, Peter en Pieter), dank voor veel, heel veel mooie apparaten en minstens evenveel gezelligheid en lol. Igno, dank voor het ontwerpen van de prachtige en uitstekend werkende fluidized bed reactor. Wim, wat had ik zonder jou moeten beginnen. Je maakte en onderhield mijn fluid bed reactor en mijn ovens. Je hebt een enorme hoeveelheid ampullen voor me gemaakt, afgesmolten en weer geopend, en last but not least heb je mijn adsorptie-opstelling gereviseerd, geoptimaliseerd en enkele malen gerepareerd. Ik beloof plechtig dat ik mijn best zal doen mijn ogen open te houden als jij in de buurt bent!

Evert en de heren en dame van de instrumentmakerij farmacie, veel dank voor de technische ondersteuning. Jullie hebben enkele mooiste kunststukjes voor me gemaakt om alles zo zuurstof- en watervrij mogelijk te houden. Victor en Henk, dank voor het gaande houden van het elektronische deel van de opstelling.

Het beschreven werk heb ik uitgevoerd in samenwerking met een aantal studenten. Het samenwerken was een zeer motiverende en leerzame ervaring die ook veel resultaten heeft opgeleverd en waar ik meestal veel plezier aan beleefde. Marieke, Micha, Ruud en Jaap veel van jullie resultaten zijn verwerkt in het boekje.
Ook scriptiestudenten Petra, Kirna, Bas en Martijn hebben ontzettend veel geholpen door literatuur te screenen en er goede, leesbare verhalen over te schrijven.

Patricia Kooyman wil ik bedanken voor schitterende TEM opnamen van kooldraden. Dat er zo veel prachtige defecten te zien zouden zijn was meteen een nieuw interessegebied. Dat jullie TEM monsters kunnen maken en overbrengen zonder blootstelling aan lucht was een geweldige uitkomst voor het onderzoek.
In opvolging van die studie heb ik met professor John Geus twee dagen achter de TEM gezeten voor de ‘heat treated’ kooldraden. John, ik wil je hier heel hartelijk voor bedanken. Prachtige opnamen, een soepele samenwerking en veel filosofie over draden, maar ook over hockey vond ik erg leuk.
Voor die “hete draden” ben ik Roland Vogels veel dank verschuldigd. Een oven die onder inert kan verhitten tot 2000°C is niet zo even voorradig. Philips Lighting Components hielp me uit de brand. Jouw gastvrijheid, interesse en hulp vond ik zeer motiverend en prettig, helaas waren de kooldraden minder onder de indruk….

Gerbrand, Frank en Daphne wil ik bedanken voor de gezelligheid bij het EXAFS avontuurtje in Grenoble. Nou weet ik ook eindelijk hoe een beamline eruit ziet!

Harry, Jules, Marjolein, Sander, Jeroen en Moniek, bedankt voor de gezelligheid, steun en lol in Limerick. Jeroen, ik wil net zo'n verjaardagscadeau als Moniek!

Tonnis, ik hoop dat ons ideetje, geboren na een dag voetballen een Debye traditie wordt.

Kamergenoten Marjolein en Tijmen, we zaten gezellig samen als de "kooldraad kids". Tijmen, onze samenwerkingen liepen vanaf het begin gesmeerd, weet je nog hoe we Esther Vercammen er tussen namen? We hebben veel samen gedaan, gepraat, gemeten, georganiseerd, gelachen en ook gehuild. Dank voor veel steun. Ik hoop dat er voor jou een periode met meer lachen aanbreekt nu en we dat dan nog vaak samen kunnen doen.
Marjolein, dank voor je eeuwige goede humeur, je leuke verhalen, al je bereidwilligheid om mij op te hoogte te houden van favoriete tv-programma's, meedenken met kooldraden dilemma's en gezelligheid op binnen- en buitenlandse uitstapjes.

Snader en Mickey Mike, bedankt voor alle ranzigheid, Friends-avondjes, goede discussies, steun, humor en jullie voor mij verhelderende mannelijke kijk op veel zaken. Houden jullie elkaar wel heel?
Alle andere collega's, bedankt voor alle koffie-, thee- en lunch-gezelligheid, borrels, LIIT's, barbecues, kerstdiners, congressen, spontane acties, filmpjes, langlaufen, zeilen, voetballen, volleyballen en alle mannen, maar in het bijzonder Dennis, bedankt voor het escorteren van de Uithof naar de bewoonde wereld in de donkere wintermaanden.

Merlijn, Dr. Nijhof! Dank voor veel vertrouwen en begrip en heel veel lol.
Karen en Stellar, scheikunde-meiden, bedankt voor alle steun en belangstelling en voor veel gezelligheid op allerlei uitjes en in de keuken.
Meiden van de culiclub, geen team meer dat ons verbindt, maar lepels en pannen en een heel goed gevoel. Ik hoop dat het een langlopende traditie gaat worden.

Jet, ruim 5 jaar geleden fietsten we elkaars leven binnen, als paranimf sta je straks naast me. Zonder jouw lay-out kennis en geduld was het boekje lang niet zo mooi geworden. Dank voor je geweldige vriendschap.
Roland, 2 minuten lopen of 24 uur vliegen, het lijntje tussen ons is sterk. Je houding naar chemie was en is een voorbeeld, je levenshouding een inspiratie en "food for thought".

Broer(tje) Jarijn, steeds ver weg, even dichtbij en nu weer wat verder. We zijn erg verschillend, maar kunnen het samen wel leuk maken. Dank voor je steun en optimisme.
Marjo en Gerard, ik kom nog steeds graag thuis. Jullie hebben in mijn studie- en promotiekeuze altijd groot vertrouwen in mijn kunnen uitgedragen. Dank voor deze fijne basis.

Reinier, jouw steun en optimistisme hielpen me als ik het zelf even niet meer zag zitten. Ieder einde is weer het begin van iets nieuws: ik wacht nog op dat aanbod van je voor mijn ideale duobaan op je Nowell "raffinaderij" en je flitsende bijlesinstituut!

Curriculum Vitae

Marije Nijkamp werd geboren op 24 december 1973 te Paramaribo, Suriname. In september 1986 begon zij aan het VWO en in juni 1992 behaalde zij het Gymnasium diploma aan het Stedelijk Gymnasium te Arnhem. In september 1992 ving zij aan met de studie Scheikunde aan de Universiteit Utrecht. Zij haalde het propedeause examen in januari 1994. In januari 1998 legde zij het doctoraalexamen *met genoegen* af met bijvakken bij de Sectie Metal Mediated Organic Synthesis (Synthese en reactiviteit van intramoleculair gecoördineerde tantaal-neofylidyn verbindingen) en bij de afdeling Zakelijke Gastoepassingen, Gastec, Apeldoorn (Adsorptie van THT aan kool) en het hoofdvak bij de sectie Anorganische Chemie en Katalyse (Hydrogenation and dehydrogenation by hydrogen absorbents based on V_2O_5). Vanaf februari 1998 was zij als Assistant in Opleiding (AIO) verbonden aan de sectie Anorganische Chemie en Katalyse van de Universiteit Utrecht., waar het onderzoek beschreven in dit proefschrift werd uitgevoerd onder supervisie van prof. dr. ir. Krijn de Jong en dr. Jos van Dillen. Dit promotie-onderzoek werd uitgevoerd in samenwerking met Shell International Oil Products (Global Solutions).